

Supporting Information for
**Structure-Guided Synthesis and Mechanistic Studies Reveal Sweetspots on
Naphthyl Salicyl Hydrazone Scaffold as Non-Nucleosidic Reversible
Inhibitors of Human Ribonucleotide Reductase**

Sarah E. Huff, Faiz Ahmad Mohammed, Mu Yang, Prashansa Agrawal; John Pink; Michael E. Harris;

Chris G. Dealwis* and Rajesh Viswanathan*

Contents

Table S1: List of FDA-Approved Antimetabolite Drugs	3
Table S2: Structures, in vitro IC ₅₀ values, predicted solubility and permeability properties for NSAH analogs.	4
Table S3. Schrödinger docking scores for NSAH analogs at the C-site, A-site, and S-site of hRRM1.	7
General Experimental Details	10
1. Reagents, Solvents and Glassware.....	10
2. Chromatography.	10
3. Structural Characterization of Synthetic Compounds.	11
General Scheme for Synthesis of NSAH and its Analogs.....	12
General Method (A) for Methyl Ester Synthesis	13
General Method (B) for Acyl Hydrazide Formation	13
General Method (C) Synthesis of Aldehydes from Acids	14
General Method (D) for Acyl Hydrazone Formation Through Aldehyde Condensation.....	15
General Method (E) for Indole Aldehyde Synthesis.....	16
Figures with docking poses for inhibitors at the C-site of hRRM1.....	17
Table S4. Enzymatic inhibition data for <i>E</i> -3A, <i>E</i> -3C, <i>E</i> -3T, and <i>E</i> -3W in the presence of ³ H-CDP substrate. IC ₅₀ values are comparable to those obtained using ¹⁴ C-ADP substrate.	26
Anaerobic Metal Chelation Assay with Fe ²⁺ and Fe ³⁺	26
Metal Chelation Assay with Mg ²⁺	27
Enzyme kinetics sigmoidal dose response curves.....	31
siRNA knockdown controls and DNA/Well measurements	31
Copies of NMR and HPLC Data.....	34

Table S1: List of FDA-Approved Antimetabolite Drugs

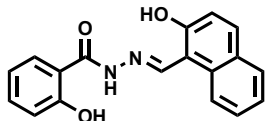
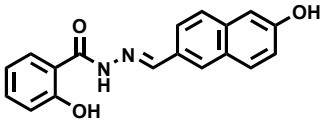
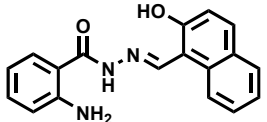
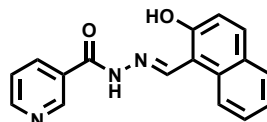
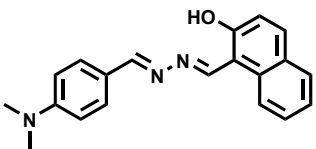
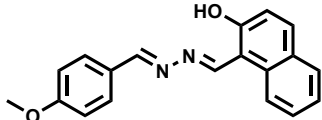
FDA approved antimetabolite drugs for the treatment of cancer

<u>Clinical agent</u>	<u>Year approved</u>
O ⁶ -methyl-arabinofuranosyl guanine (nelarabine)	2005
2'-fluoro-2'-deoxyarabinofuranosyl-2-chloroadenine (clofarabine)	2004
N ⁴ -pentylloxycarbonyl-5'-deoxy-5-fluorocytidine (capecitabine)	1998
2,2-difluoro-2'-deoxycytidine (gemcitabine)	1996
2-chloro-2'-deoxyadenosine (cladribine)	1992
arabinofuranosyl-2-fluoroadenine (fludarabine)	1991
2'-deoxycoformycin (pentostatin)	1991
5-fluoro-2'-deoxyuridine	1970
arabinofuranosylcytosine (cytarabine)	1969
6-thioguanine	1966
5-fluorouracil	1962
methotrexate	1953
6-mercaptopurine	1953
Hydroxyurea [§]	1967
Triapine [§]	(Currently in Phase 2 trials)

§ - Non-antimetabolite class of inhibitors.

Table S2: Structures, in vitro IC₅₀ values, predicted solubility and permeability properties

for NSAH analogs. Cellular IC₅₀ values are averaged from HCT116 and MDA-MB-231 cell lines. ClogP and membrane permeability parameters were predicted using Qikprop. Permeability is reported as a diffusion rate in nanometers/second.

Structure	Name	Enzymatic IC ₅₀	Cellular IC ₅₀		ClogP (octanol/water)	Permeability (nm/s)	
			HCT116	MDA-MB-231		Caco-2	MDCK
	NSAH-E-3A	19 μM	0.225 μM	0.300 μM	3.558	541	254
	NSAH-E-3C	7.3 μM	>10 μM	>10 μM	3.485	333	150
	NSAH-E-3E	23.8 μM	>10 μM	>10 μM	3.181	529	248
	NSAH-E-3F	5.3 μM	>10 μM	>10 μM	2.758	552	260
	NSAH-E-3H	95.2 μM	>10 μM	>10 μM	3.017	605	287
	NSAH-E-3I	94.1 μM	>10 μM	>10 μM	4.046	1012	501

Structure	Name	Enzymatic IC ₅₀	Cellular IC ₅₀		ClogP (octanol/water)	Permeability (nm/s)	
			HCT116	MDA-MB-231		Caco-2	MDCK
	NSAH-E-3J	86.8 μM	>10 μM	>10 μM	3.967	1032	511
	NSAH-E-3K	39.4 μM	>10 μM	>10 μM	3.811	2617	1399
	NSAH-E-3L	21.5 μM	>10 μM	>10 μM	4.473	2700	3832
	NSAH-E-3M	70.1 μM	>10 μM	>10 μM	2.849	311	140
	NSAH-E-3N	21.1 μM	>10 μM	>10 μM	2.629	171	73
	NSAH-E-3O	121.8 μM	10 μM	>10 μM	2.772	737	356
	NSAH-E-3P	130.7 μM	>10 μM	>10 μM	3.341	670	321
	NSAH-E-3Q	43.7 μM	>10 μM	>10 μM	2.211	79	31

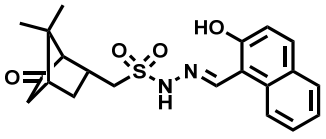
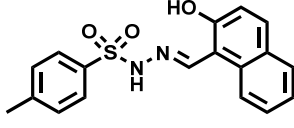
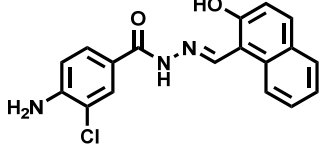
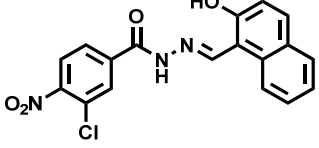
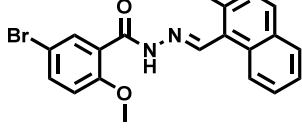
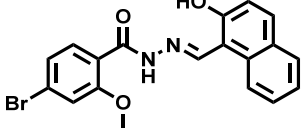
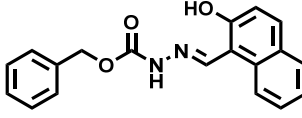
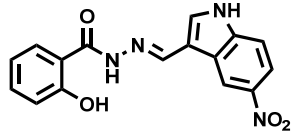
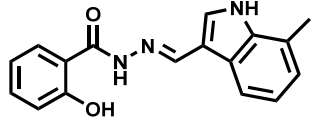
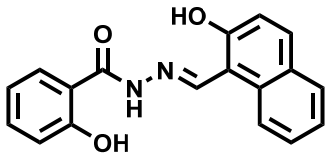
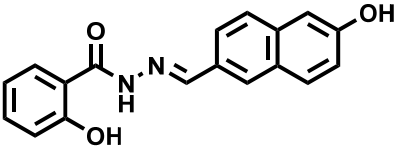
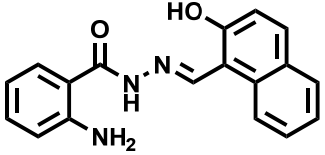
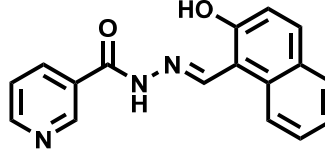
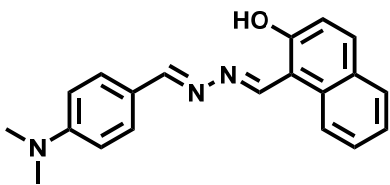
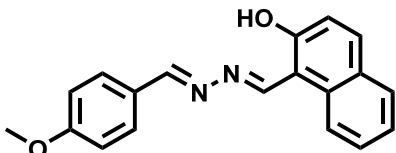
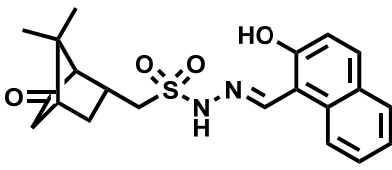
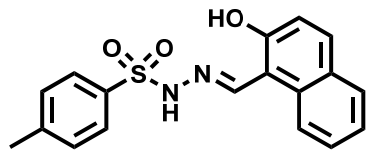
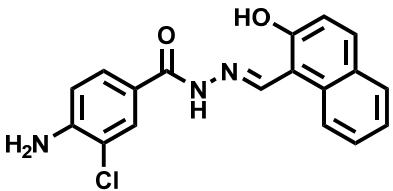
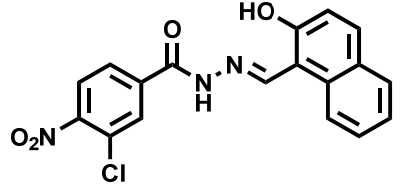
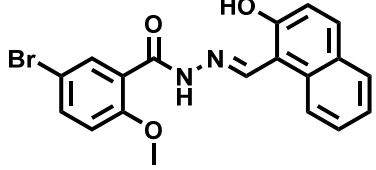
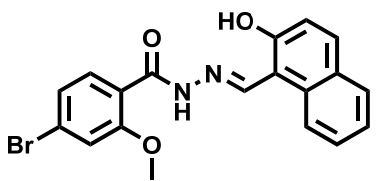
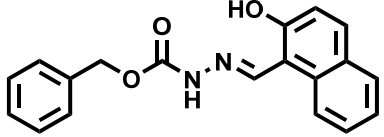
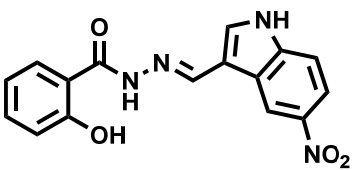
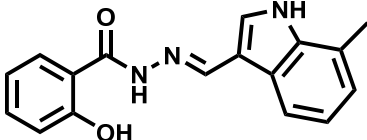
Structure	Name	Enzymatic IC ₅₀	Cellular IC ₅₀		ClogP (octanol/water)	Permeability (nm/s)	
			HCT116	MDA-MB-231		Caco-2	MDCK
	NSAH-E-3R	297.7 μM	>10 μM	>10 μM	-	-	-
	NSAH-E-3S	6.8 μM	>10 μM	>10 μM	3.248	605	288
	NSAH-E-3T	6.1 μM	>10 μM	>10 μM	3.145	346	358
	NSAH-E-3U	16.7 μM	>10 μM	>10 μM	3.428	137	118
	NSAH-E-3V	16.6 μM	1 μM	>1 μM	4.216	1053	1392
	NSAH-E-3W	13.6 μM	<10 μM	>1 μM	4.362	1061	1392
	NSAH-E-3X	120.3 μM	>10 μM	>10 μM	4.137	624	297
	NSAH-E-3Y	20.7 μM	>10 μM	>10 μM	2.742	62	24
	NSAH-E-3Z	10.2 μM	>10 μM	>10 μM	3.788	685	329

Table S3. Schrödinger docking scores for NSAH analogs at the C-site, A-site, and S-site of hRRM1.

Structure	Name	Docking scores		
		C-site	A-site	S-site
	NSAH-E-3A	-6.97	-4.22	-3.85
	NSAH-E-3C	-6.71	-4.71	-5.30
	NSAH-E-3E	-6.26	-3.99	-3.97
	NSAH-E-3F	-6.96	-3.15	-4.22
	NSAH-E-3H	-7.18	-4.13	-3.91
	NSAH-E-3I	-6.36	-4.07	-3.35

Structure	Name	Docking scores		
		C-site	A-site	S-site
	NSAH-E-3J	-6.56	-5.23	-4.19
	NSAH-E-3K	-7.39	-4.96	-3.77
	NSAH-E-3L	-6.75	-4.66	-3.65
	NSAH-E-3M	-6.31	-5.11	-4.01
	NSAH-E-3N	-7.03	-4.93	-2.16
	NSAH-E-3O	-7.20	-4.17	-4.67
	NSAH-E-3P	-7.76	-3.88	-4.24
	NSAH-E-3Q	-7.60	-3.39	-4.51

Structure	Name	Docking scores		
		C-site	A-site	S-site
	NSAH-E-3R	-6.48	-3.04	-5.41
	NSAH-E-3S	-7.15	-2.99	-4.07
	NSAH-E-3T	-6.97	-3.33	-3.22
	NSAH-E-3U	-7.20	-3.57	-3.18
	NSAH-E-3V	-6.51	-4.10	-1.95
	NSAH-E-3W	-6.50	-4.22	-1.98
	NSAH-E-3X	-7.26	-3.09	-3.90
	NSAH-E-3Y	-6.88	-4.16	-2.11

Structure	Name	Docking scores		
		C-site	A-site	S-site
	NSAH-E-3Z	-7.07	-4.52	-2.97

General Experimental Details

1. Reagents, Solvents and Glassware. Unless otherwise specified, all reactions were carried out under standard atmosphere. Dry reactions were carried out under a blanket of nitrogen, using standard syringe-septum, and cannulation techniques.¹ Dry dichloromethane was prepared by distillation over calcium hydride. Anhydrous ether was obtained from an m-Braun solvent purification system (charged with A2 alumina as a desiccant).²

2. Chromatography. Analytical thin-layer chromatography (TLC) was performed with silica Gel 60 Å (230-400 mesh) to monitor the progress of each chemical reaction and to serve as a guide for purification of the ensuing mixtures. TLC was conducted on glass plates (7.5 x 2.5 and 7.5 x 5.0 cm) coated with silica gel G containing 13% calcium sulphate as binder or on pre-coated 0.2 mm thick 60 F₂₅₄ silica plates and various combinations of ethyl acetate and hexane were used as eluent. Visualization of spots after TLC was accomplished by exposure to iodine vapour and/or UV light (254 nm). All compounds were purified using flash column chromatography³ (Silica gel

¹ Pirrung, M. C.; Chapter 8: Conducting the Reaction Itself, *The Synthetic Organic Chemist's Companion*, John Wiley & Sons Inc., Hoboken, NJ, 2007, 69-91.

² Pangborn, A. B.; Giardello, M. A.; Grubbs, R. H.; Rosen, R. K. Timmers, F. J. Safe and Convenient Procedure for Solvent Purification. *Organometallics*, **1996**, *15*, 1518 -1520.

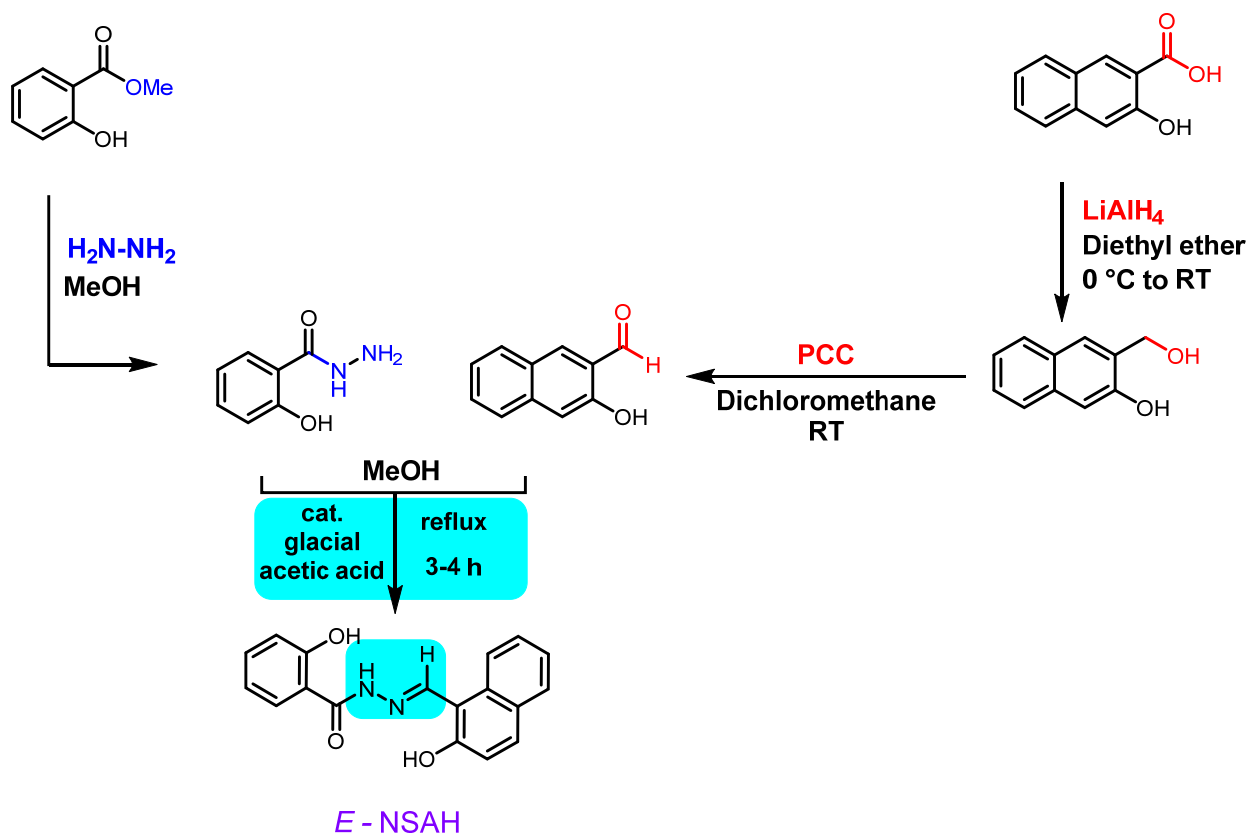
grade: 200-400 mesh, 40-63 μm) at medium pressure (20 psi). Yields refer to compounds isolated to analytical purity after chromatography. All compounds were purified to > 95%.

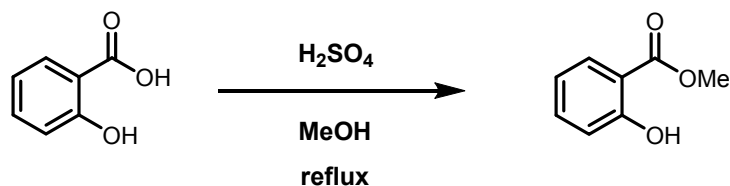
3. Structural Characterization of Synthetic Compounds. NMR spectroscopic analyses (^1H NMR, ^{13}C NMR) were conducted for all new compounds. ^1H NMR spectra were recorded on a 500 MHz spectrometer (^1H : 500 MHz and ^{13}C : 125 MHz), with the exception of a few compounds recorded on a 400 MHz spectrophotometer (^1H : 400 MHz and ^{13}C : 100 MHz). Chemical shift values (δ) for NMR spectra are reported in parts per million (ppm) relative to the residual (indicated) solvent peak (CDCl_3 , $(\text{CD}_3)_2\text{OS}$, or CD_3CN). Additional peaks other than the compound in question, if any, are calibrated based on reported values for trace impurities.⁴ Coupling constants (J) are reported in Hz. Data for ^1H NMR are reported as follows: chemical shift (δ , ppm), multiplicity (s = singlet, brs = broad singlet, d = doublet, t = triplet, q = quartet, dd = doublet of doublets, dt = doublet of triplets), integration corresponding to the number of protons followed by coupling constants in Hz. For ^{13}C NMR spectra, the nature of the carbons (C, CH, CH₂ or CH₃) was determined by recording the Distortionless Enhancement by Polarization Transfer (DEPT) experiment, and notations are provided in parentheses. ^{13}C NMR (125 MHz) data is reported in parts per million (δ) relative to the residual (indicated) solvent peak. All melting points for solids were determined on a Buchi B-540 instrument and are reported uncorrected. IR spectra were recorded on a FT-IR spectrophotometer. HPLC analyses for products were performed using a Shimadzu LC-20-AT Series separations module equipped with Shimadzu SPD-M20A PDA (photo diode array) multiple wavelength detector (180nm-800nm). The system (CBM-20)

⁴ (a). Gottlieb, H. E.; Kotlyar, V.; Nudelman, A. NMR Chemical Shifts of Common Laboratory Solvents as Trace Impurities *J. Org. Chem.* **1997**, *62*, 7512-7515 and (b). Fulmer, G. R.; Miller, A. J. M.; Sherden, N. H.; Gottlieb, H. E.; Nudelman, A.; Stoltz, B. M.; Bercaw, J. E.; Goldberg, K. I. NMR Chemical Shifts of Trace Impurities: Common Laboratory Solvents, Organics, and Gases in Deuterated Solvents Relevant to the Organometallic Chemist *Organometallics*, **2010**, *29*, 2176-2179.

was controlled using LC Solutions software. Separations were carried out on a Princeton C18 reverse phase column (10 μm 4.6 x 250 mm column, 300 Å diameter) using an isocratic mobile phase of 5:1 Acetonitrile:Water. Samples were run over 45 minutes at a flow rate of 1 mL/min. NSAH-*E*-3A, C, N, Y, and Z were run in a mobile phase of Acetonitrile with 0.5% trifluoroacetic acid. Raw data was plotted using Origin[®] software program after exporting absorbance data as an ASCII-formatted file. High-resolution mass spectrometry (HRMS) data for synthetic compounds reported herein were obtained by direct infusion of sodium acetate solutions on a HDMS QTOF mass spectrometer.

General Scheme for Synthesis of NSAH and its Analogs





General Method (A) for Methyl Ester Synthesis

Salicylic acid (0.70 g, 5 mmol) was dissolved in 30 mL of methanol and heated to reflux.

Concentrated H₂SO₄ (0.80 mL, 15 mmol) was added to catalyze the reaction. The flask was left under reflux for approximately 12 h. The solution was diluted with distilled water

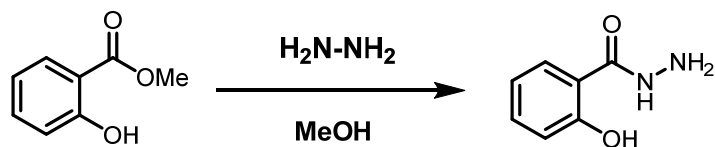
(approximately 20 mL) and the pH was adjusted to 7.0 with NaHCO₃ (sat. solution,

approximately 15 mL) then concentrated *in vacuo* to remove MeOH. The remaining aqueous

solution was transferred to a separatory funnel and extracted thrice with ethyl acetate (10 mL).

The organic layers were dried with Na₂SO₄, filtered, and concentrated to obtain a yellow oil.

Following this general procedure, several distinct methyl esters were obtained. An average yield of 90% was obtained using this procedure.

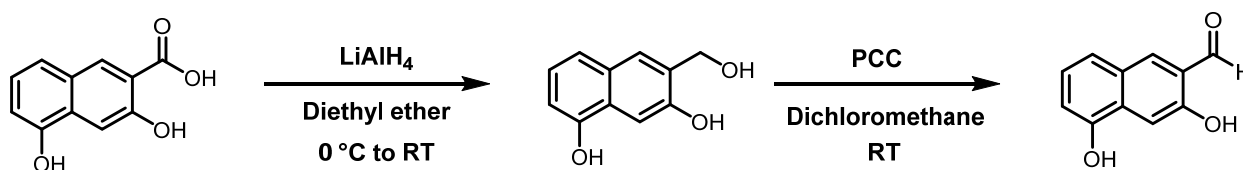


General Method (B) for Acyl Hydrazide Formation

Methyl-2-hydroxybenzoate (0.76 g, 5 mmol) was dissolved in methanol under a nitrogen

atmosphere at room temperature (rt). A syringe was used to transfer 0.5 mL (15 mmol) of

anhydrous hydrazine to the stirring solution and reaction was refluxed for 6 h. The solution was concentrated and the remaining aqueous oil was transferred to a separatory funnel and extracted thrice with ethyl acetate (15 mL). The organic layers were dried with Na₂SO₄, filtered, and concentrated to obtain a white solid. Following this general procedure, several distinct acyl hydrazides were obtained. An average yield of 81% was obtained using this procedure.

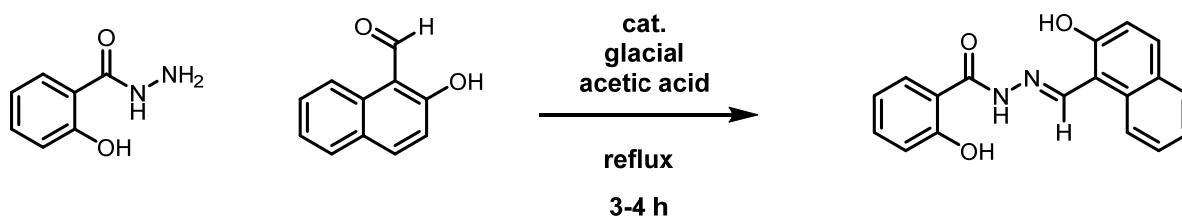


General Method (C) Synthesis of Aldehydes from Acids

Step 1. Reduction using Lithium Aluminum Hydride: A 100 mL round bottomed flask charged with a stirbar and 1.72 g (10 mmol) of 6-hydroxy-2-naphthoic acid was placed under a nitrogen atmosphere. The carboxylic acid was dissolved in approximately 50 mL of dry diethyl ether and cooled to 0 °C in an ice bath. 0.76 g (20 mmol) of LiAlH₄ was mixed in dry diethyl ether under a nitrogen blanket and the resulting suspension was added dropwise to the stirring solution (containing the carboxylic acid) using a syringe. The reaction was left stirring at 0 °C and then slowly warmed to room temperature and stirring continued for 12 h. The reaction flask was then quenched with approximately 100 mL of deionized water and the mixture was vacuum filtered over a sintered glass funnel. The filtrate was saturated with (approximately 4.0 g) Rochelle's salt and left stirring vigorously at room temperature for 2 hours. The saturated solution was then transferred to a separatory funnel and extracted five times with ethyl acetate (10 mL). The combined organic layers were dried with anhyd. Na₂SO₄, filtered, and then concentrated *in vacuo*

to obtain a white solid. Alcohol obtained through this step was traced using TLC, and the product was generally used for the oxidation step without any purification.

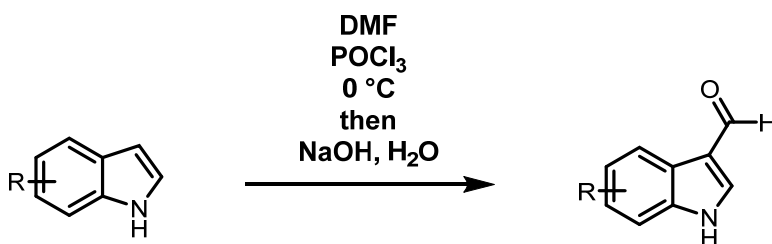
Step 2. Oxidation using PCC: A 300 mL round bottom flask charged with a stirbar and 10 mmol of 6-(hydroxymethyl)naphthalene-1,7-diol was placed under a nitrogen atmosphere and dissolved in approximately 30 mL of dry dichloromethane. In a separate flask, 3.23 g (15 mmol) of PCC was dissolved in 30 mL of dry dichloromethane under nitrogen. A syringe was used to transfer the PCC solution dropwise to the stirring alcohol solution at room temperature. The reaction was left stirring for 12 h. Excess PCC was then quenched with isopropanol (approximately 20 mL) and the flask was concentrated, producing a wet, green solid. This solid was dissolved in ethyl acetate and transferred to a separatory funnel and extracted with deionized water (3 x 15 mL). The aqueous layer was then extracted with additional ethyl acetate to recover any lost aldehyde product (2 x 10 mL). The organic layers were dried with anhyd. Na₂SO₄, filtered, and concentrated to obtain a light brown solid. Following this general procedure, several distinct aldehydes were obtained using this two-step procedure. An average yield of 74% was obtained using this two-step procedure.



General Method (D) for Acyl Hydrazone Formation Through Aldehyde Condensation

A 1:1 molar ratio of salicylic hydrazide and 2-hydroxy-1-naphthaldehyde (5 mmol each) was dissolved in 30 mL of MeOH and heated to reflux. Several drops of glacial acetic acid were

added to catalyze the reaction and the flask was left under reflux for 3-4 h. The reaction mixture was filtered to collect the crude product (a yellow precipitate), and the compound was purified by silica gel column chromatography (Ethyl acetate/Hexanes 2:3, $R_f = 0.45$). Following this general procedure, several distinct acyl hydrazones were obtained. An average yield of 62% was obtained using this procedure.



General Method (E) for Indole Aldehyde Synthesis

Indole aldehydes were prepared by a Vilsmeier-Haack formylation reaction⁵. In a 50 mL, 3-necked round bottomed flask, 5 mL of DMF was placed under a nitrogen atmosphere and chilled on an ice bath for 30 min. A syringe was used to add 0.14 mL (1.5 mmol) of phosphorous oxychloride to the chilled DMF solution dropwise over 30 minutes. The reaction mixture turned light pink in color. In a glass vial, 0.12 g (1 mmol) of indole was dissolved in approximately 5 mL of DMF. This solution was then added dropwise to the reaction flask over 1 h. The reaction was heated at 35 °C until the mixture became bright yellow and pasty (approximately 1 h and 15 min). Crushed ice was then added to the mixture to produce a red aqueous solution. This solution was washed with 1.5 mmol of NaOH in ice, forming a suspension. The suspension was heated

⁵ Chatterjee, A., Biswas, K.M. Acylation of Indoles by Duff Reaction and Vilsmeier-Haack Formylation and Conformation of N-Formylindole. *J. Org. Chem.*, **1973**, 38, pp-4002.

rapidly to boiling, then cooled to room temperature and stored overnight at 4 °C. The crude product was collected by vacuum filtration and used without further purification.

Figures with docking poses for inhibitors at the C-site of hRRM1.

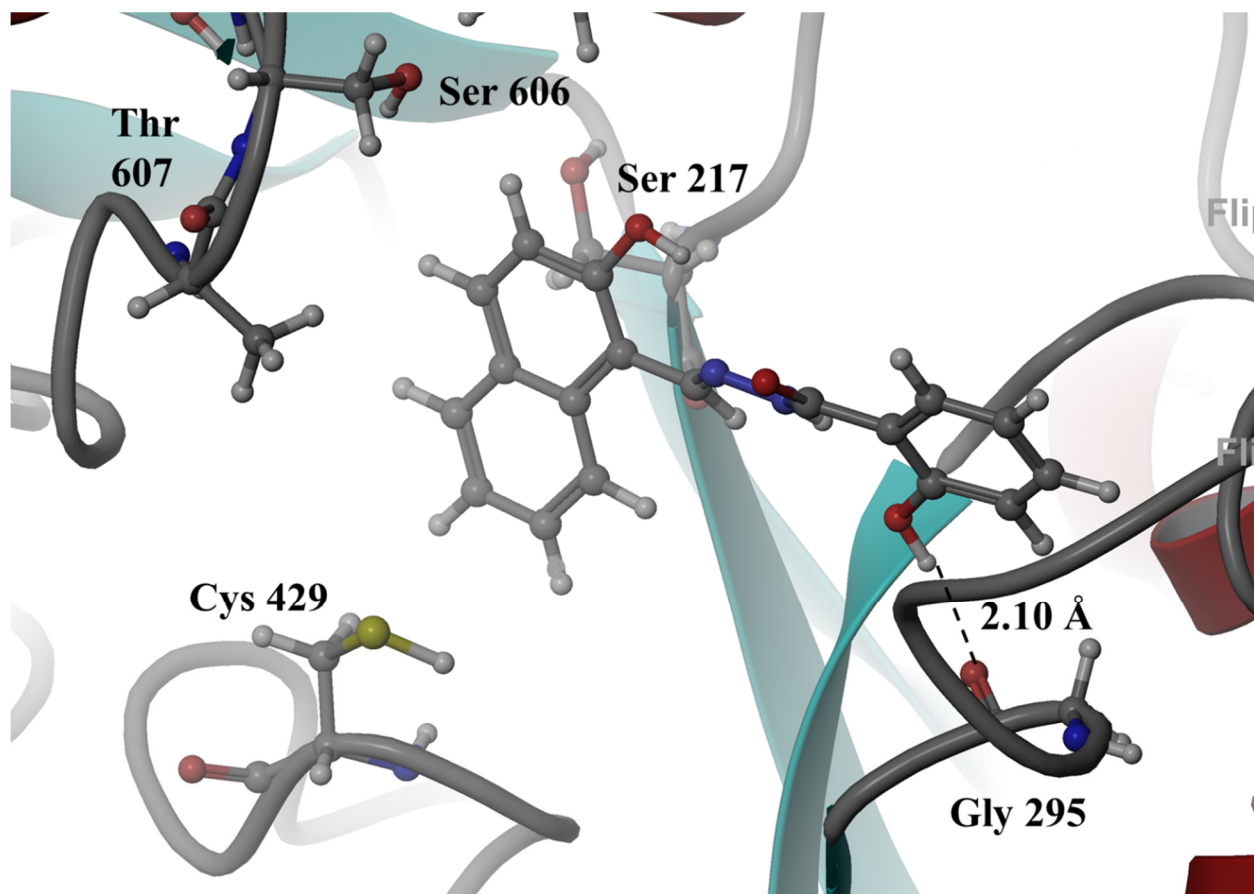


Figure S1. *E-3A* docked in the catalytic site of hRRM1. The majority of the protein-ligand interactions are predicted to be hydrophobic in nature. A hydrogen bond is observed between the C2' hydroxyl group of *E-3A* and the carbonyl group of the protein backbone in Gly 295. Further Van der Waals contacts are made with Thr 607, Ser 606, Ser 217, and Cys 429.

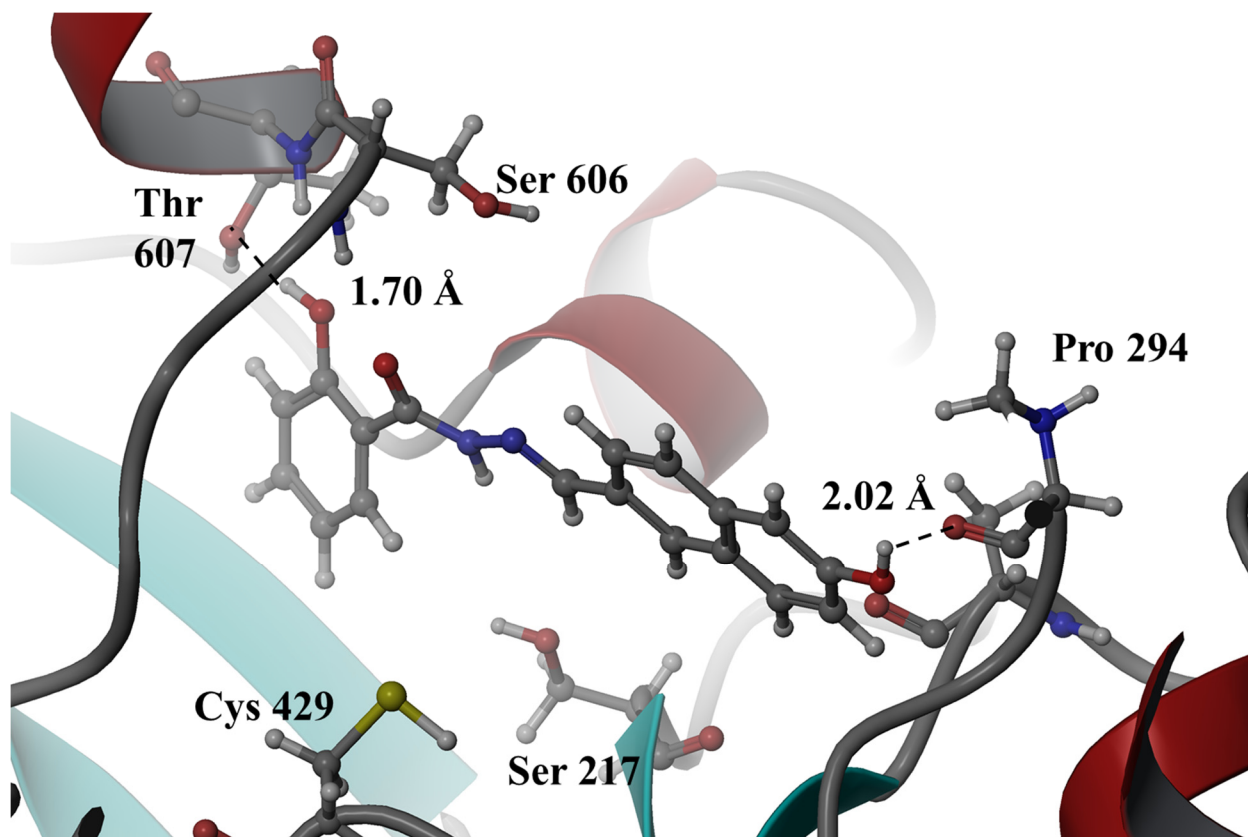


Figure S2. *E-3C* docked in the catalytic site of hRRM1. A hydrogen bond is observed between the 2' hydroxyl group of *E-3C* and the hydroxyl group of Thr 607. A second hydrogen bond is observed between the C6 hydroxyl group of *E-3C* and the carbonyl group of the protein backbone in Pro 294. Further Van der Waals contacts are made with Ser 606, Ser 217, and Cys 429.

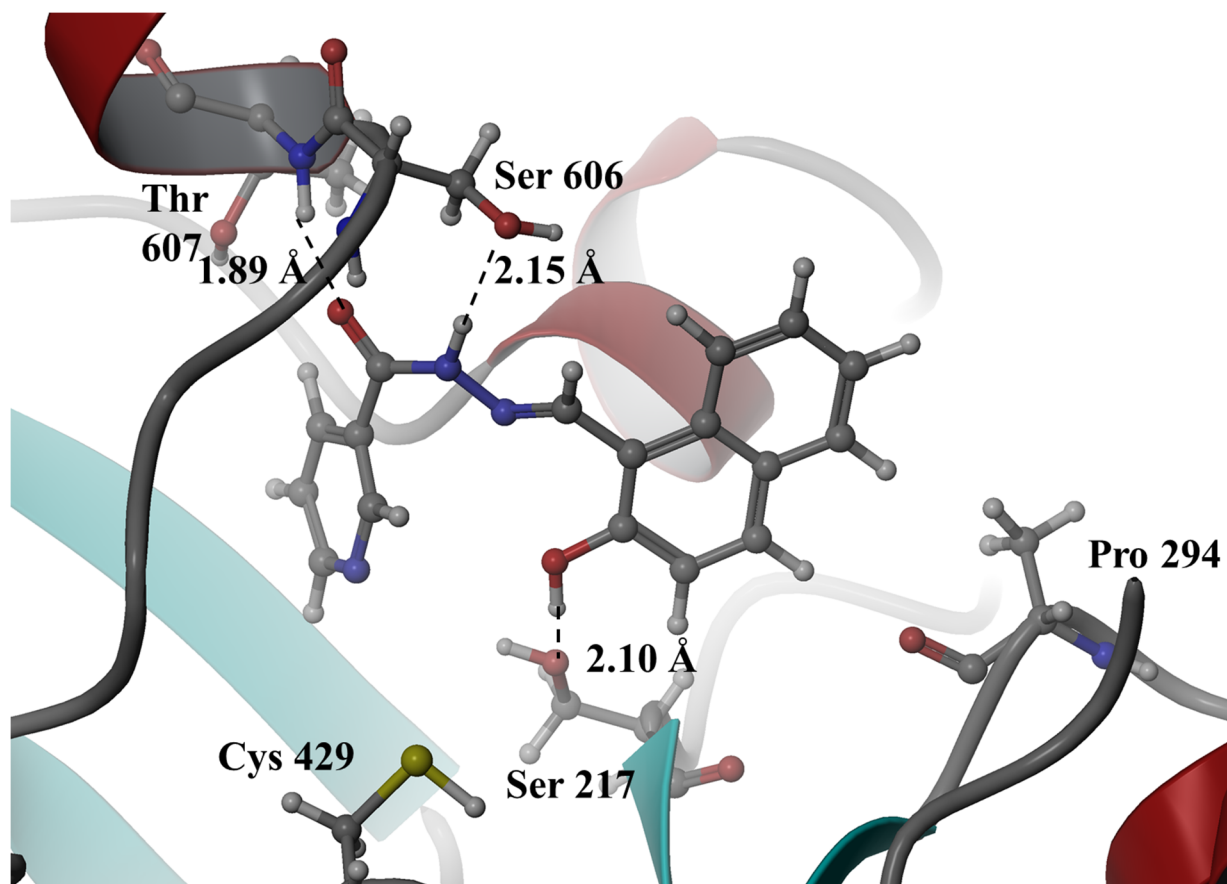


Figure S3. *E-3F* docked in the catalytic site of hRRM1. A hydrogen bond is observed between the hydrazone carbonyl group of *E-3F* and the amide group of the protein backbone in Thr 607. The hydroxyl group of Ser 606 is also observed to form hydrogen bond to the hydrazone backbone of *E-3F*. A third hydrogen bond is found between the hydroxyl group of Ser 217 and the hydroxyl group of C2. Further Van der Waals contacts are made with Pro 294 and Cys 429.

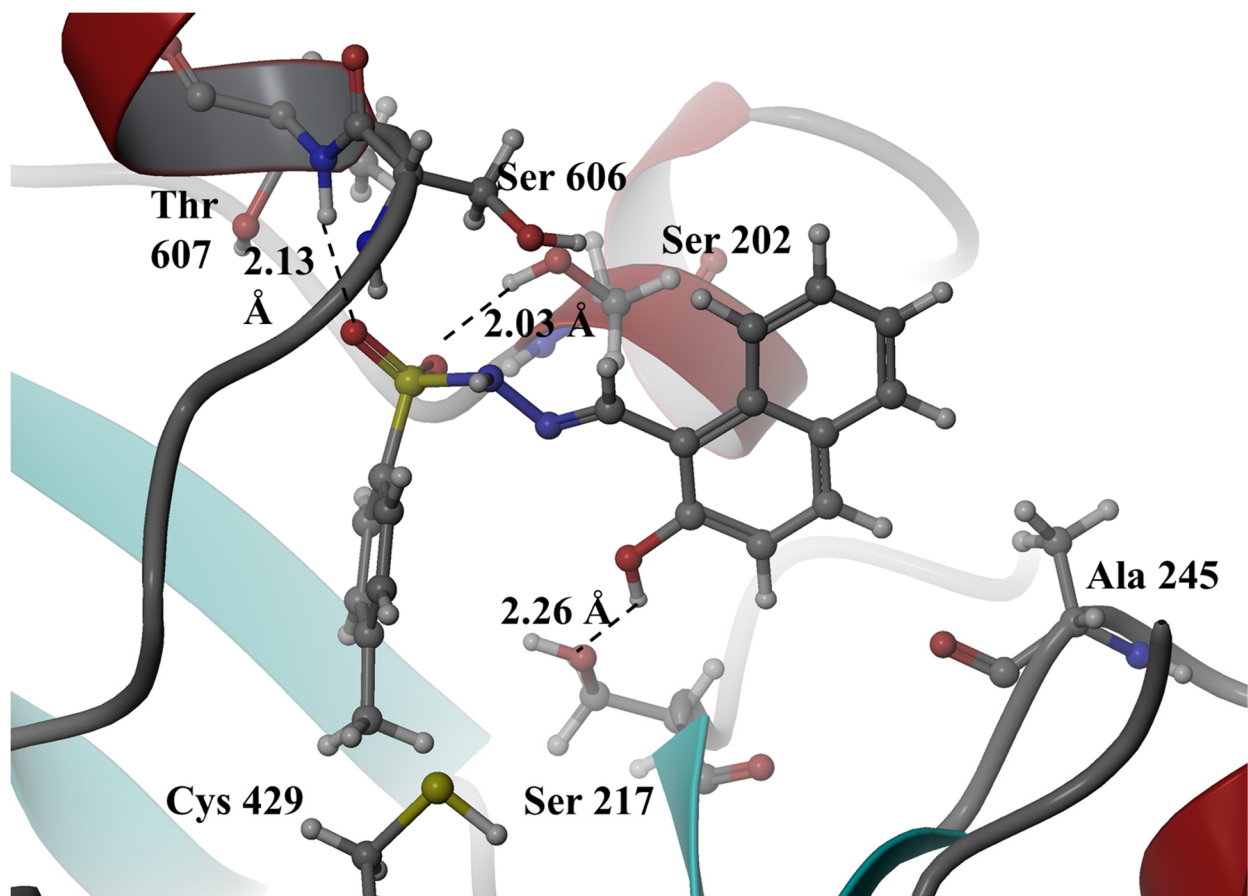


Figure S4. *E-3S* docked in the catalytic site of hRRM1. A hydrogen bond is observed between the C2 hydroxyl group of *E-3S* and the hydroxyl group of Ser 217. The sulfonyl oxygen atoms of *E-3S* both form hydrogen bonds with Thr 607 and Ser 202. Further Van der Waals contacts are made with Ser 606, Ala 245, and Cys 429.

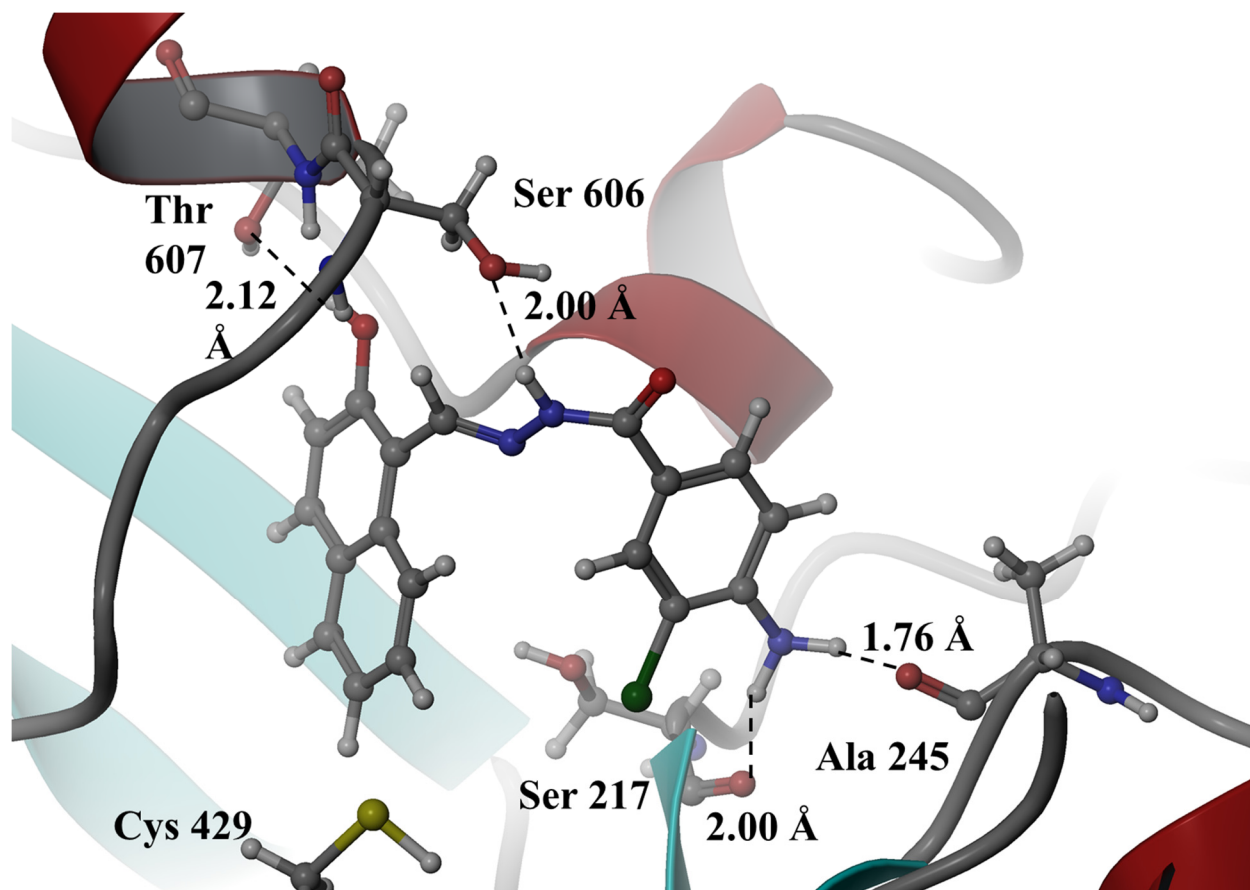


Figure S5. *E-3T* docked in the catalytic site of hRRM1. A hydrogen bond is observed between the C2 hydroxyl group of *E-3T* and the hydroxyl group of Thr 607. The hydrazone backbone of *E-3T* is observed to hydrogen bond with the hydroxyl group of Ser 606. The amino group on C4' of *E-3T* forms two hydrogen bonds with the protein backbones of Ala 245 and Ser 217. Further Van der Waals contacts are made with Cys 429.

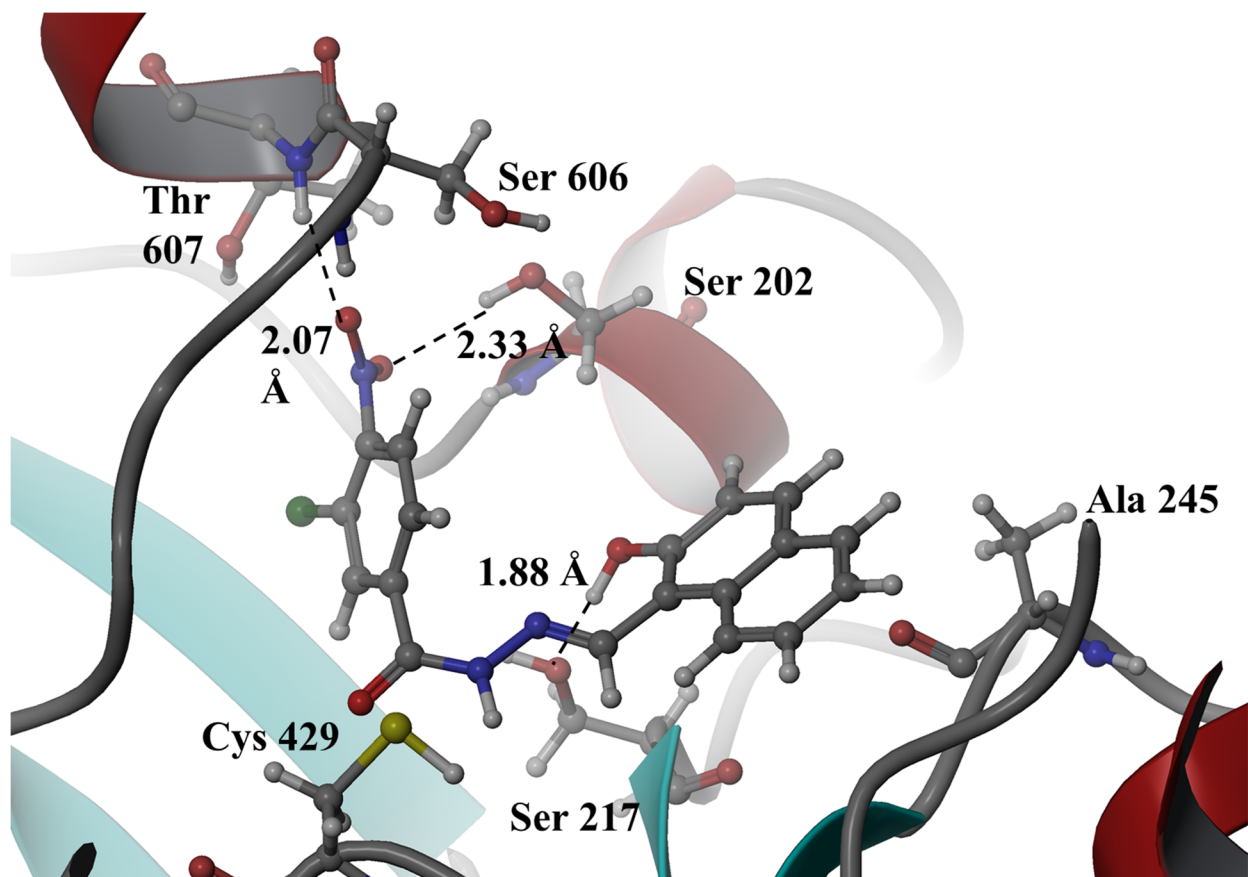


Figure S6. *E*-3U docked in the catalytic site of hRRM1. A hydrogen bond is observed between the C2 hydroxyl group of *E*-3U and the hydroxyl group of Ser 217. The nitro group of C4' of *E*-3U forms hydrogen bonds with both Thr 607 and Ser 202. Further Van der Waals contacts are made with Ala 245, Ser 606, and Cys 429.

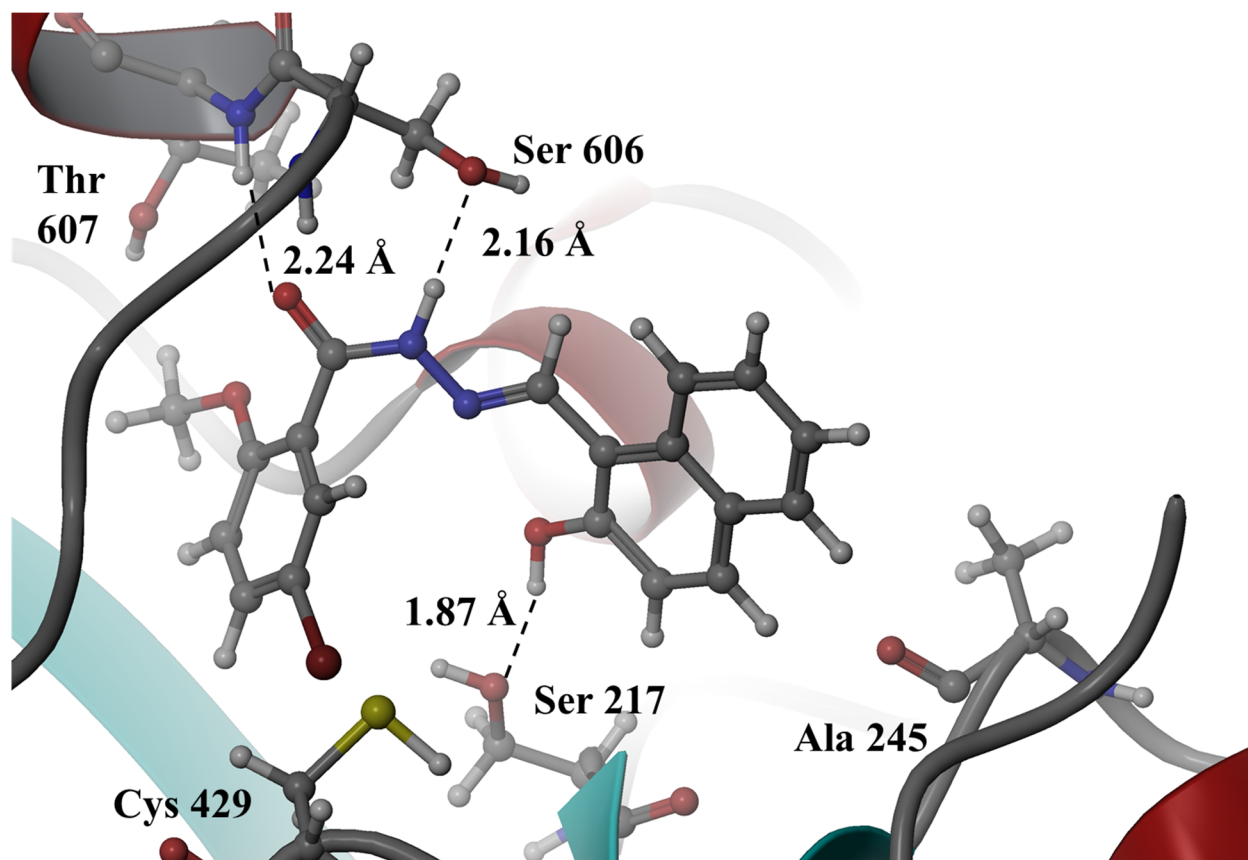


Figure S7. *E-3V* docked in the catalytic site of hRRM1. A hydrogen bond is observed between the C2 hydroxyl group of *E-3V* and the hydroxyl group of Ser 217. The hydrazone backbone is observed to hydrogen bond both Thr 607 and Ser 606. Further Van der Waals contacts are made with Ala 245 and Cys 429.

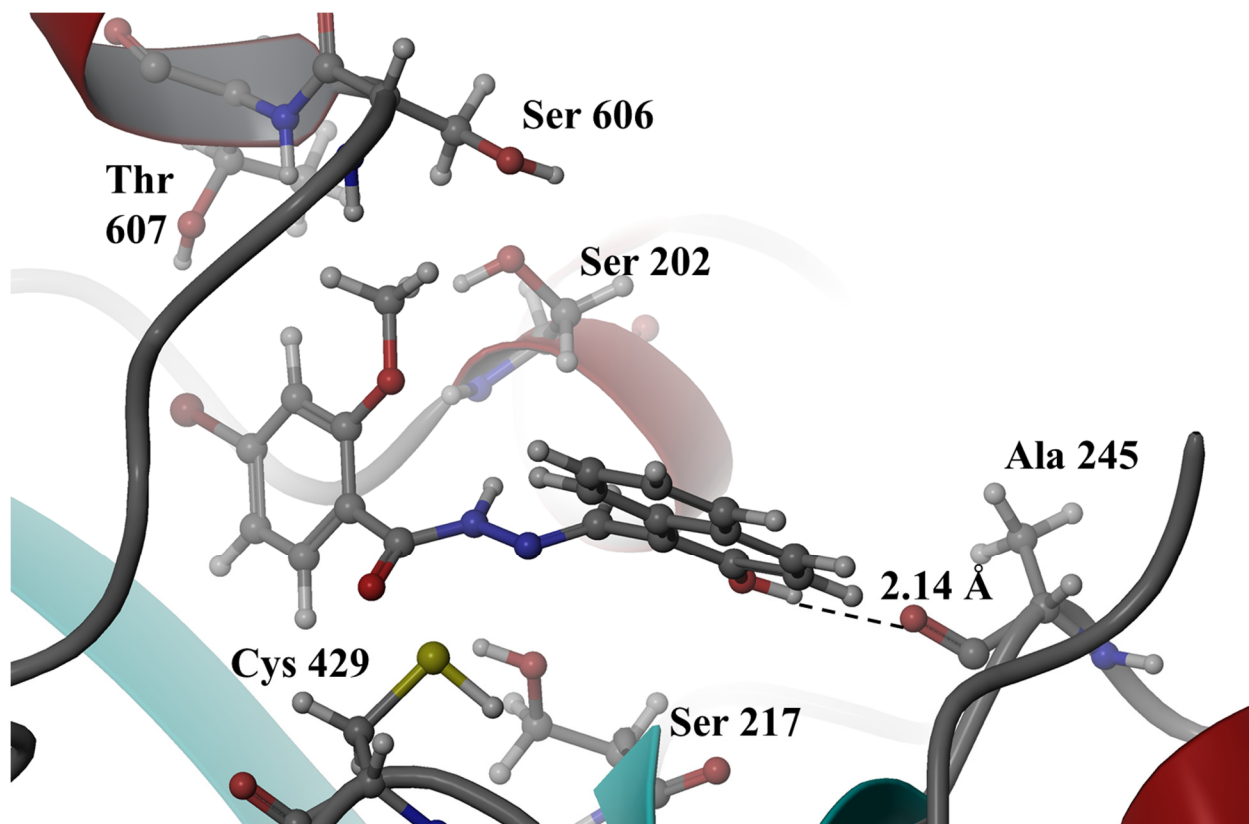


Figure S8. *E-3W* docked in the catalytic site of hRRM1. The binding interactions are predicted to be mostly hydrophobic interactions. A hydrogen bond is observed between the C2 hydroxyl group of *E-3W* and the carbonyl group of the protein backbone in Ala 245. Further Van der Waals contacts are made with Thr 607, Ser 606, Ser 202, Ser 217, and Cys 429.

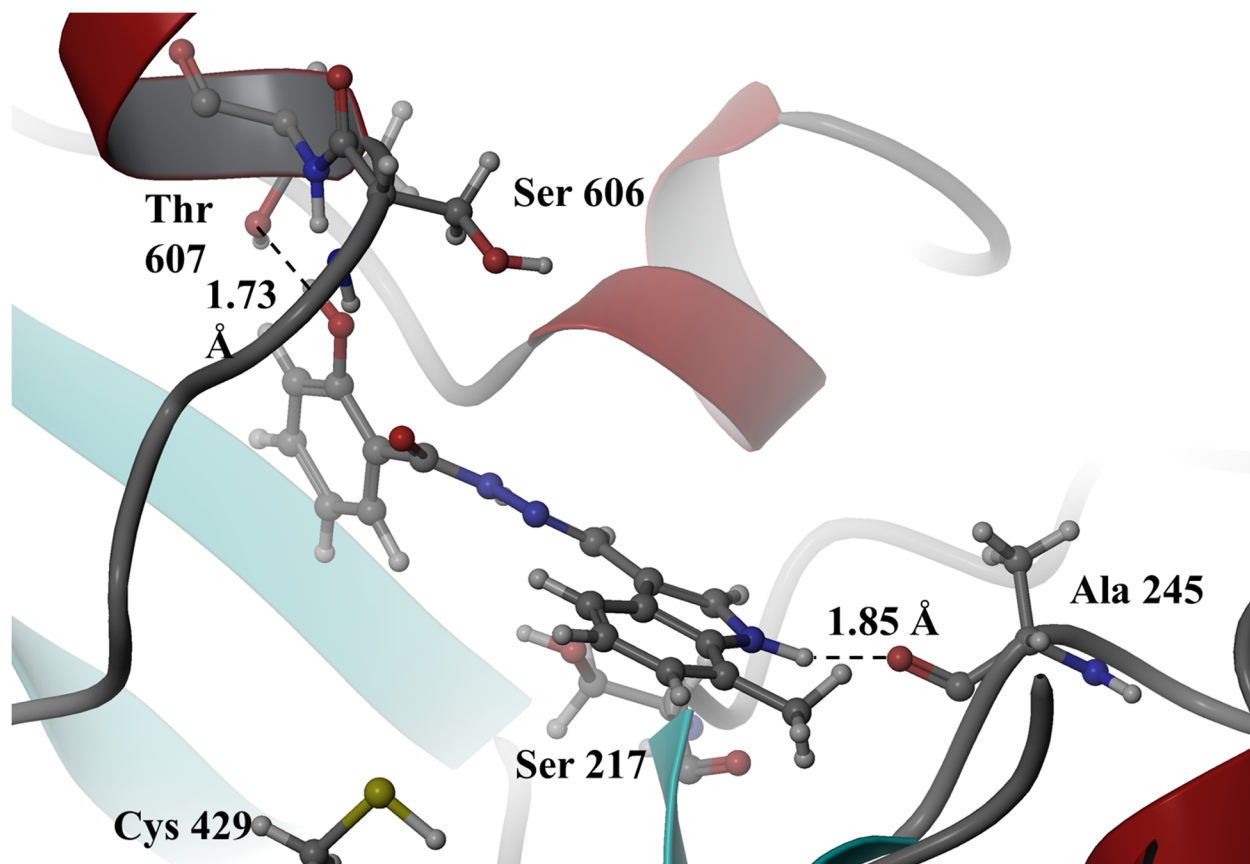


Figure S9. *E-3Z* docked in the catalytic site of hRRM1. A hydrogen bond is observed between the 2' hydroxyl group of *E-3Z* and the hydroxyl group of Thr 607. A second hydrogen bond is observed between the indole NH moiety and the protein backbone of Ala 245. Further Van der Waals contacts are made with Ser 606, Ser 217, and Cys 429.

Table S4. Enzymatic inhibition data for *E-3A*, *E-3C*, *E-3T*, and *E-3W* in the presence of ³H-CDP substrate. IC₅₀ values are comparable to those obtained using ¹⁴C-ADP substrate.

Compound	wt R1	Average specific activity (nmol min ⁻¹ mg ⁻¹)					Estimated IC ₅₀ (μM)
		5 μM	10 μM	25 μM	50 μM	100 μM	
3A	450.1	404.1	341.3	172.4	84.9	35.2	24.1
3C	411.9	285.6	209.6	124.5	86.2	55.3	7.1
3T	481.3	305.2	244.9	144.3	100.7	64.6	6.4
3W	465.2	321.5	250.8	162.4	80.9	29.9	17.1

Anaerobic Metal Chelation Assay with Fe²⁺ and Fe³⁺

In separate round bottom flasks, a solution of 10mM ammonium acetate buffer (pH 7.0), 50 mM of *E-3A* in DMSO were flash-frozen in liquid nitrogen, then degassed under vacuum. The degassed solutions were stored under Argon atmosphere. Once thawed, the solutions were transferred to a glovebox, where the following buffer mixtures were prepared under nitrogen: 100 μM *E-3A*; 100 μM *E-3A*: 100 μM FeCl₂·6H₂O; 100 μM *E-3A*: 200 μM FeCl₂·6H₂O; 100 μM *E-3A*: 300 μM FeCl₂·6H₂O; 100 μM *E-3A*: 400 μM FeCl₂·6H₂O; 100 μM *E-3A*: 500 μM FeCl₂·6H₂O; 100 μM *E-3A*: 600 μM FeCl₂·6H₂O; 100 μM *E-3A*: 700 μM FeCl₂·6H₂O; 100 μM *E-3A*: 800 μM FeCl₂·6H₂O; 100 μM *E-3A*: 900 μM FeCl₂·6H₂O; 100 μM *E-3A*: 1,000 μM FeCl₂·6H₂O; 100 μM *E-3A*: 2,000 μM FeCl₂·6H₂O; 100 μM *E-3A*: 5,000 μM FeCl₂·6H₂O. The samples were transferred to sealed cuvettes under nitrogen atmosphere and the UV profile was recorded over 200-800 nm, with a 1 nm slit width. The same procedure was repeated with

FeCl₃·6H₂O. Results for binding to Fe²⁺ and Fe³⁺ ions are depicted in **Figures S10** and **S11** respectively.

Metal Chelation Assay with Mg²⁺

In 10 mM ammonium acetate buffer (pH 7.0), 100 μM of *E-3A* was titrated with either MgCl₂·6H₂O at concentrations of Mg²⁺ ranging from 100 μM to 1 mM. The ratios of *E-3A*: M²⁺ tested were 1:1, 1:2, 1:3, 1:4, 1:5, 1:6, 1:7, 1:8, 1:9, and 1:10. The UV emission spectrum was recorded over 200-800 nm at each concentration. The slit width was held constant at 1 nm. As a control, the same procedure was repeated with 100 μM phenanthroline. Results for binding to Mg²⁺ ions are depicted in **Figure S12**.

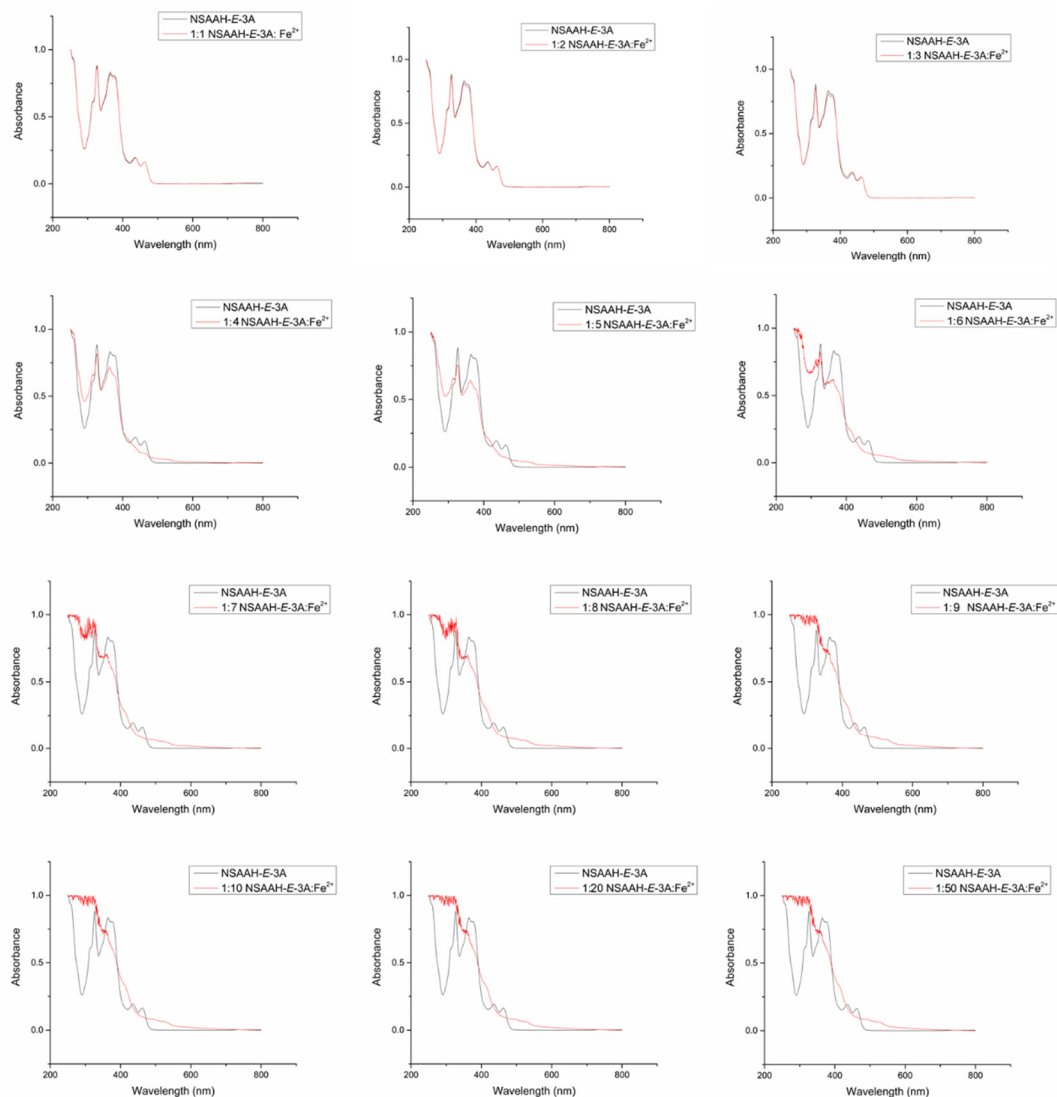


Figure S10. Chelation study for *E-3A* with Fe(II) ion. Under anaerobic conditions, solutions of 100 μM of *E-3A* in 10mM ammonium acetate buffer (pH 7.0) were prepared with $\text{FeCl}_2 \cdot 6\text{H}_2\text{O}$ at concentrations of metal ranging from 100 μM to 5 mM (ratios of *E-3A*: M^{2+} of 1:1, 1:2, 1:3, 1:4, 1:5, 1:6, 1:7, 1:8, 1:9, 1:10, 1:20, and 1:50). The emission spectrum was recorded over 200-800 nm in sealed cuvettes and is presented as a normalized absorbance (0-100%). Changes in absorbance are observed at concentrations of 400 μM Fe^{2+} (greater than a four-fold excess of Fe^{2+}) and higher, indicating that in the presence of an excess of Fe^{2+} , *E-3A* can chelate metals.

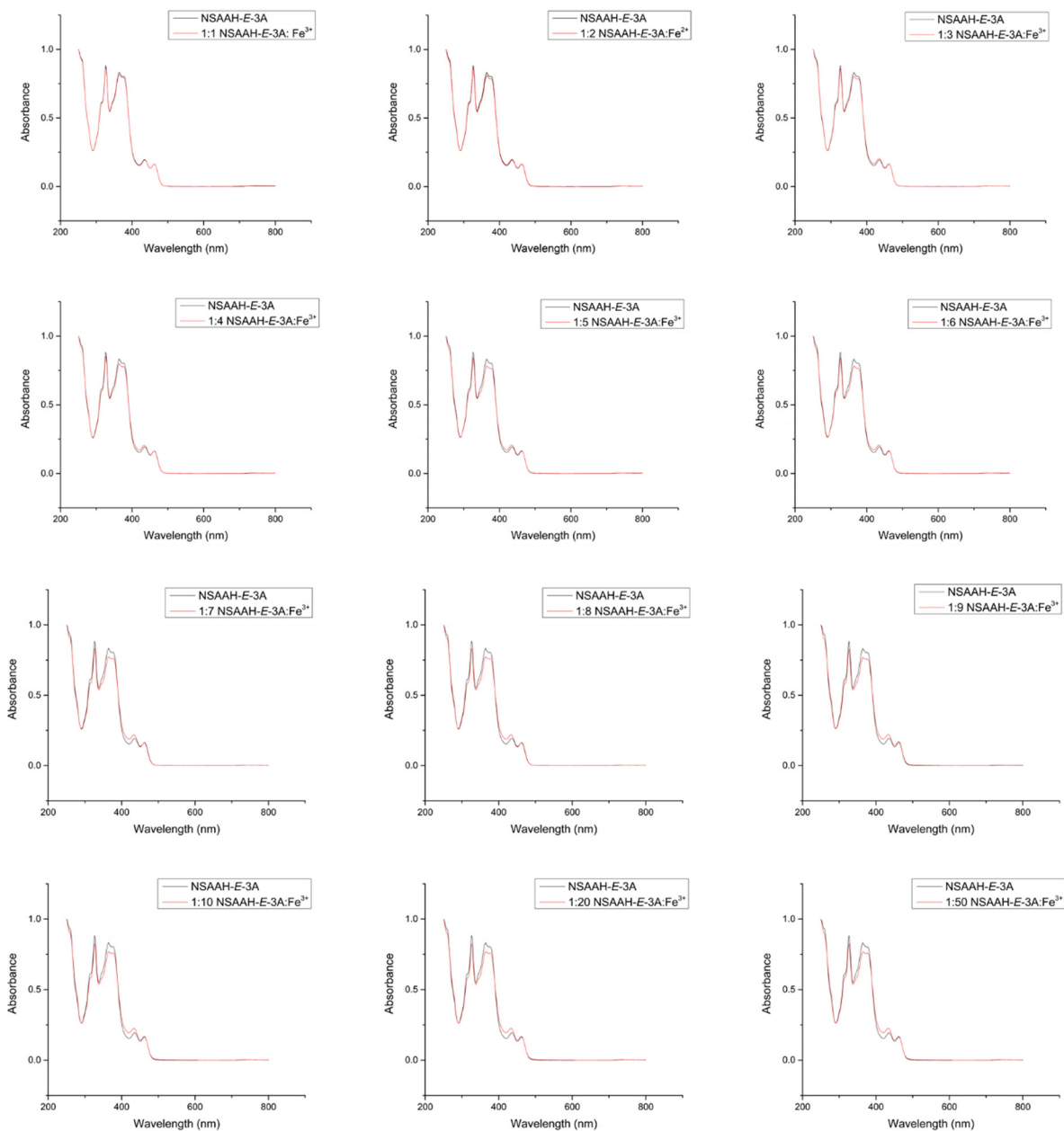


Figure S11. Chelation study for *E-3A* with Fe(III) ion. Under anaerobic conditions, solutions of 100 μM of *E-3A* in 10mM ammonium acetate buffer (pH 7.0) were prepared with $\text{FeCl}_3 \cdot 6\text{H}_2\text{O}$ at concentrations of metal ranging from 100 μM to 5 mM (ratios of *E-3A*: M^{2+} of 1:1, 1:2, 1:3, 1:4, 1:5, 1:6, 1:7, 1:8, 1:9, 1:10, 1:20, and 1:50). The emission spectrum was recorded over 200-800 nm in sealed cuvettes and is presented as a normalized absorbance (0-100%). No significant chelation was observed.

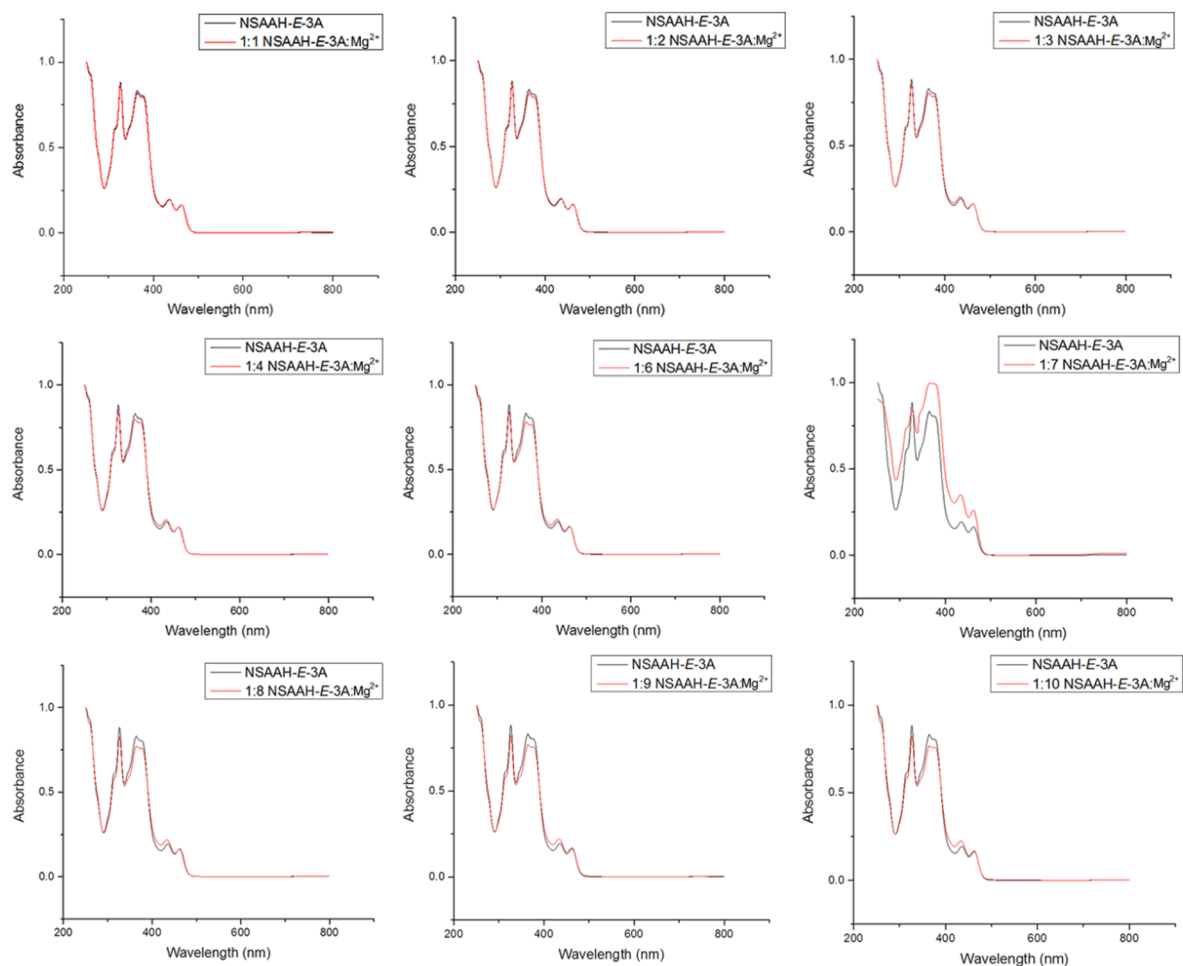


Figure S12. Chelation study for *E-3A* with Mg(II) ion. No significant change in absorbance is observed in the presence of Mg²⁺ at any concentration tested.

Enzyme kinetics sigmoidal dose response curves

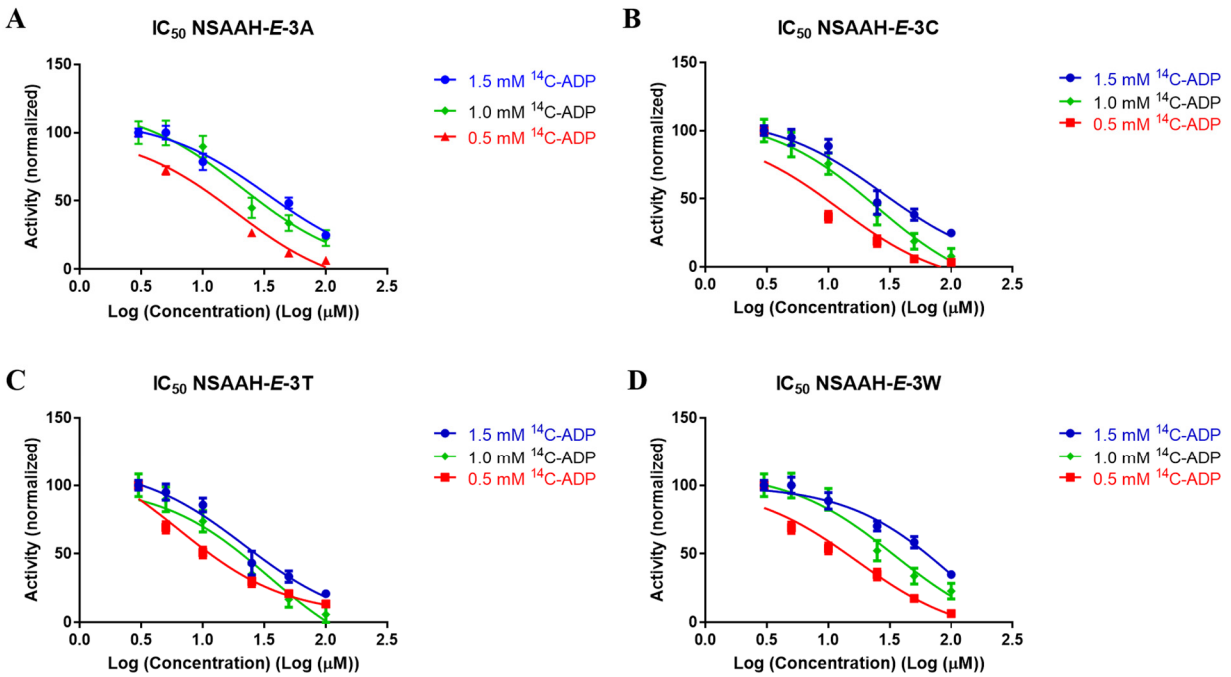


Figure S13. A. Sigmoidal dose-response curve for *E-3A*. As the ¹⁴C-ADP substrate concentration increased from 1.0 mM to 1.5 mM, the IC₅₀ was also observed to increase from 32.6 to 44.3 μM. At 0.5 mM ¹⁴C-ADP, the IC₅₀ was observed to decrease to 10.5 μM. B. Sigmoidal dose-response curve for *E-3C*. IC₅₀ values were determined as 7.5, 20.3, 34.6 μM at 0.5, 1.0, and 1.5 mM ¹⁴C-ADP, respectively. C. Sigmoidal dose-response curves for *E-3T*. IC₅₀ values were determined as 13.1, 18.9, and 29.7 μM at 0.5, 1.0, and 1.5 mM ¹⁴C-ADP, respectively. D. Sigmoidal dose-response curves for *E-3W*. IC₅₀ values were determined as 13.4, 35.2, and 64.7 μM at 0.5, 1.0, and 1.5 mM ¹⁴C-ADP, respectively.

siRNA knockdown controls and DNA/Well measurements

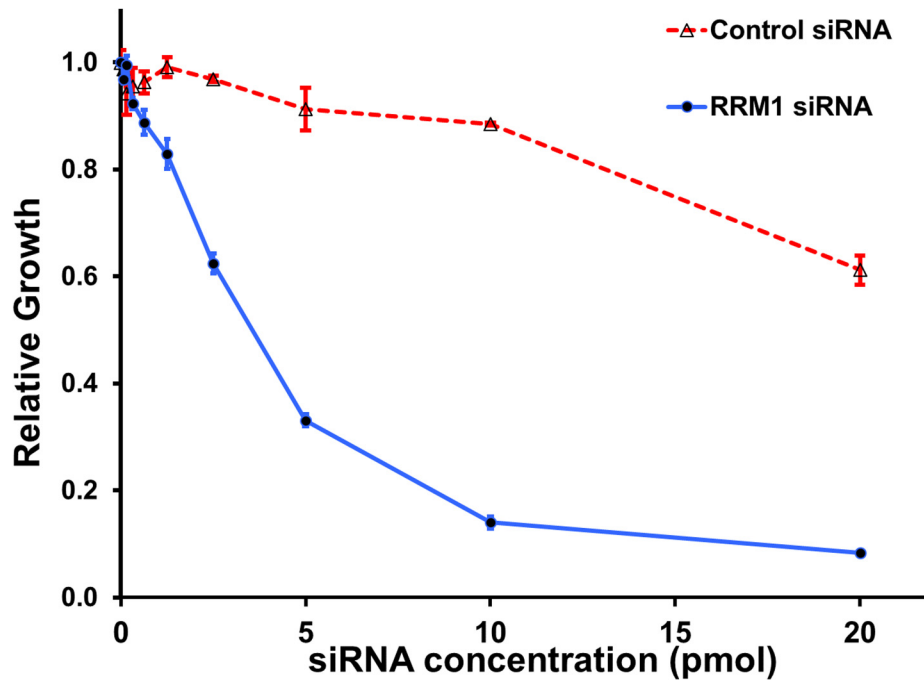


Figure S14. siRNA-mediated knockdown RRM1 leading to growth inhibition of MDA-MB-231 breast cancer cells. Control scrambled siRNA causes only marginal inhibition at the highest levels. Average of triplicates with standard error of the means (SEM) is shown.

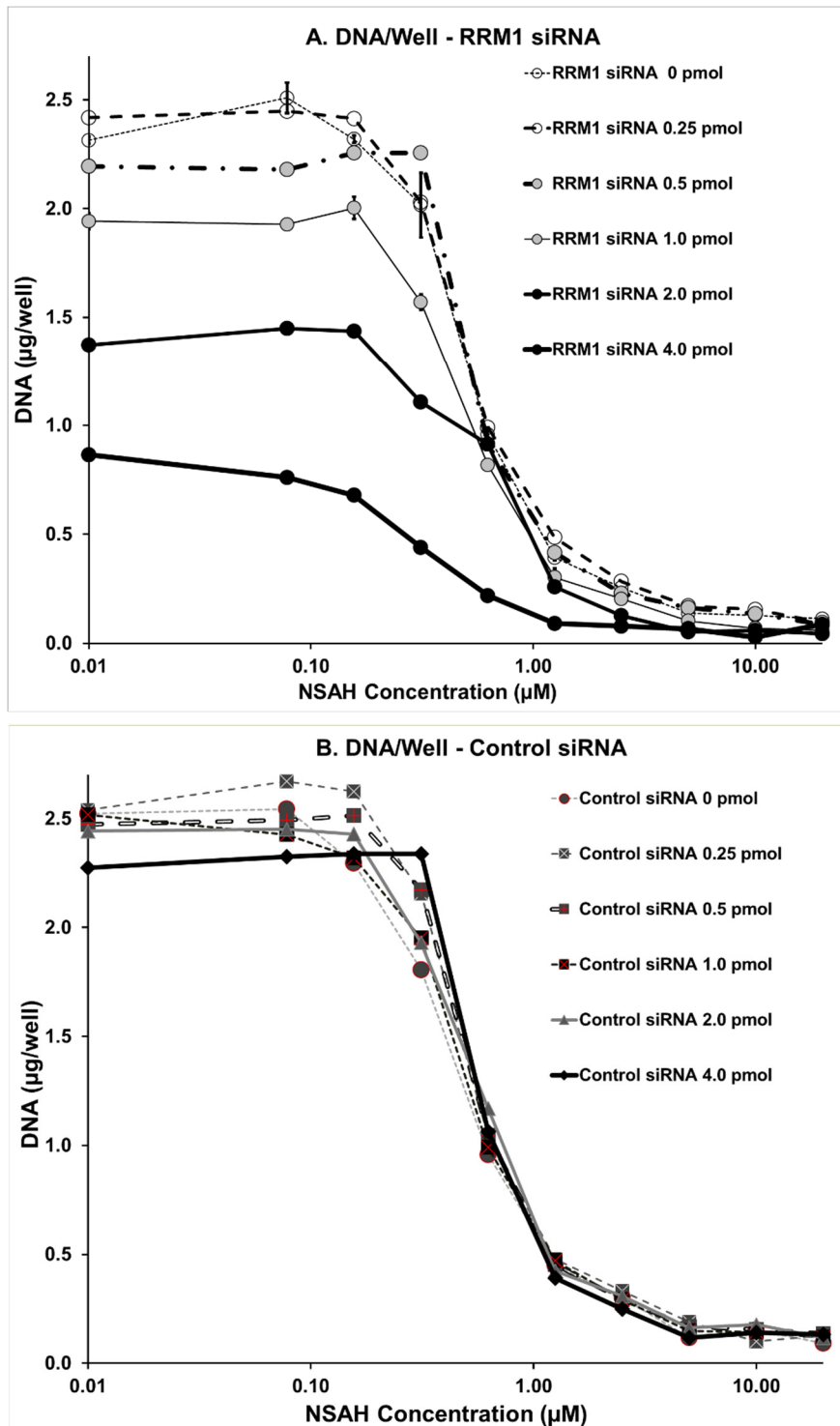
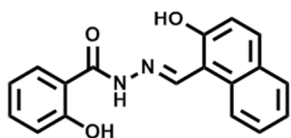


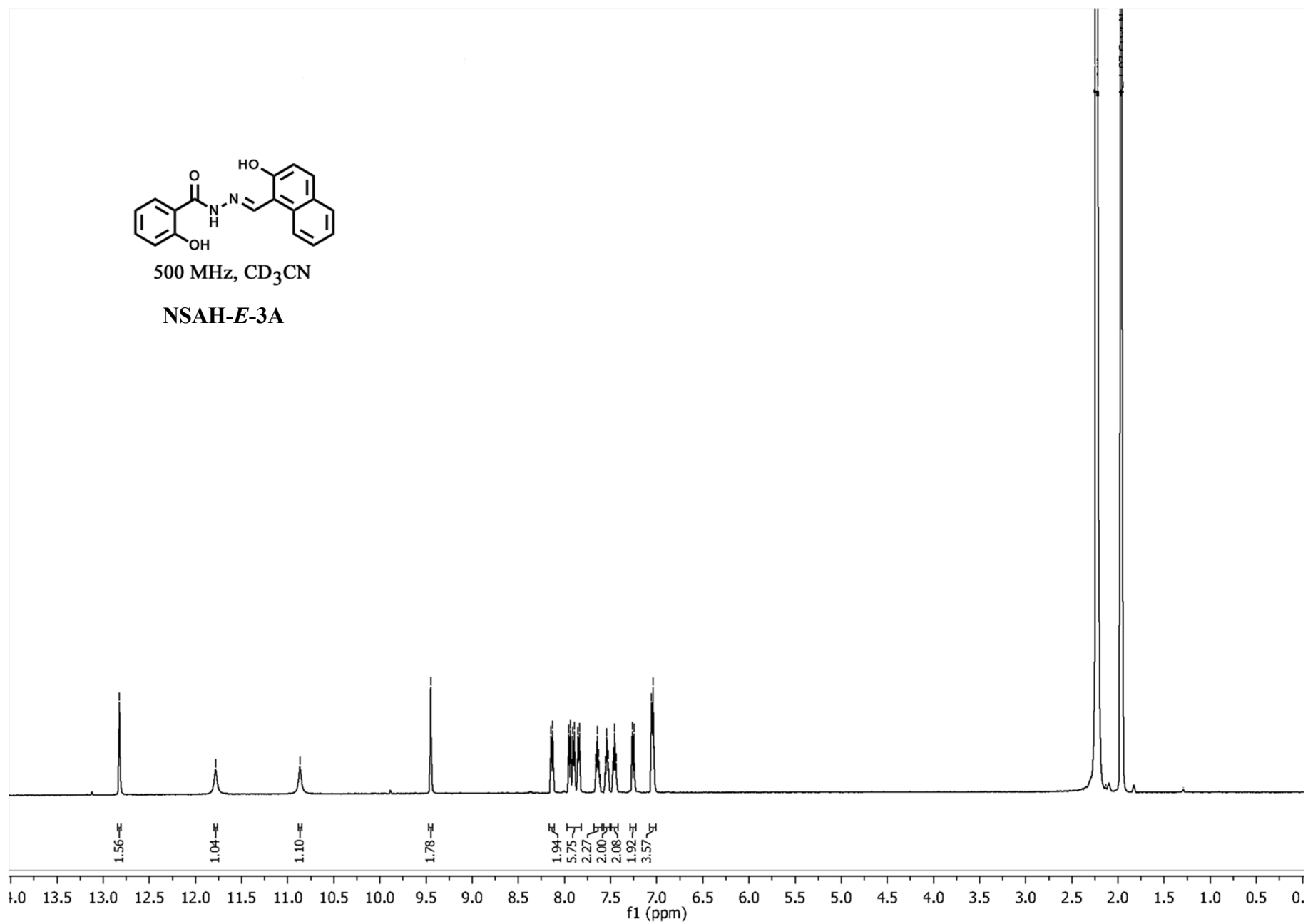
Figure S15. DNA per well determined after transfection and growth for 5 days with NSAH. **A)** after RRM1 siRNA transfection and **B)** after Control scrambled siRNA transfection. Note the lack of growth inhibition by Control scrambled siRNA transfection alone (0 µM NSAH), in contrast to the dose dependent growth inhibition after transfection with RRM1 siRNA alone (0 µM NSAH).

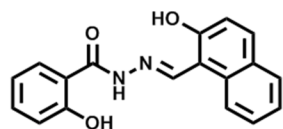
Copies of NMR and HPLC Data



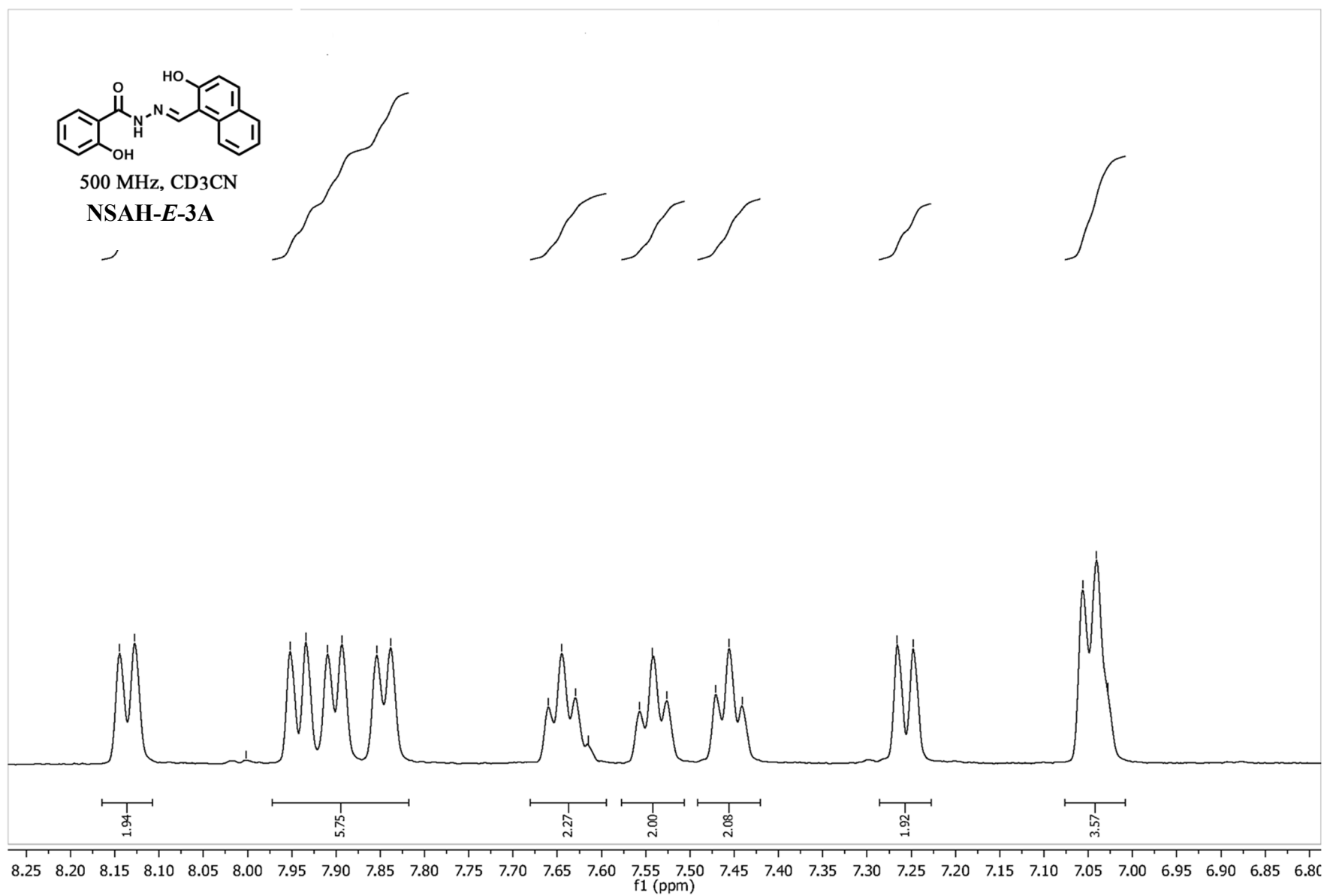
500 MHz, CD₃CN

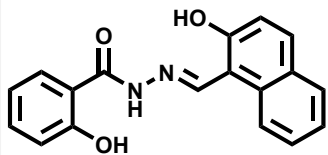
NSAH-E-3A





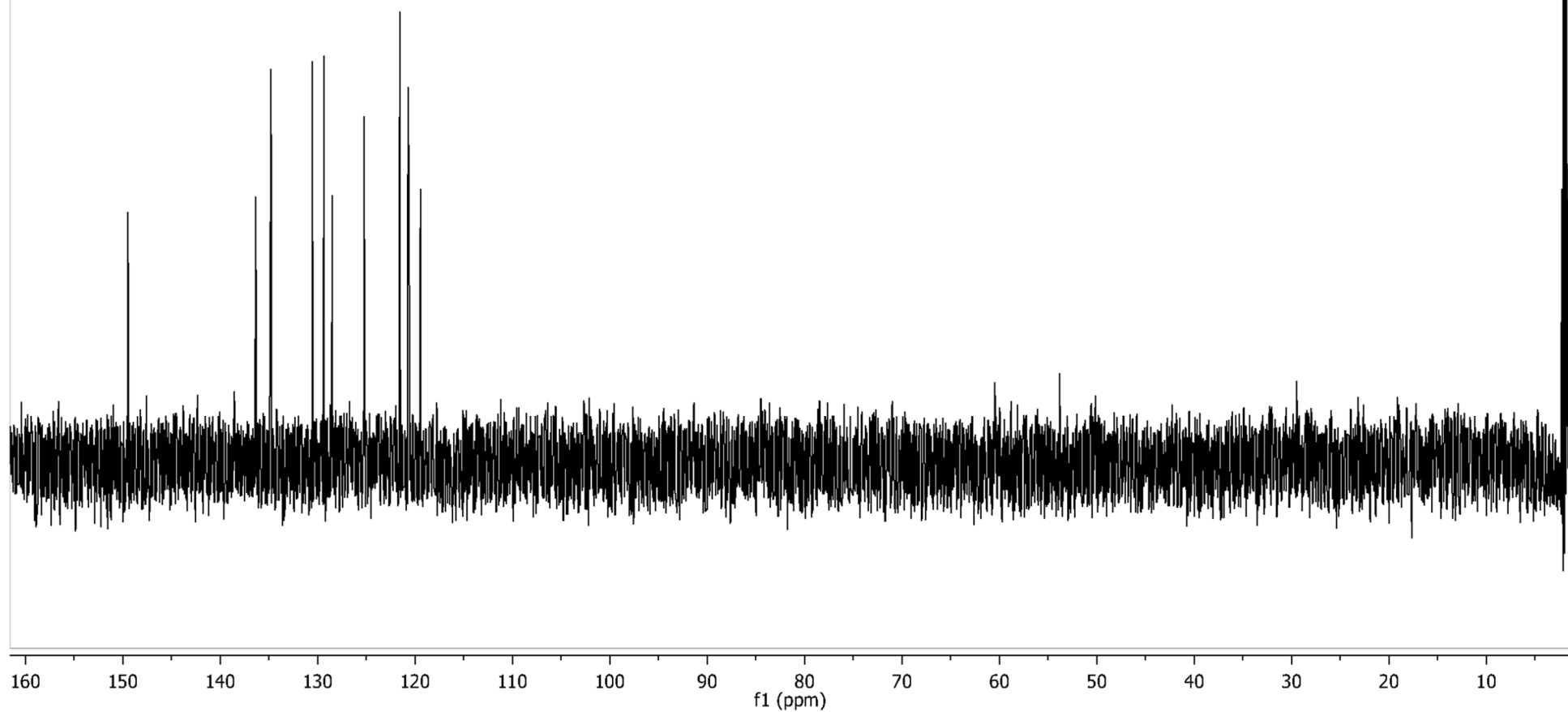
500 MHz, CD₃CN
NSAH-E-3A

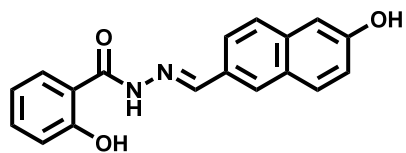




125 MHz, CD₃CN

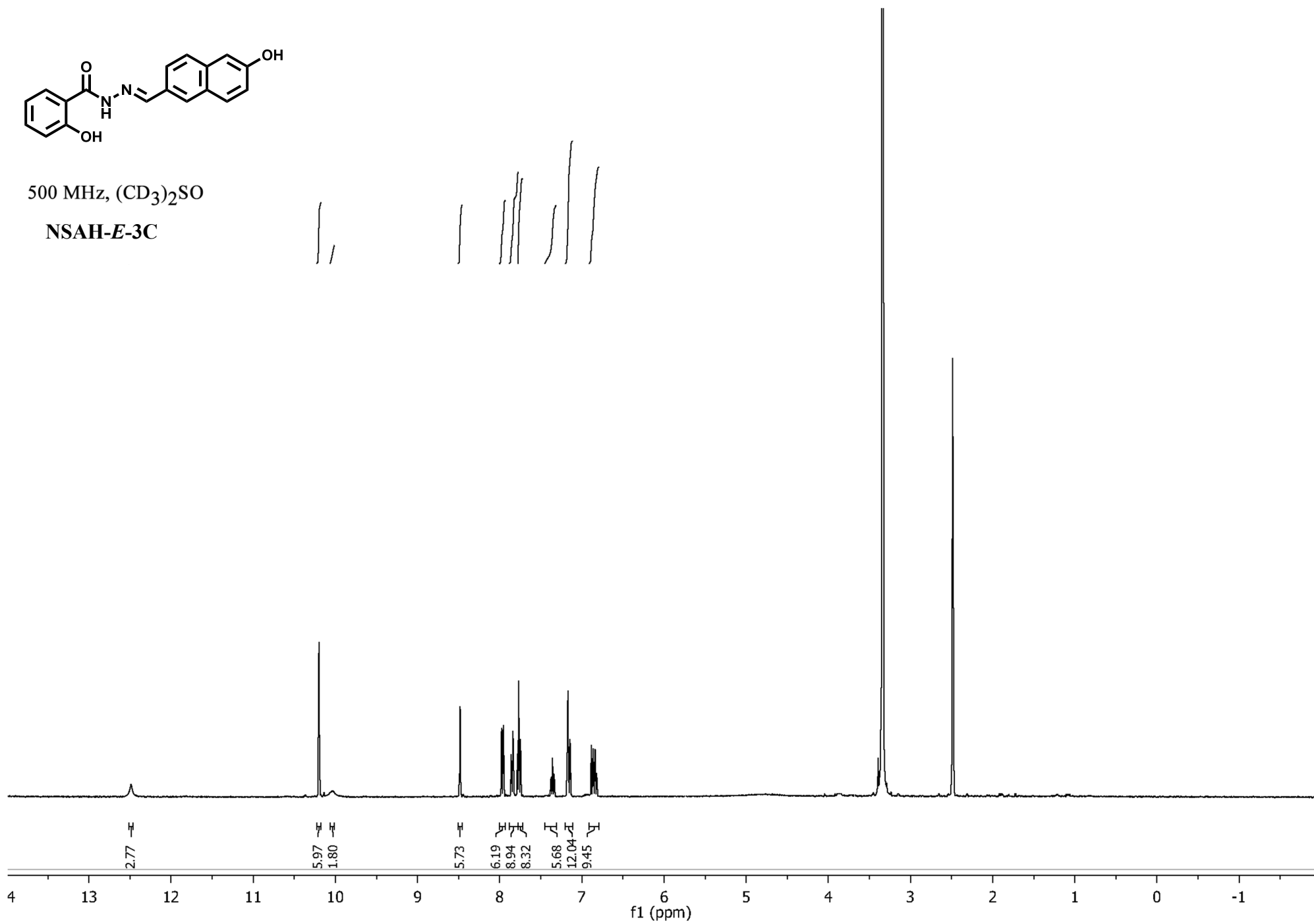
NSAH-E-3A

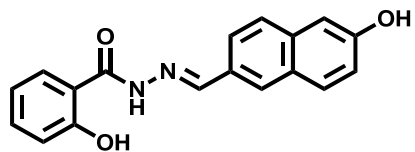




500 MHz, (CD₃)₂SO

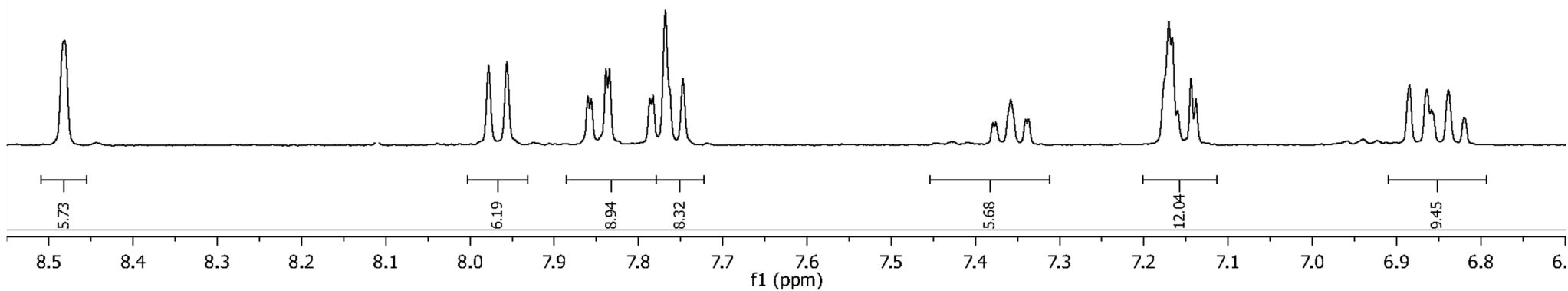
NSAH-*E*-3C

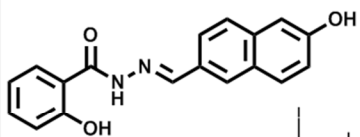




500 MHz, (CD₃)₂SO

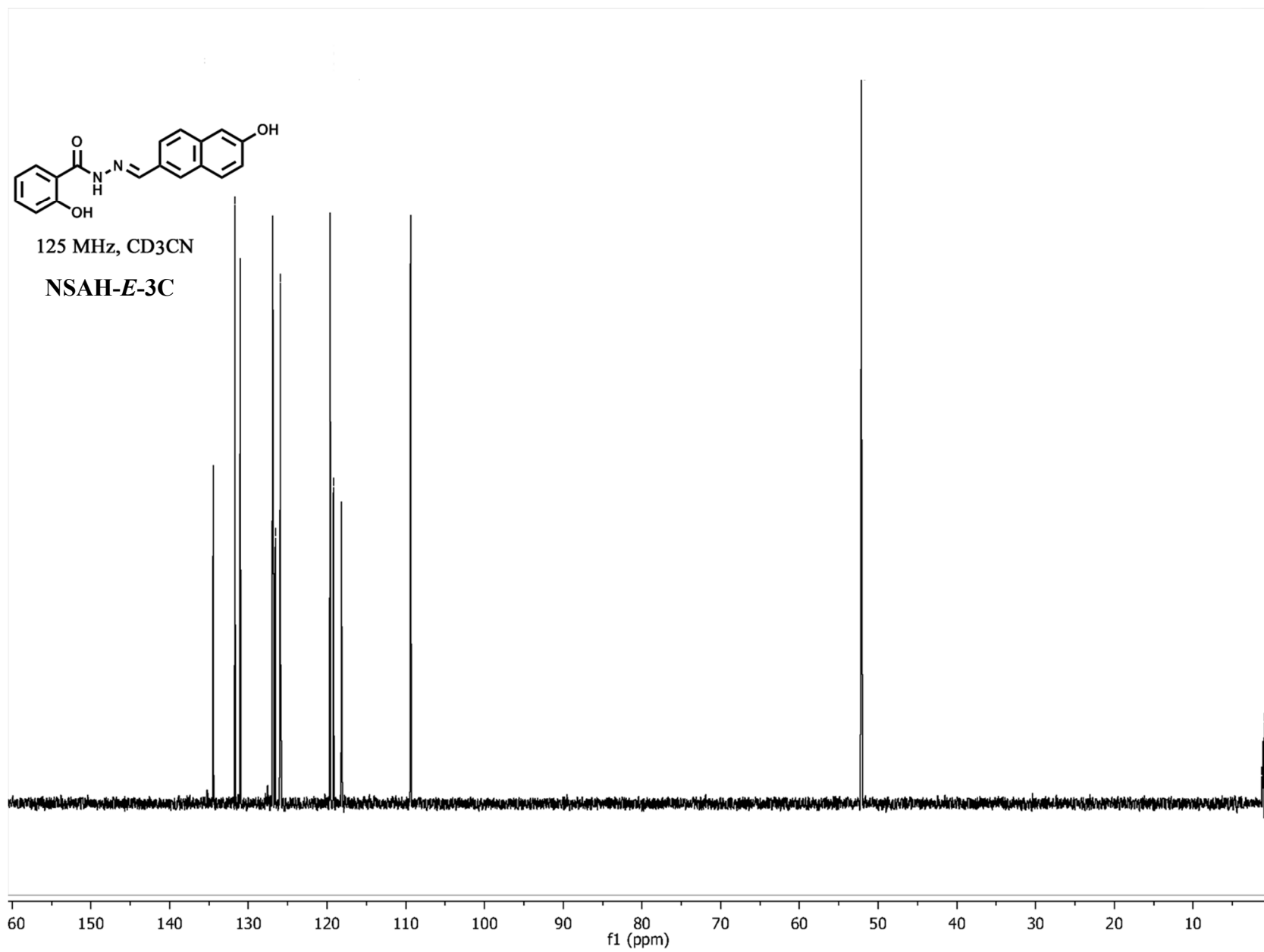
NSAH-E-3C

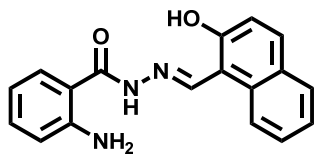




125 MHz, CD₃CN

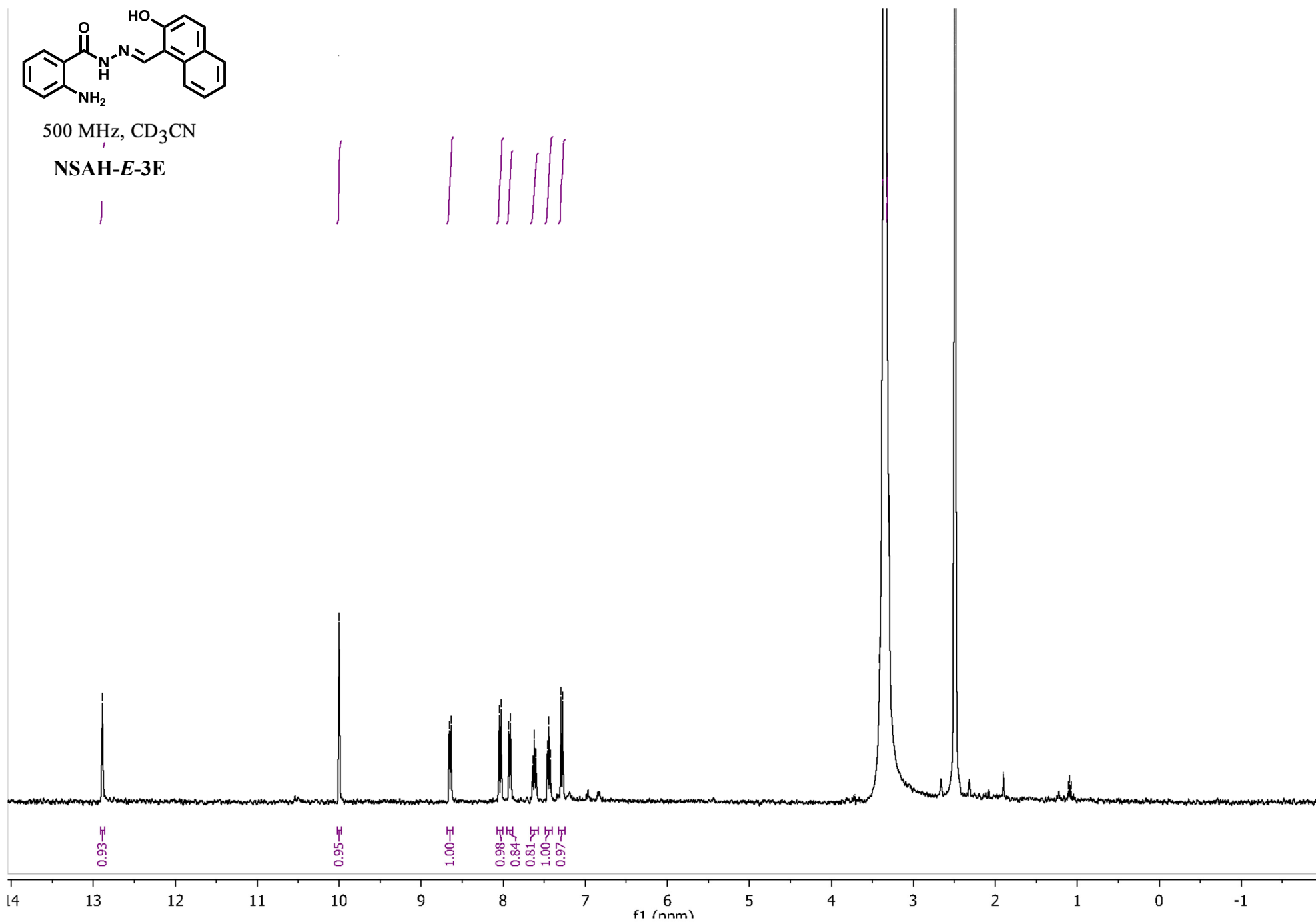
NSAH-*E*-3C

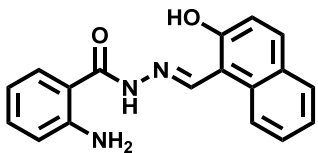




500 MHz, CD₃CN

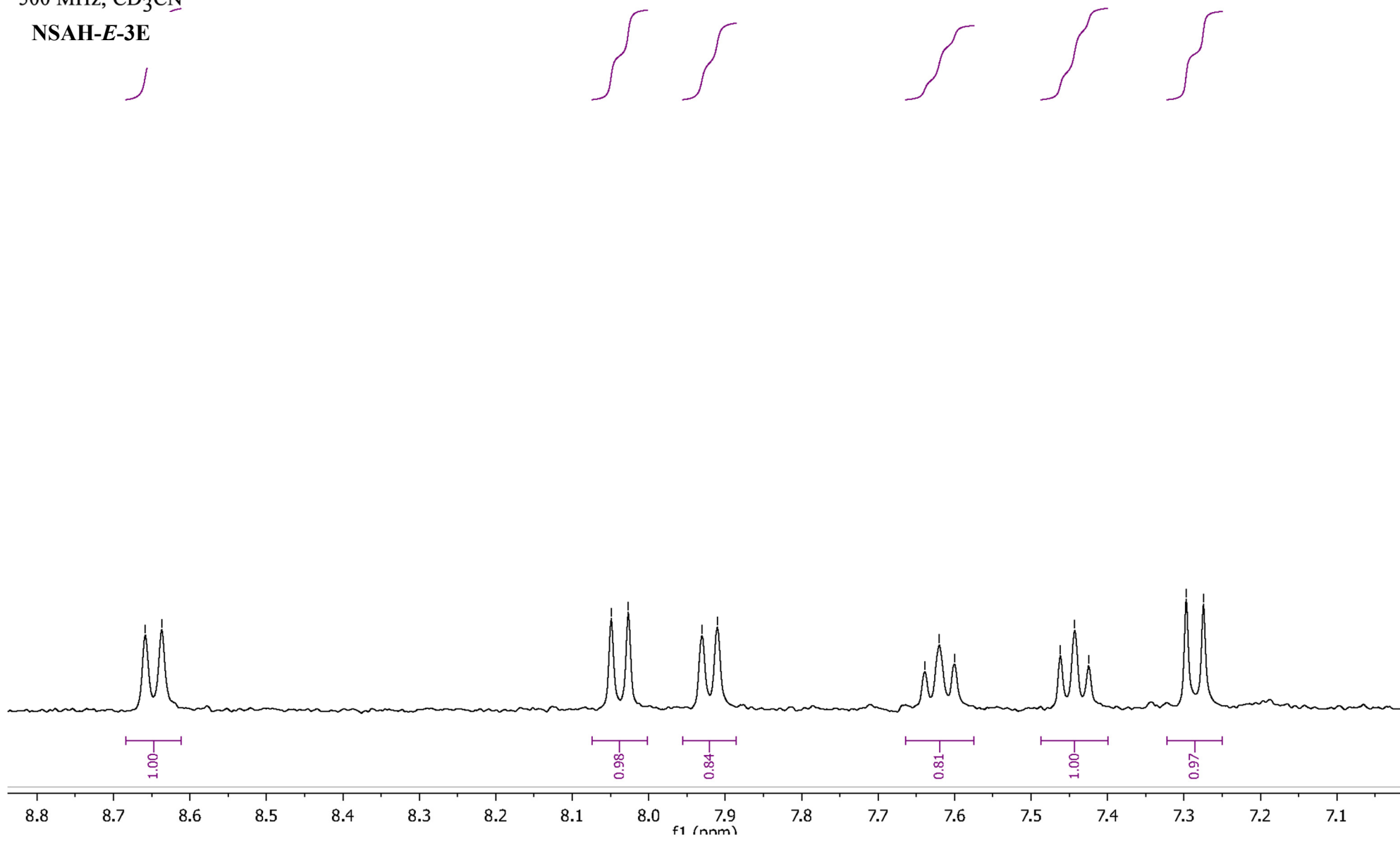
NSAH-*E*-3E

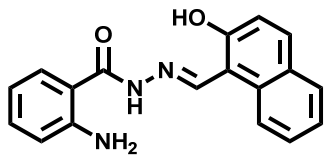




500 MHz, CD₃CN

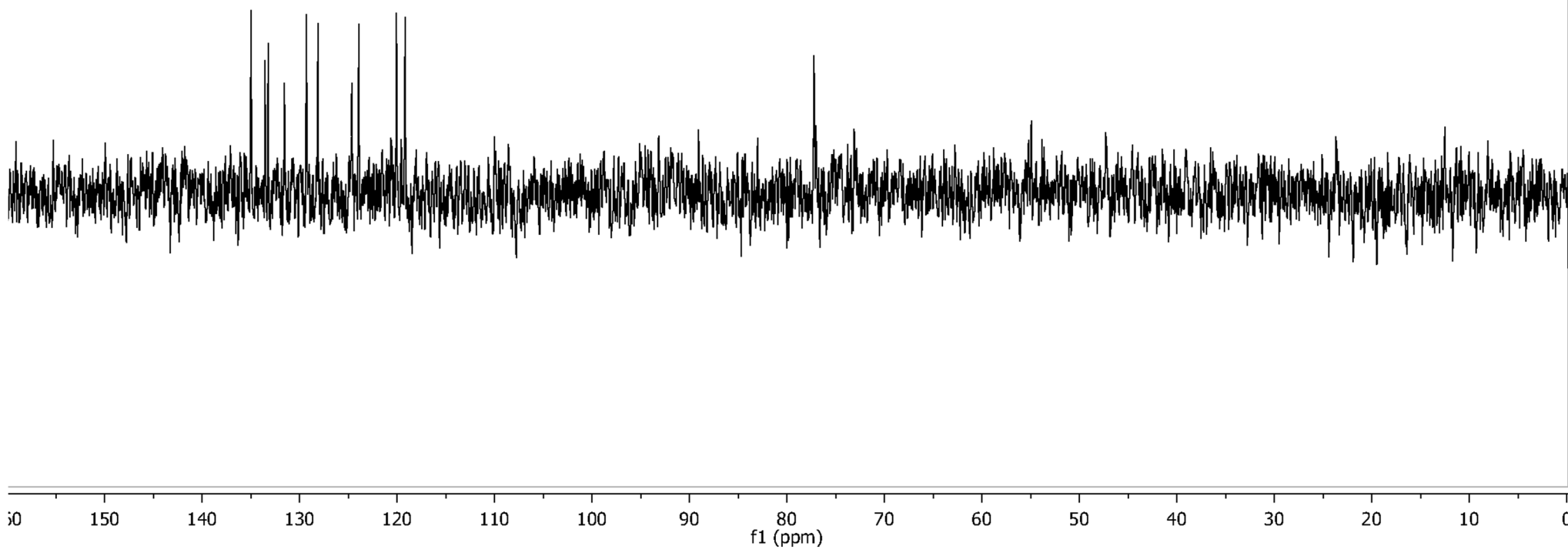
NSAH-E-3E

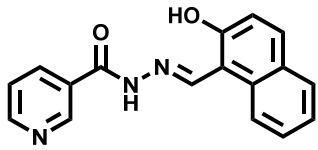




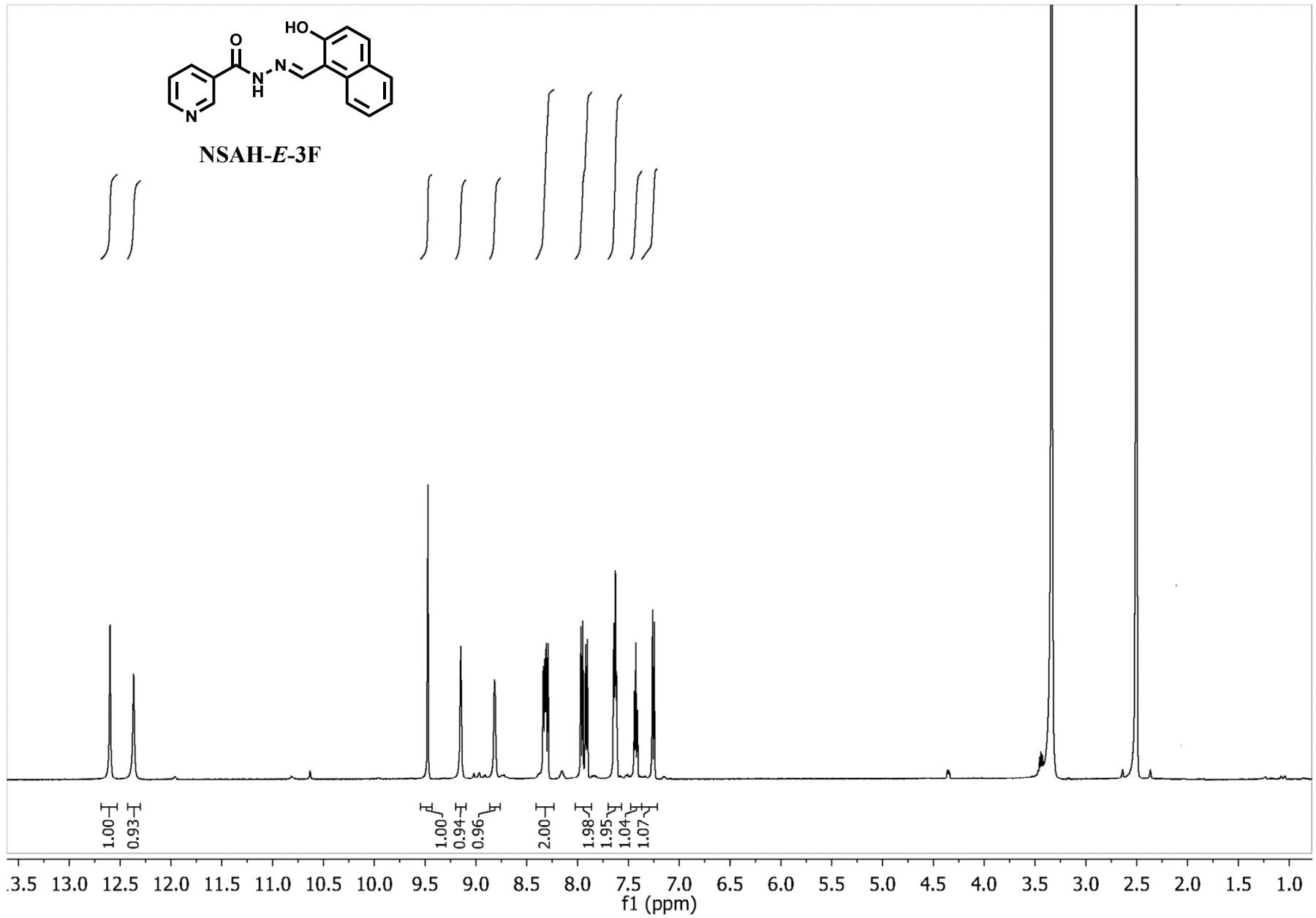
125 MHz, CDCl₃

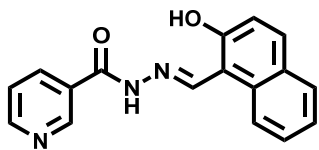
NSAH-E-3E



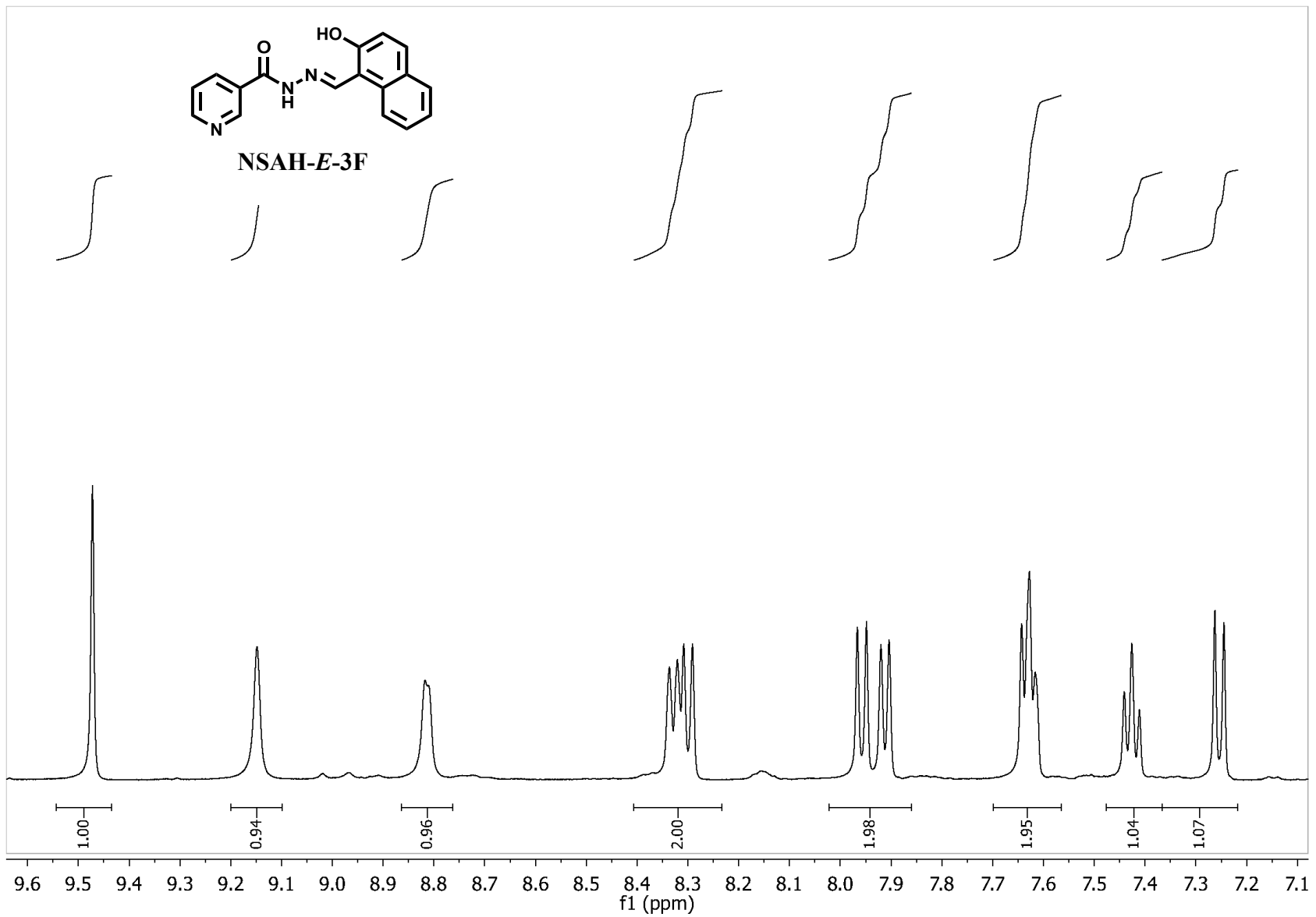


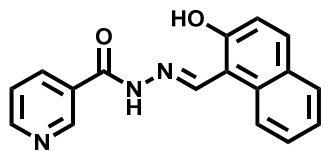
NSAH-E-3F





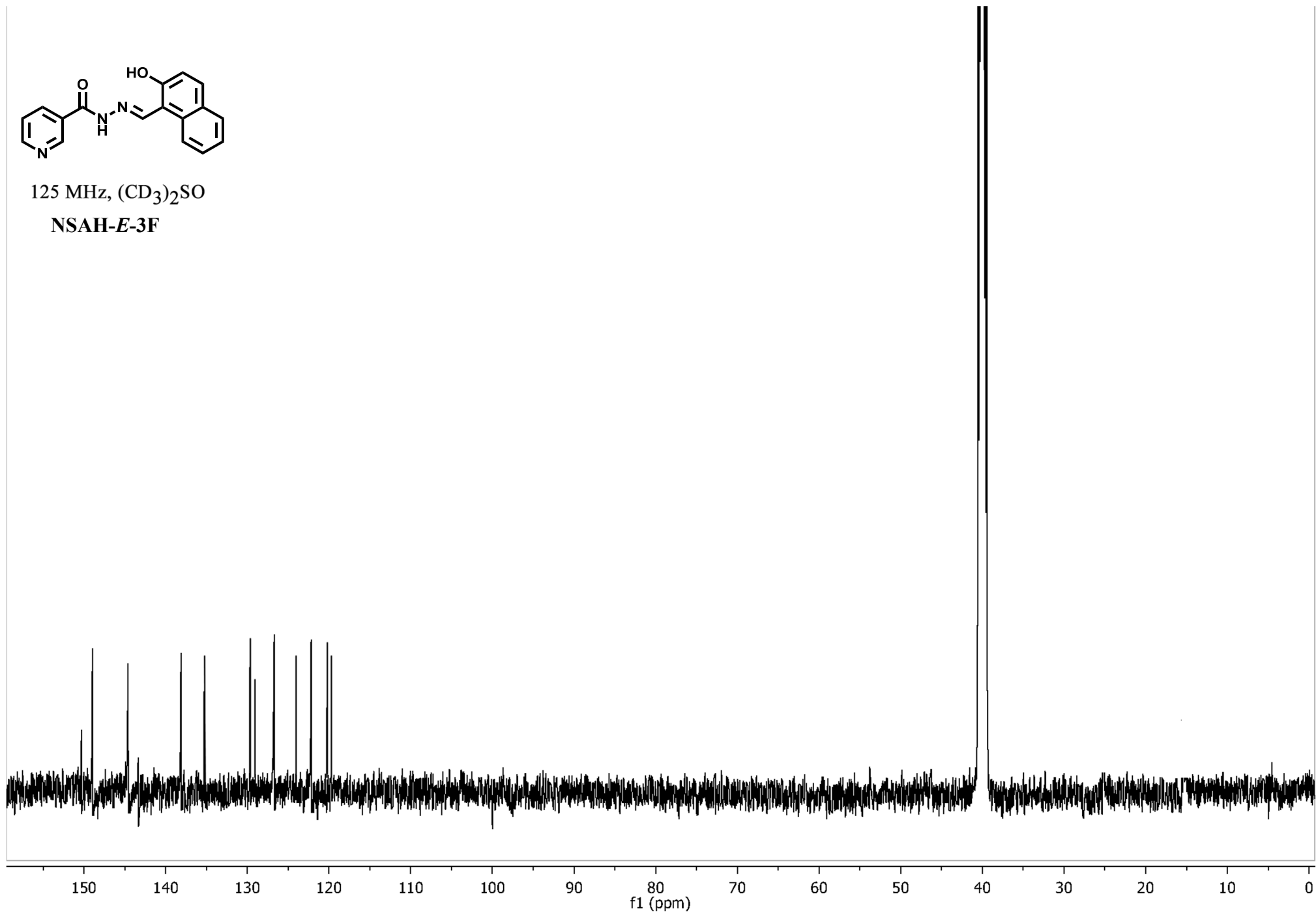
NSAH-E-3F

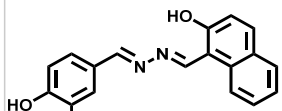




125 MHz, (CD₃)₂SO

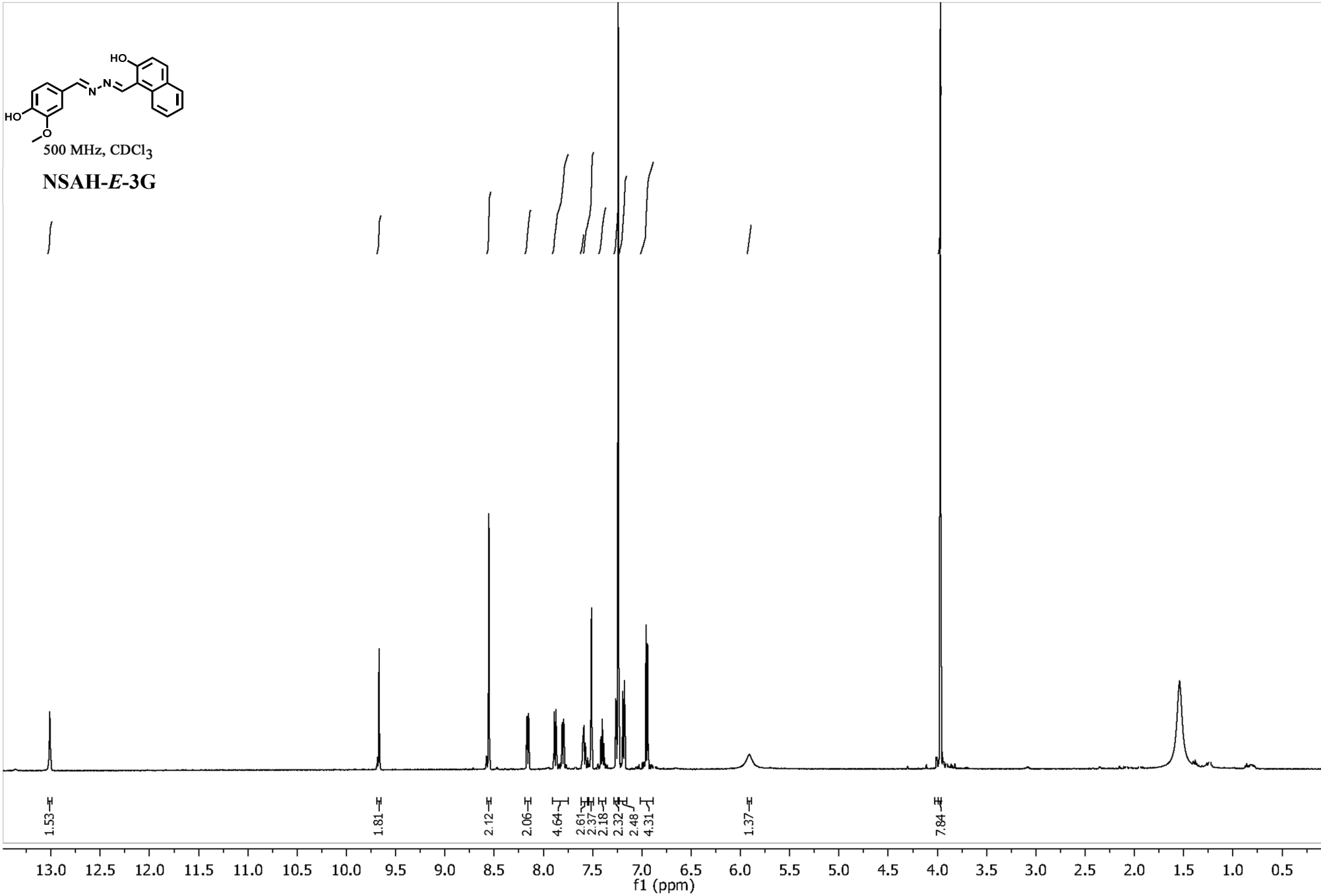
NSAH-E-3F

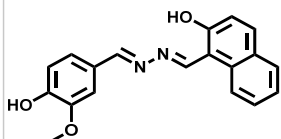




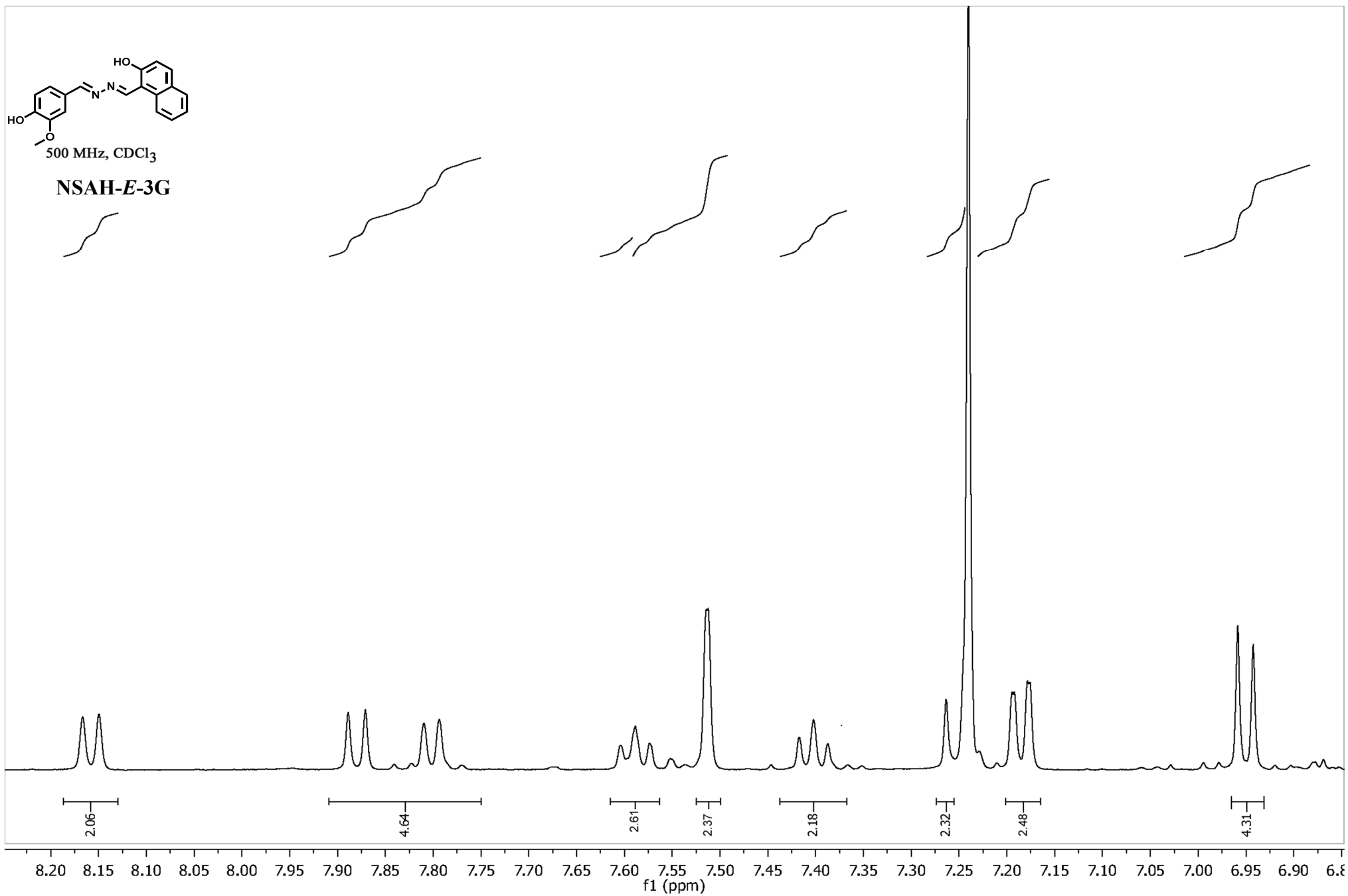
500 MHz, CDCl₃

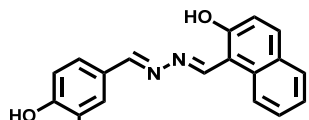
NSAH-E-3G





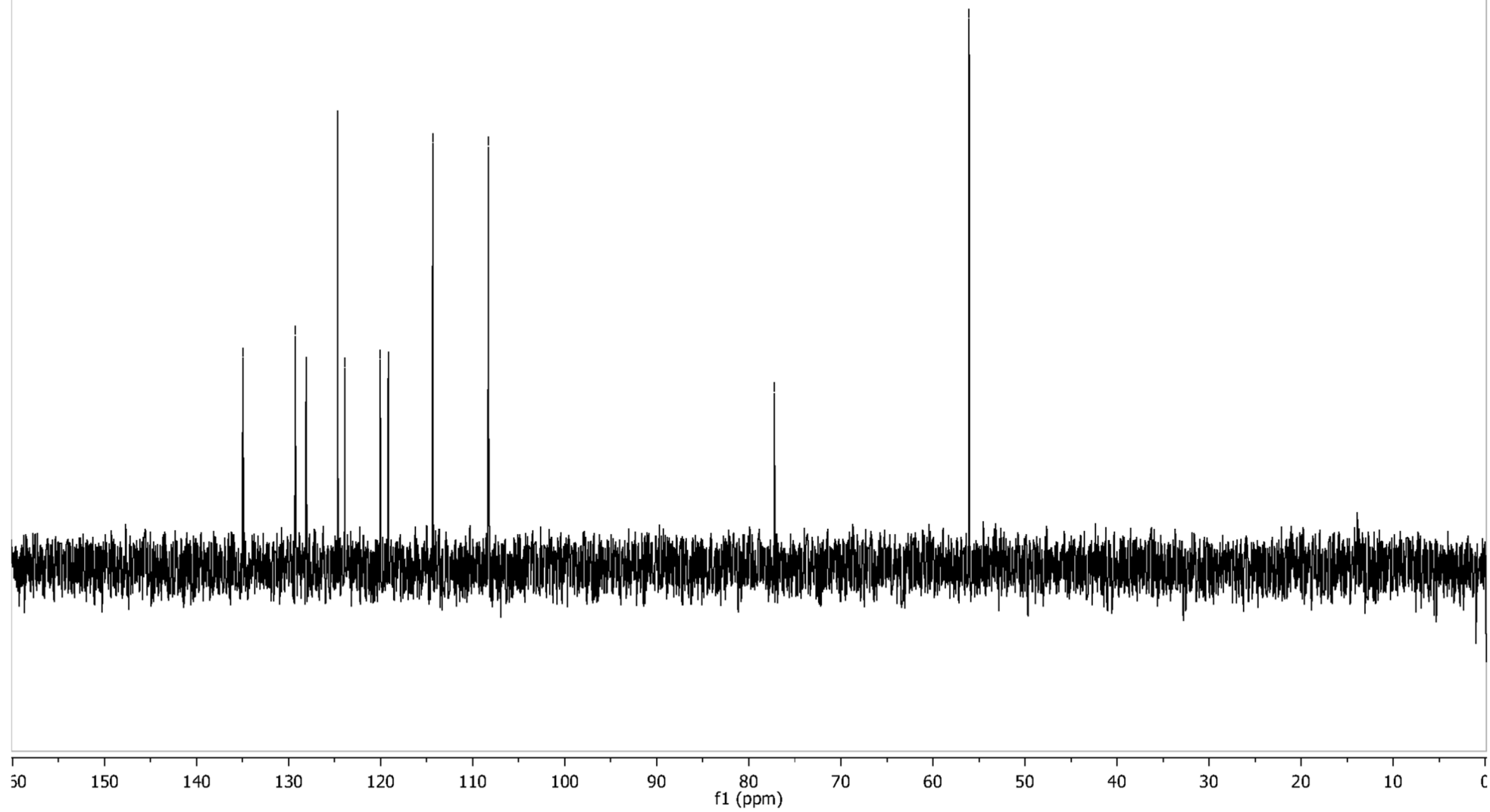
NSAH-E-3G

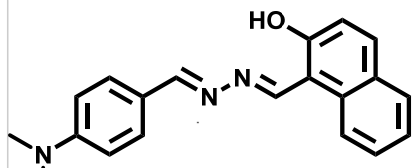




125 MHz, CD₃CN

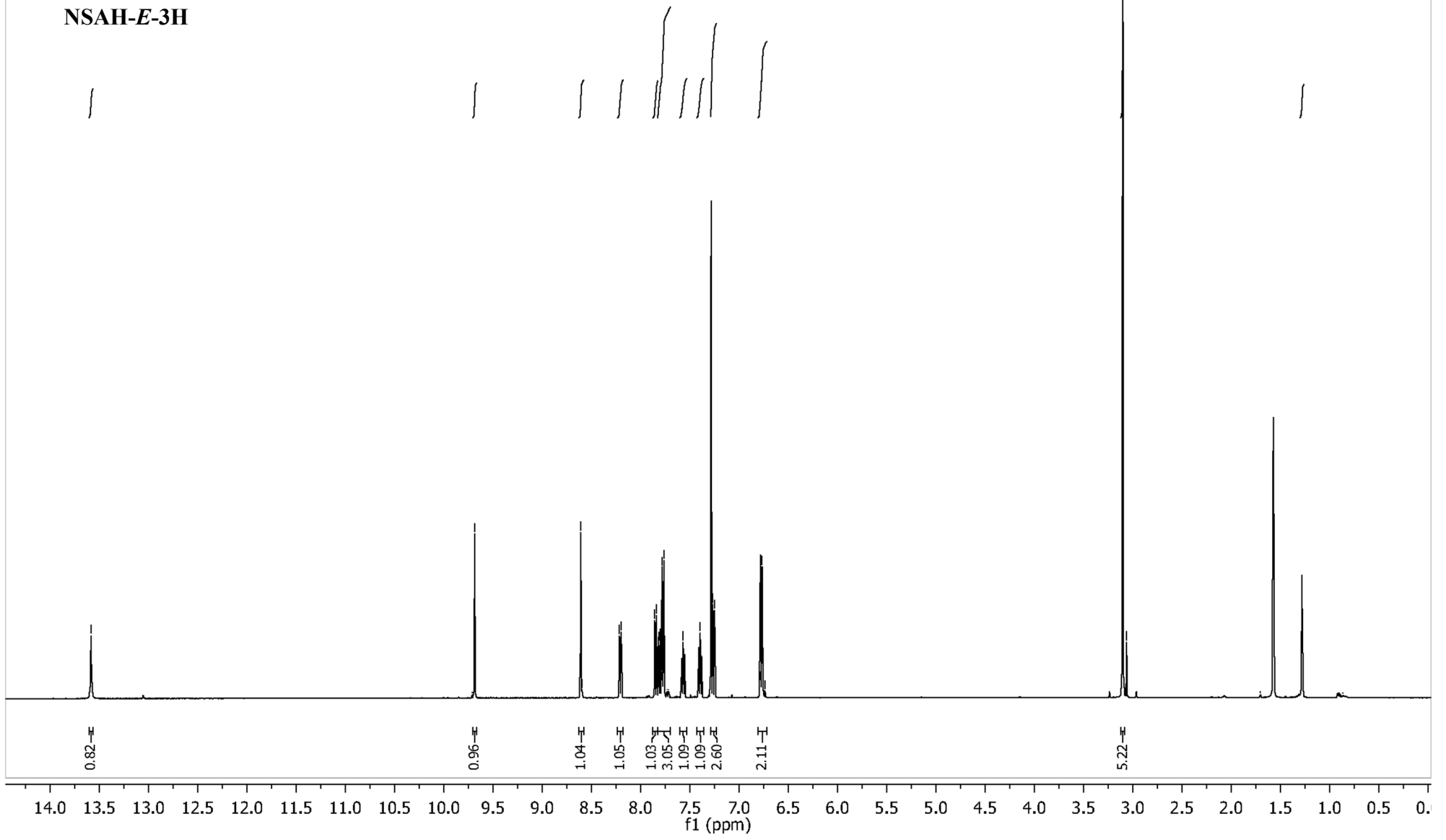
NSAH-*E*-3G

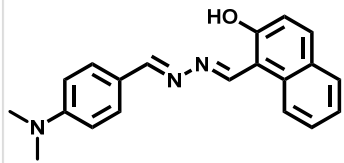




500 MHz, CD₃CN

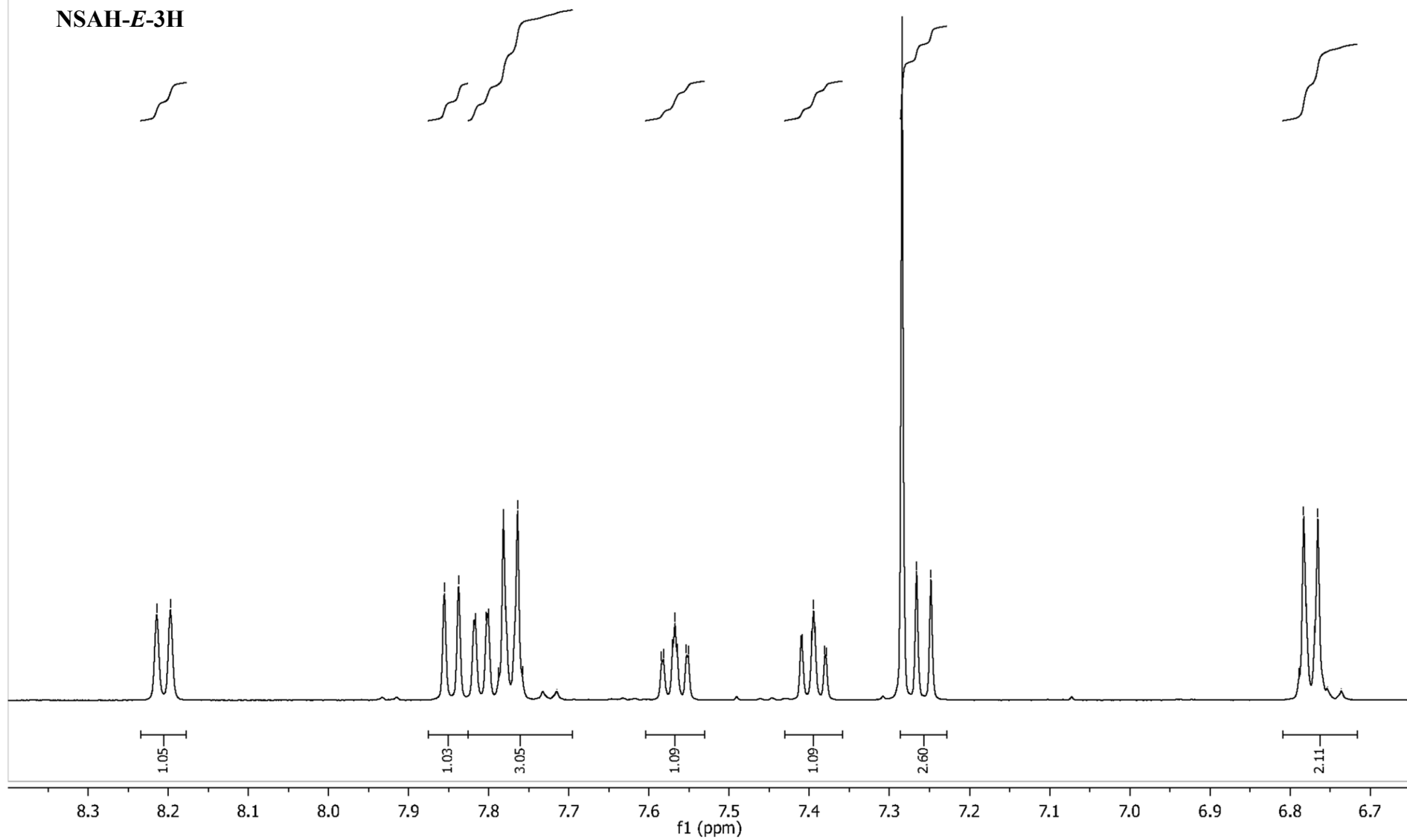
NSAH-E-3H

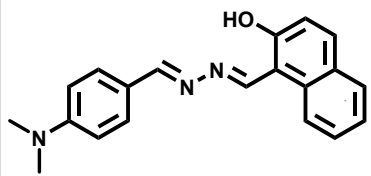




500 MHz, CD₃CN

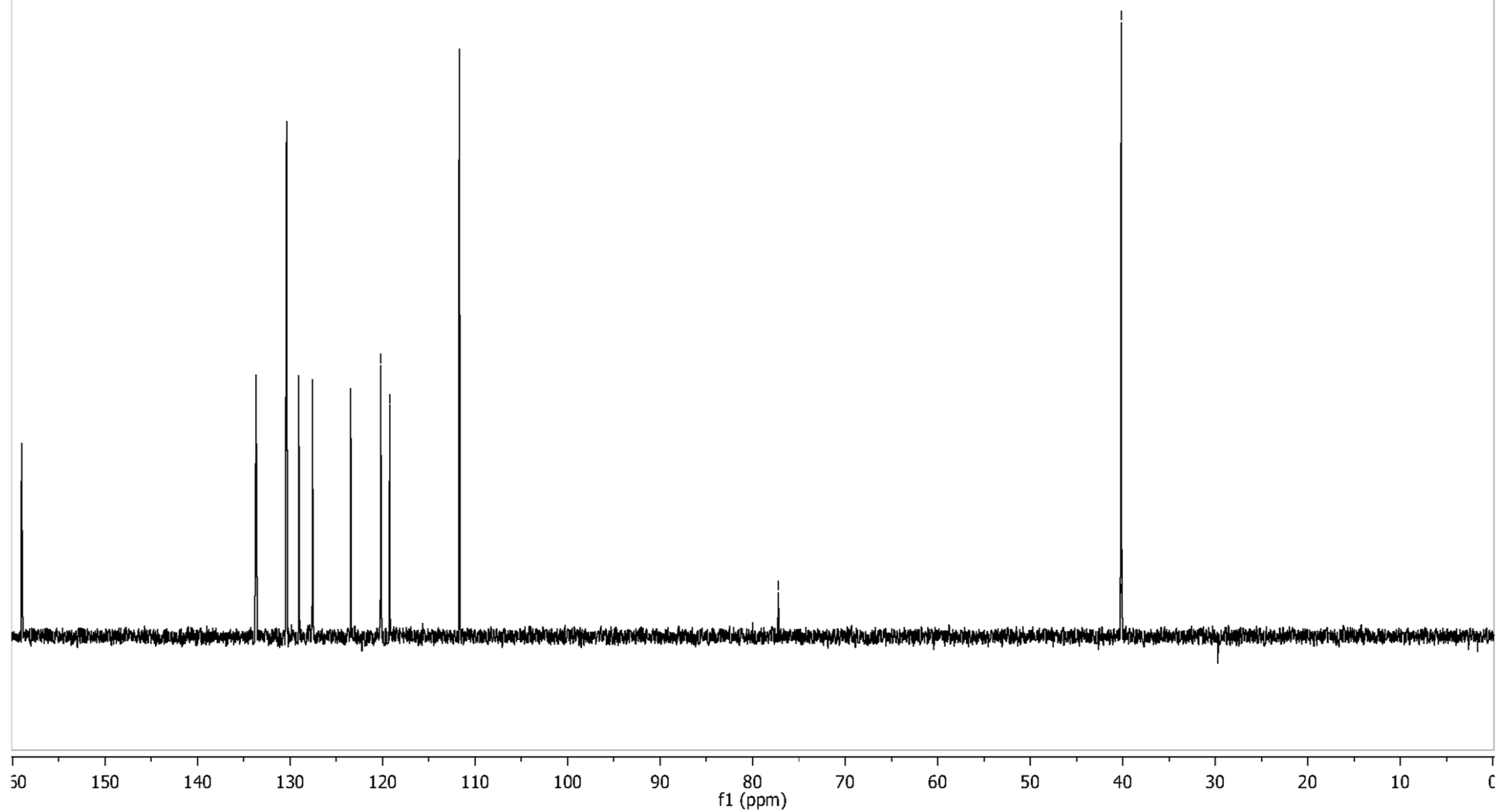
NSAH-E-3H

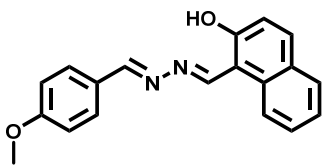




125 MHz, CD₃CN

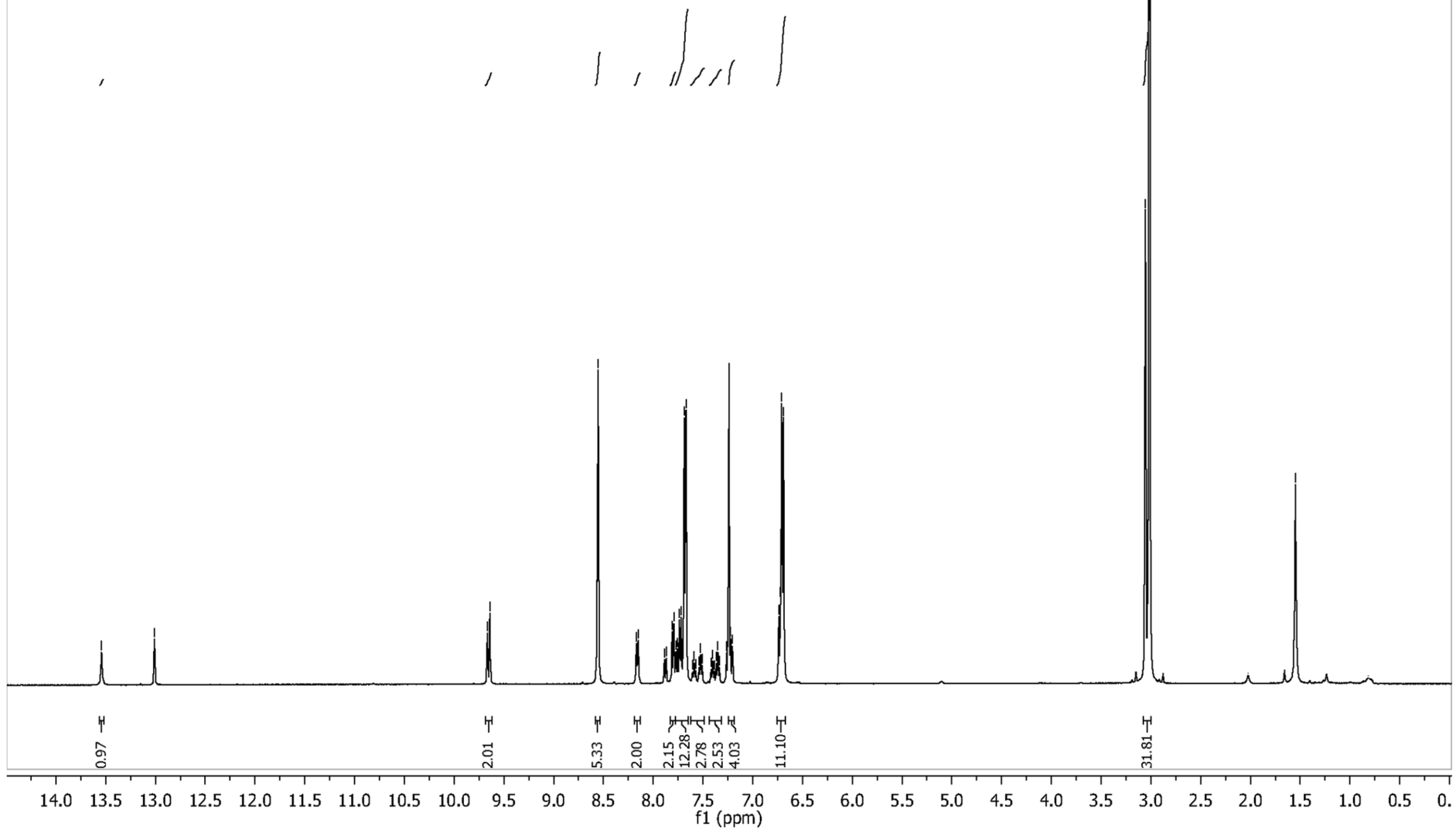
NSAH-E-3H

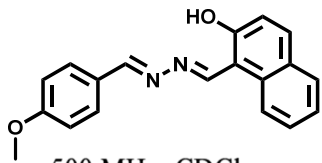




500 MHz, CDCl₃

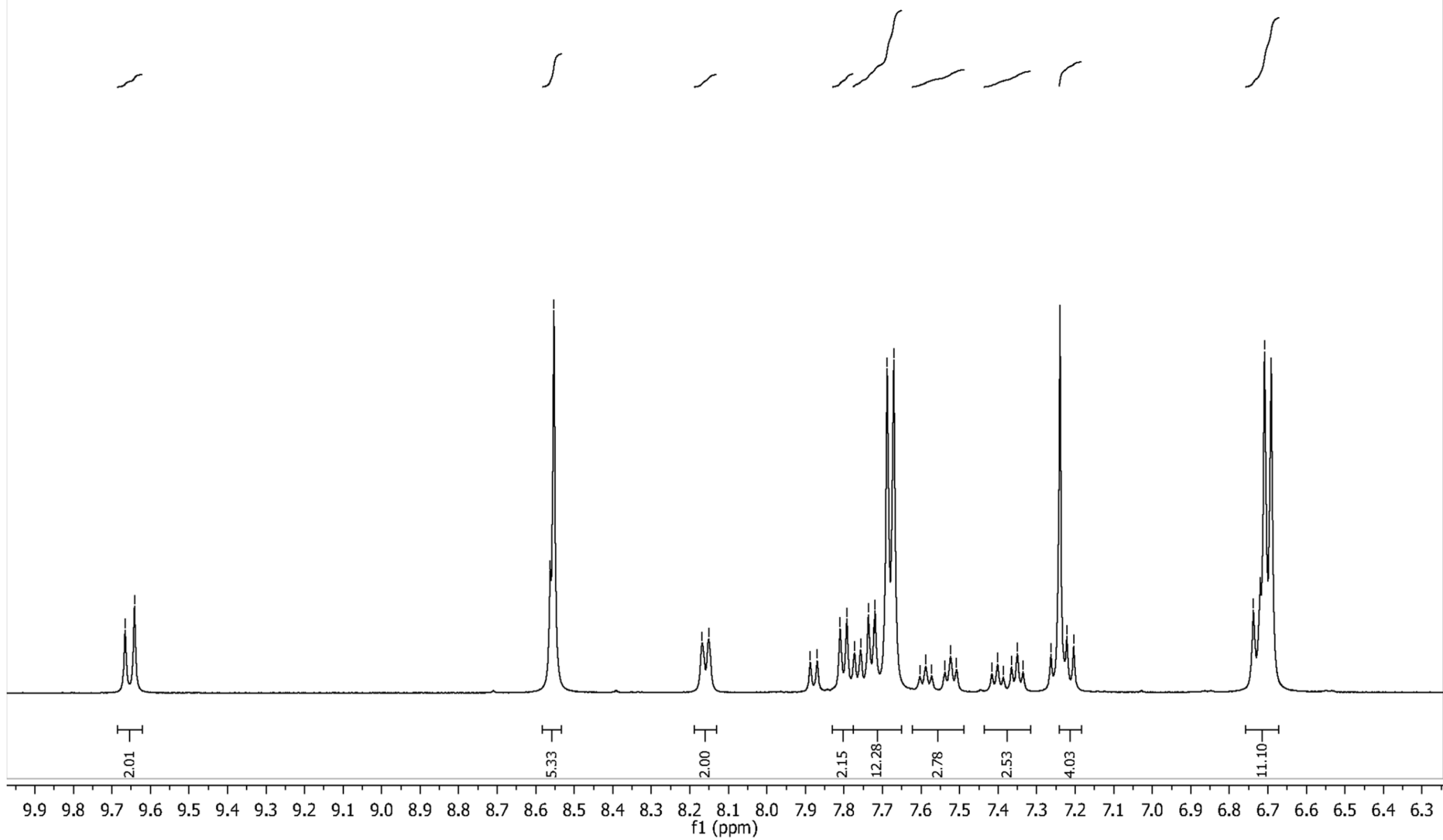
NSAH-E-3I

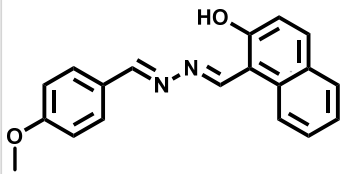




500 MHz, CDCl₃

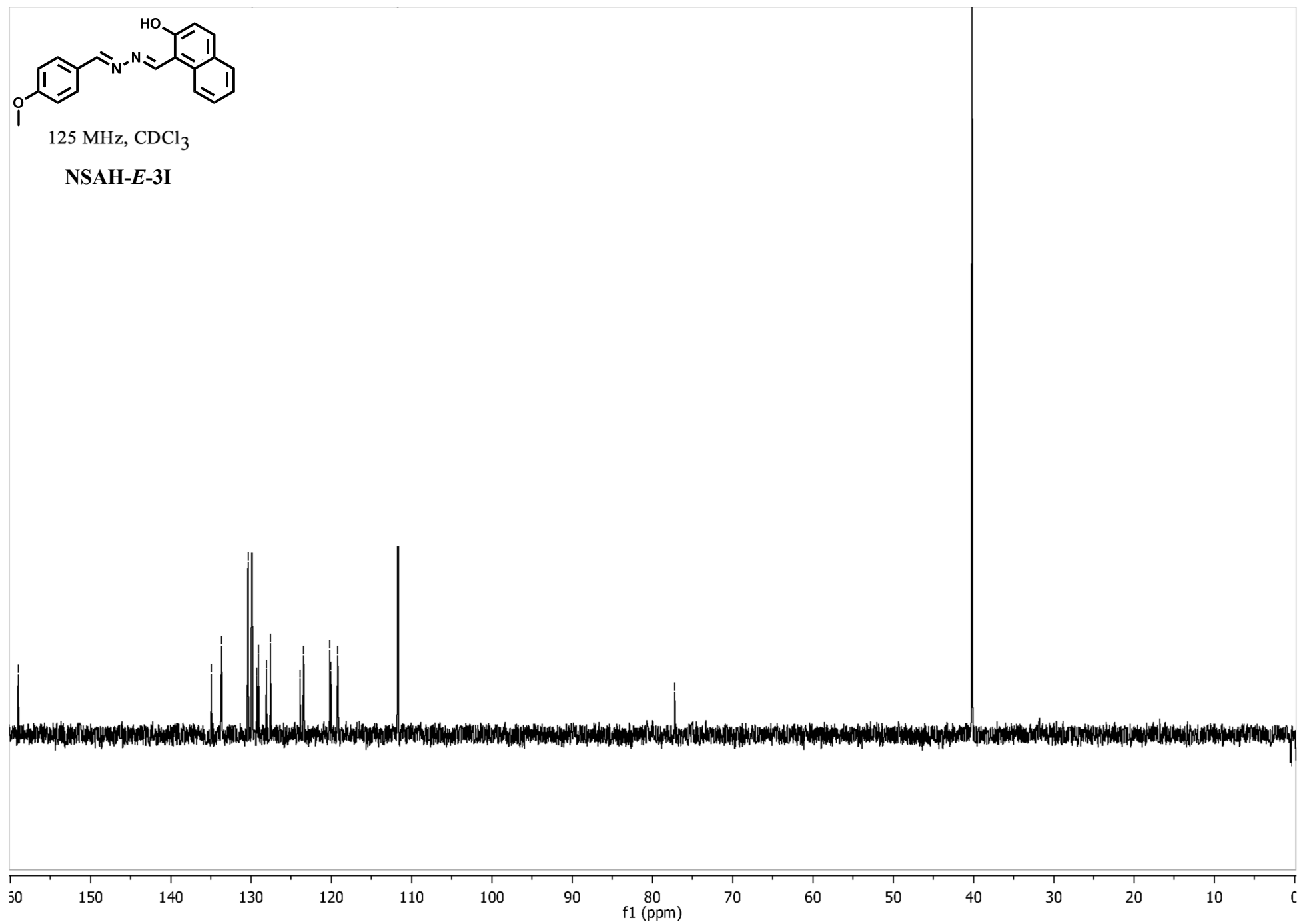
NSAH-E-3I

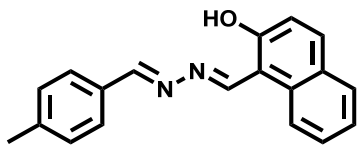




125 MHz, CDCl₃

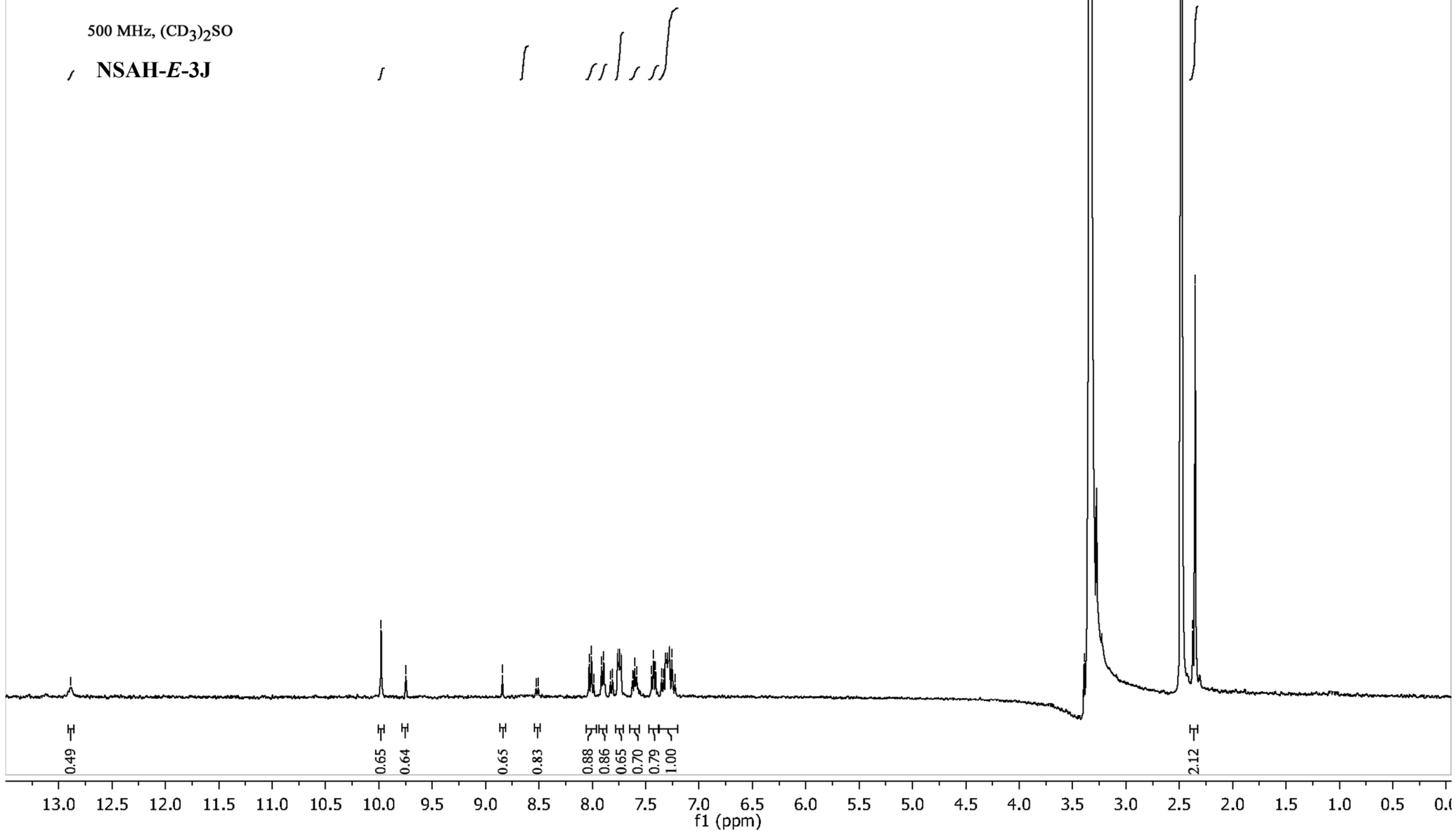
NSAH-E-3I

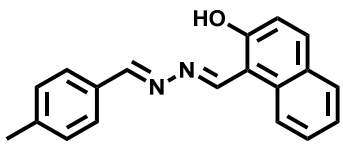




500 MHz, (CD₃)₂SO

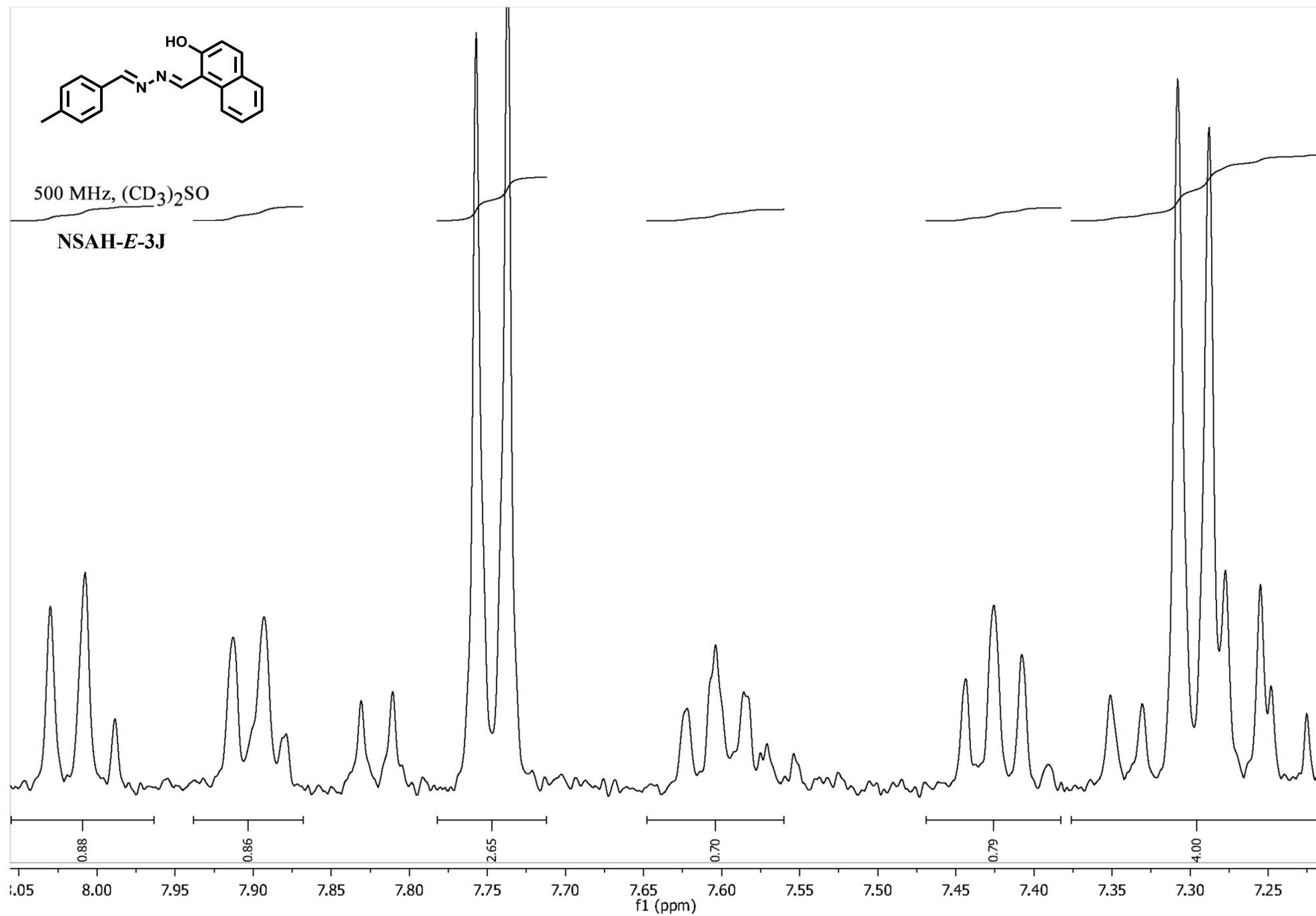
NSAH-E-3J

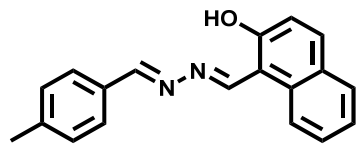




500 MHz, (CD₃)₂SO

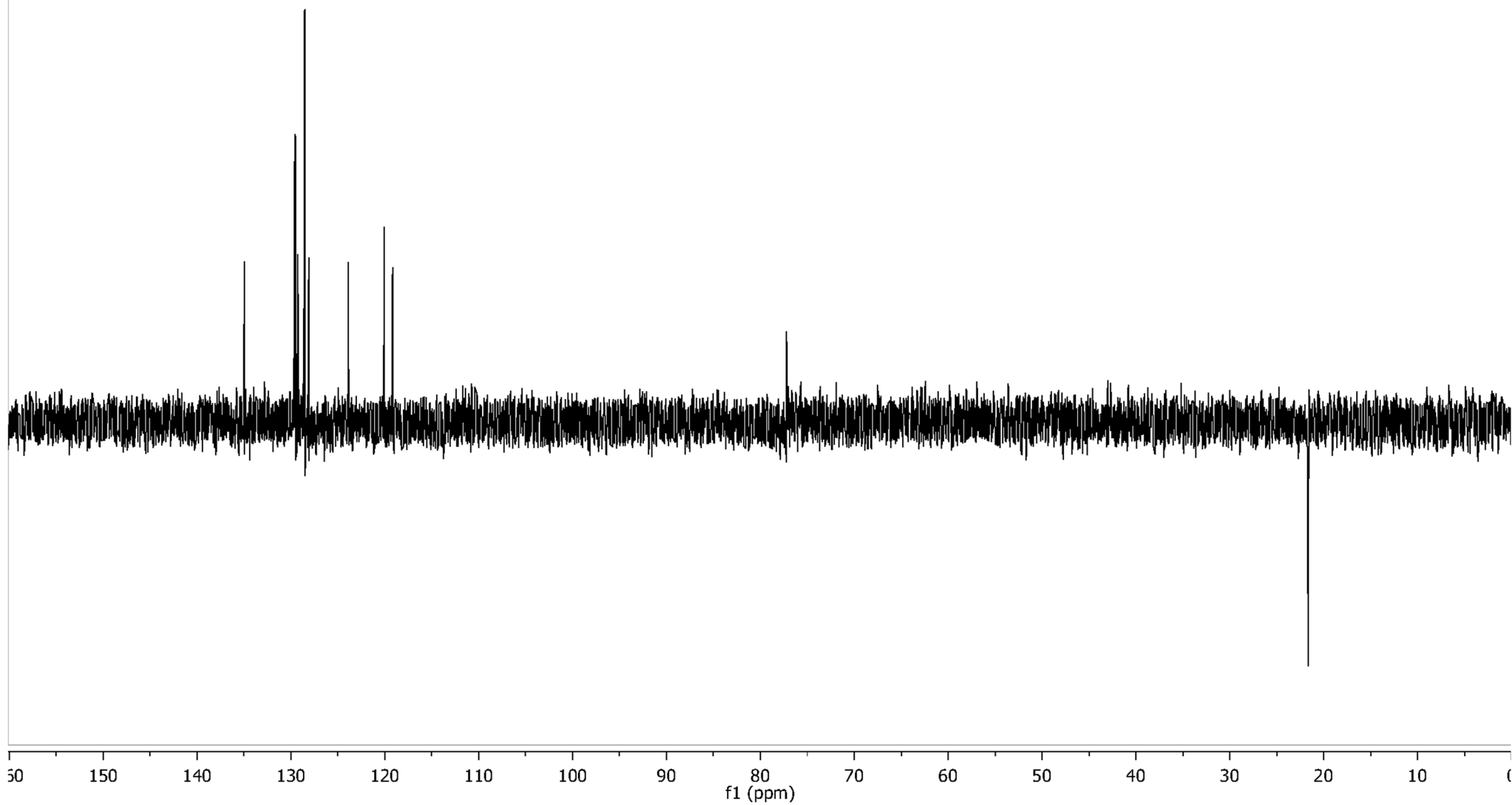
NSAH-E-3J

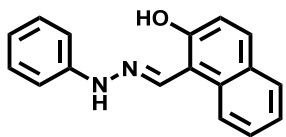




125 MHz, CDCl₃

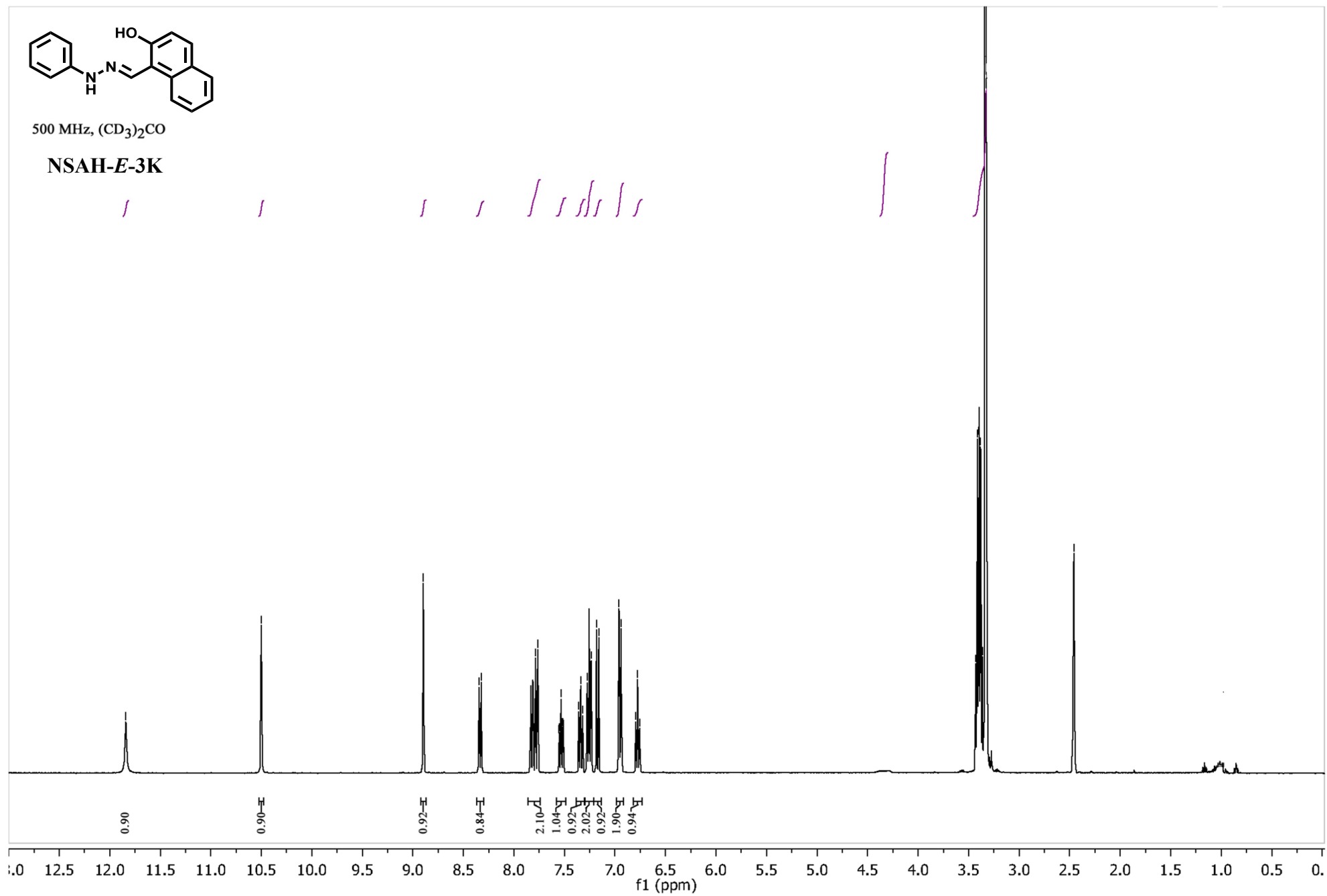
NSAH-E-3J

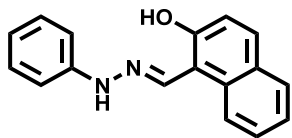




500 MHz, (CD₃)₂CO

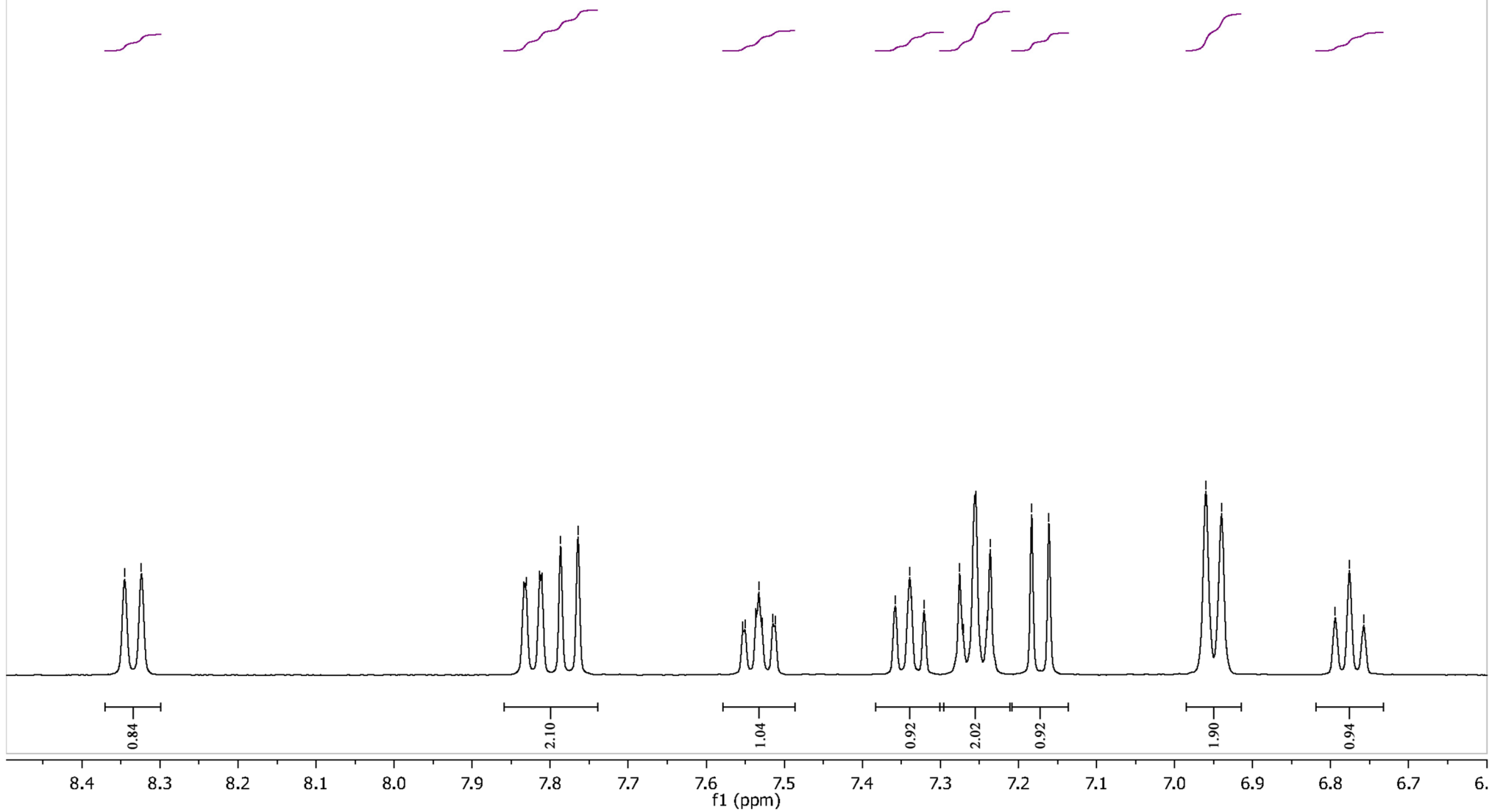
NSAH-E-3K

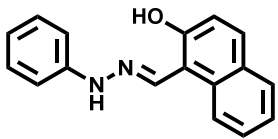




500 MHz, (CD₃)₂CO

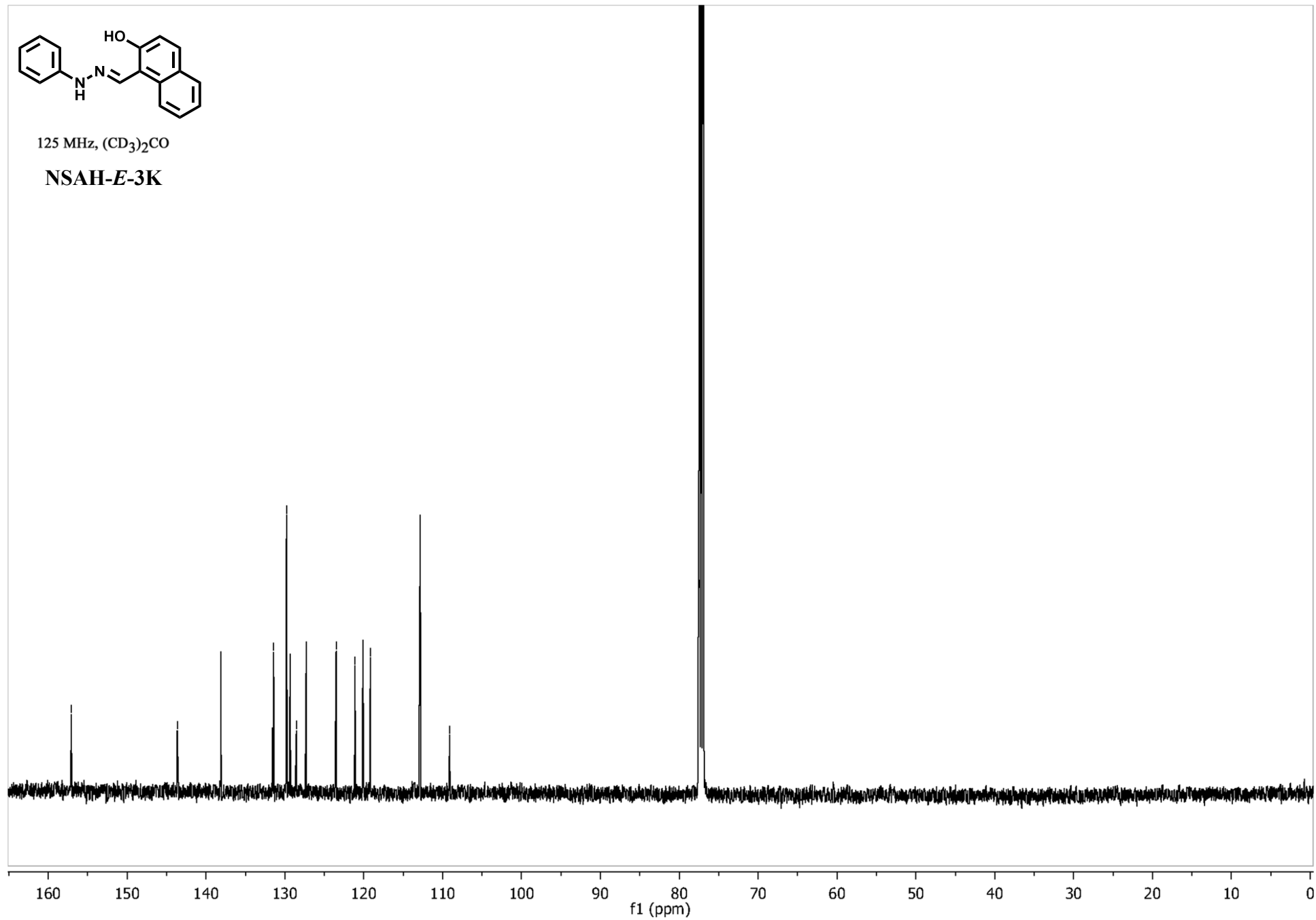
NSAH-E-3K

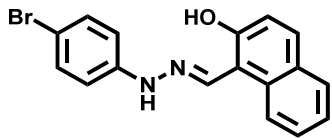




125 MHz, (CD₃)₂CO

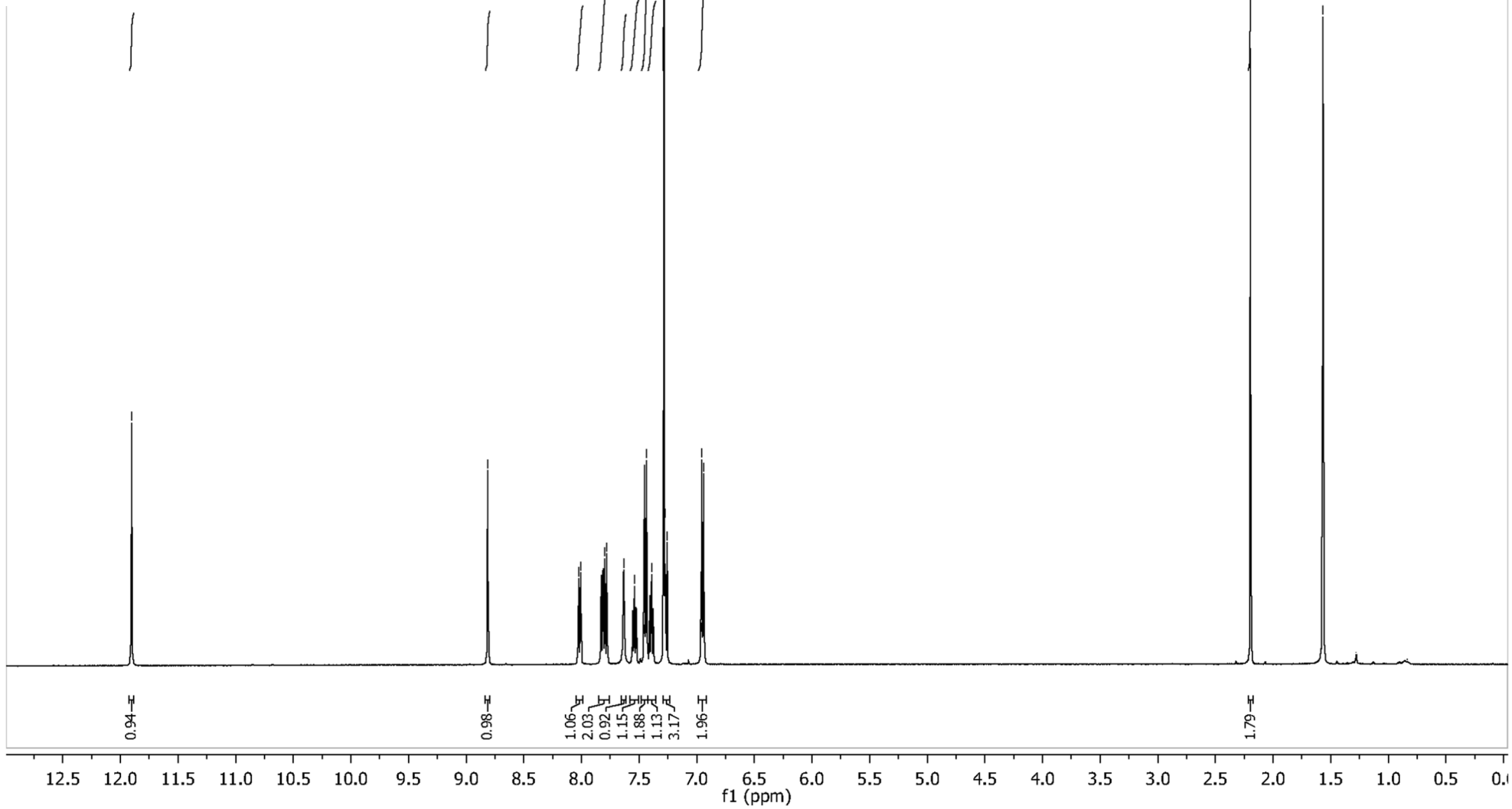
NSAH-E-3K

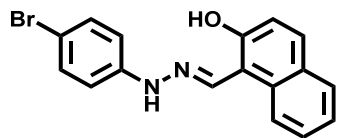




500 MHz, CDCl₃

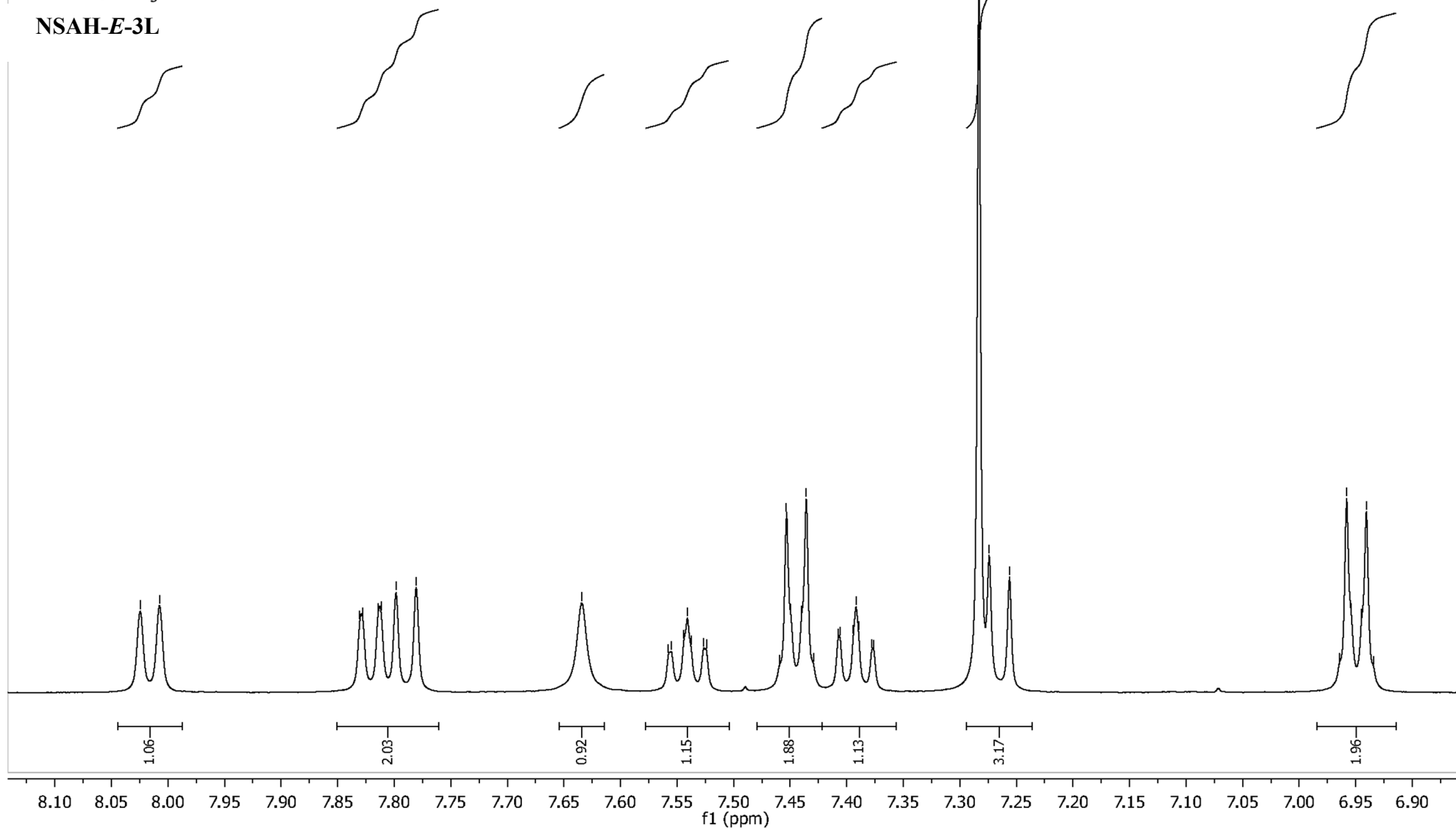
NSAH-E-3L

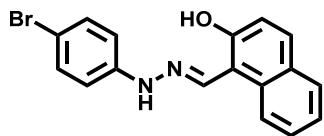




500 MHz, CDCl₃

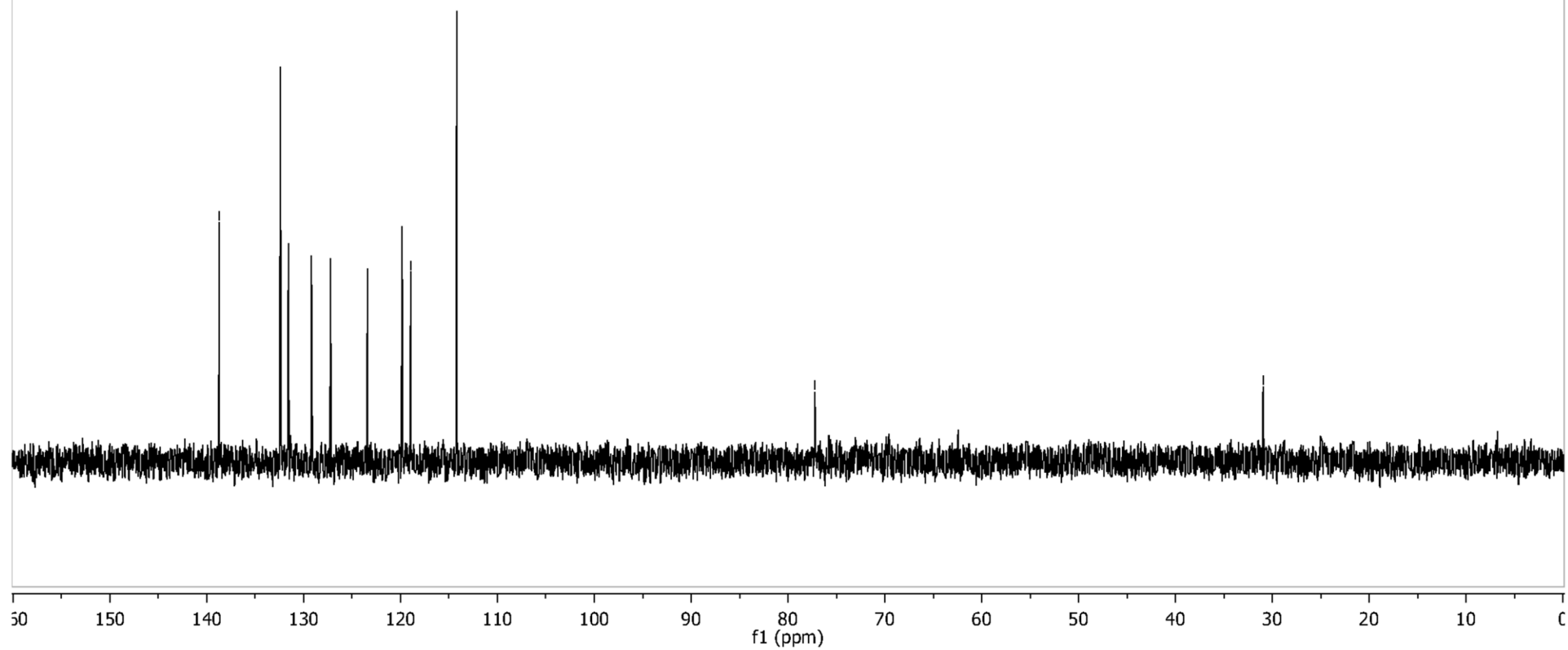
NSAH-E-3L

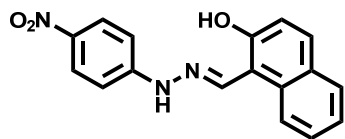




125 MHz, CDCl₃

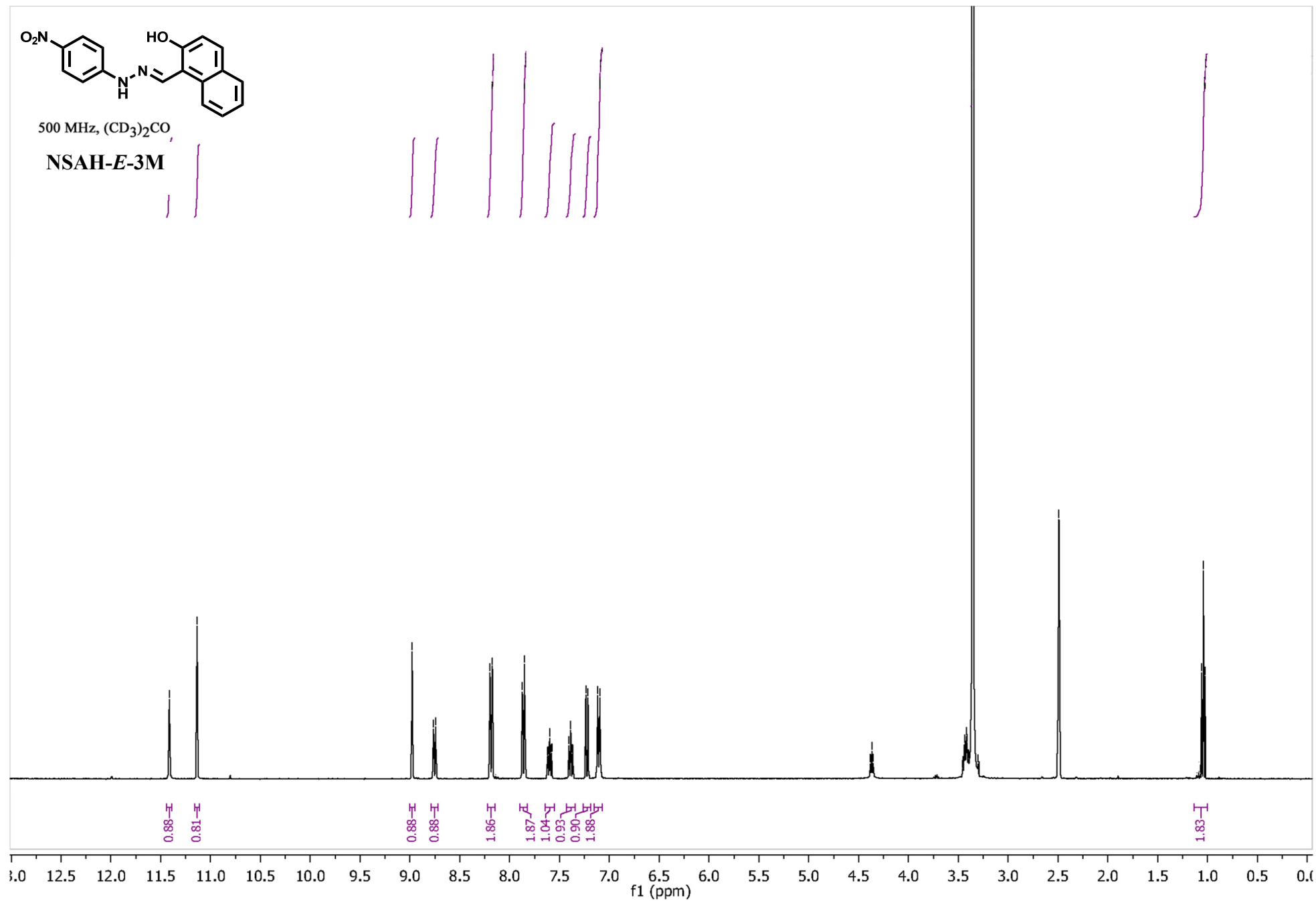
NSAH-E-3L

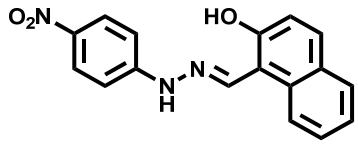




500 MHz, (CD₃)₂CO

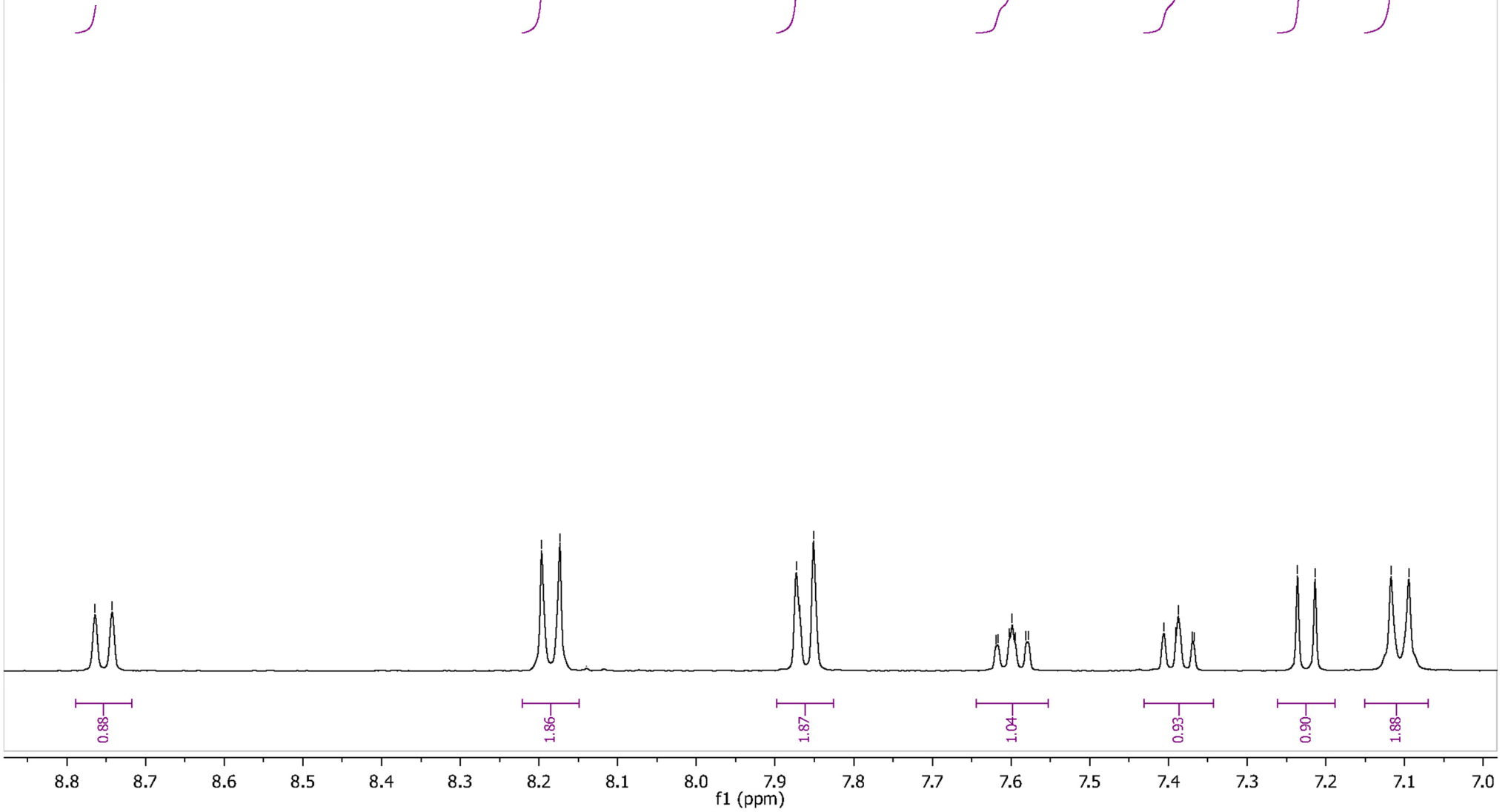
NSAH-E-3M

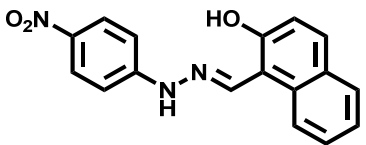




500 MHz, (CD₃)₂CO

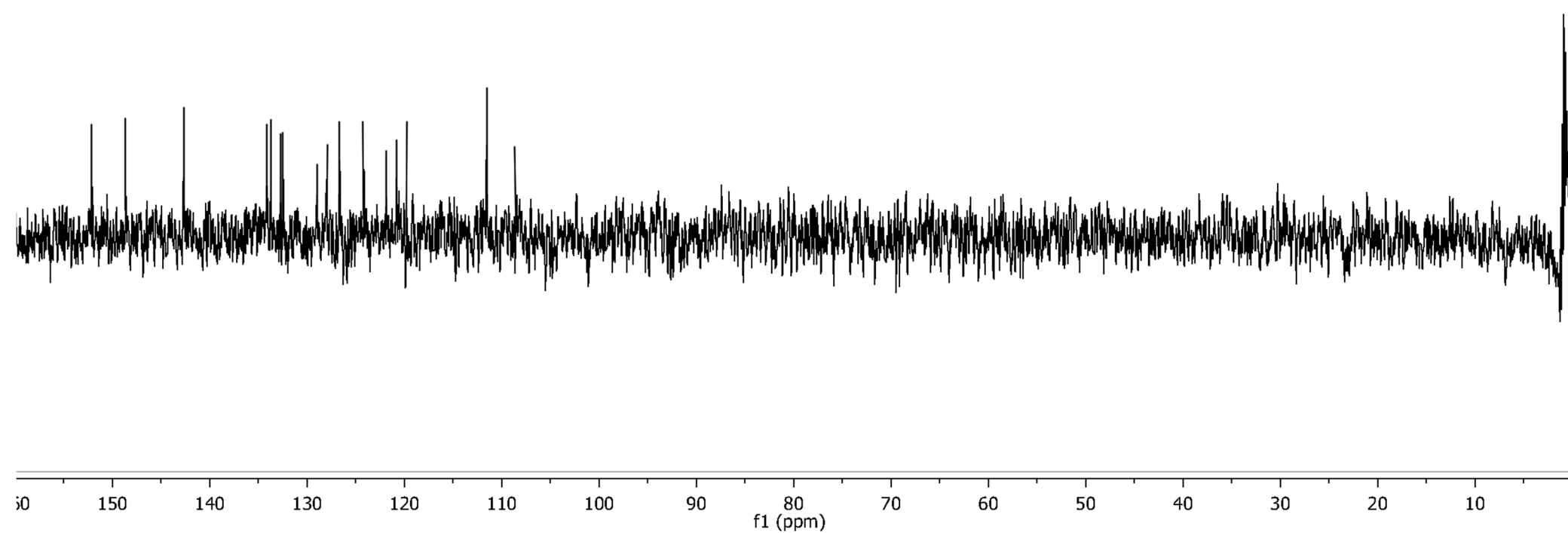
NSAH-*E*-3M

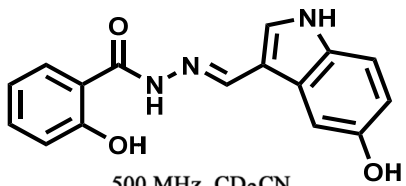




125 MHz, CD₃CN

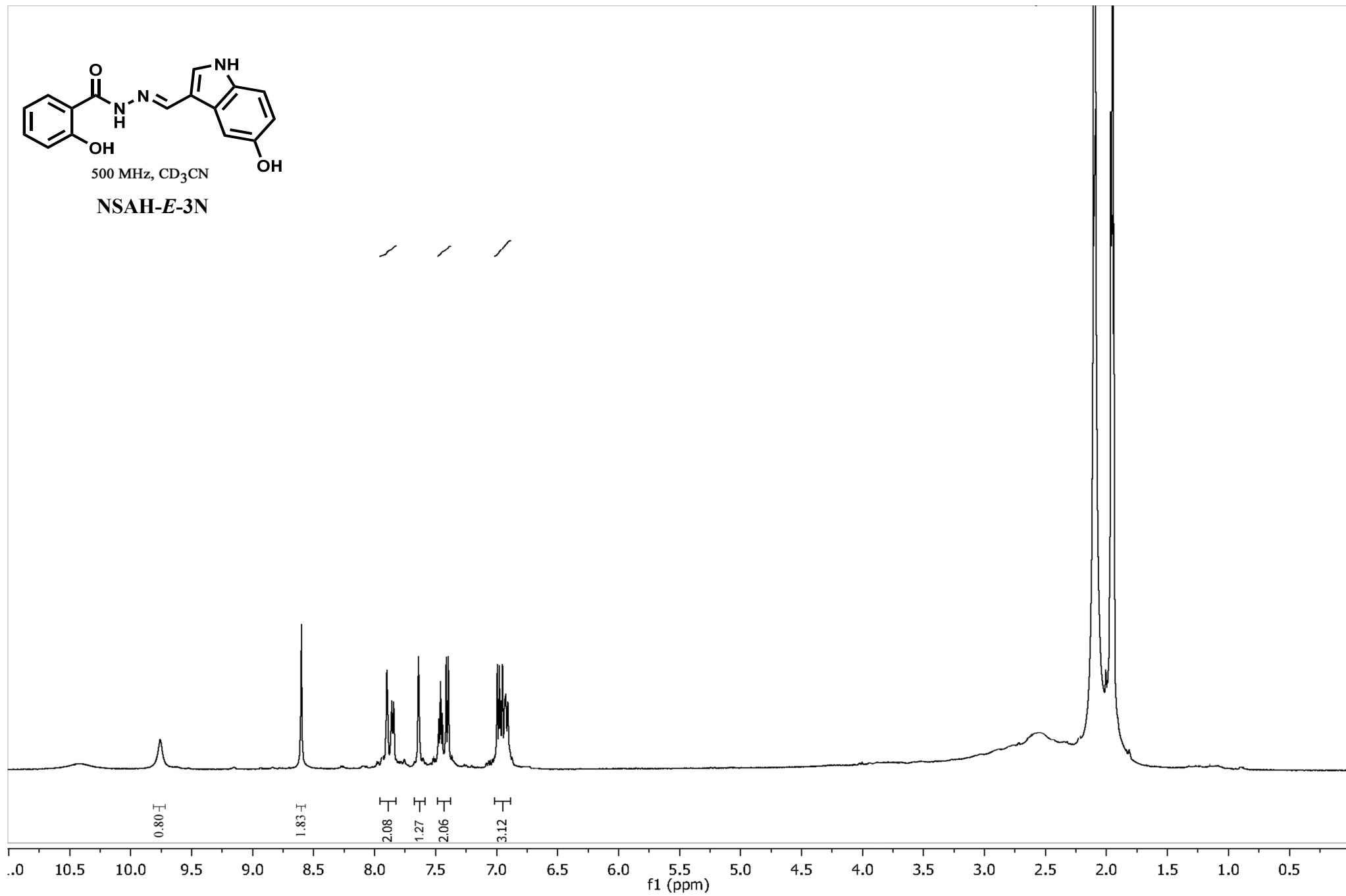
NSAH-*E*-3M

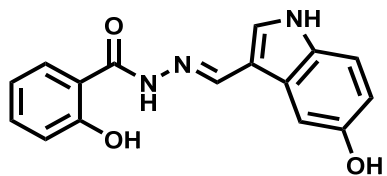




500 MHz, CD₃CN

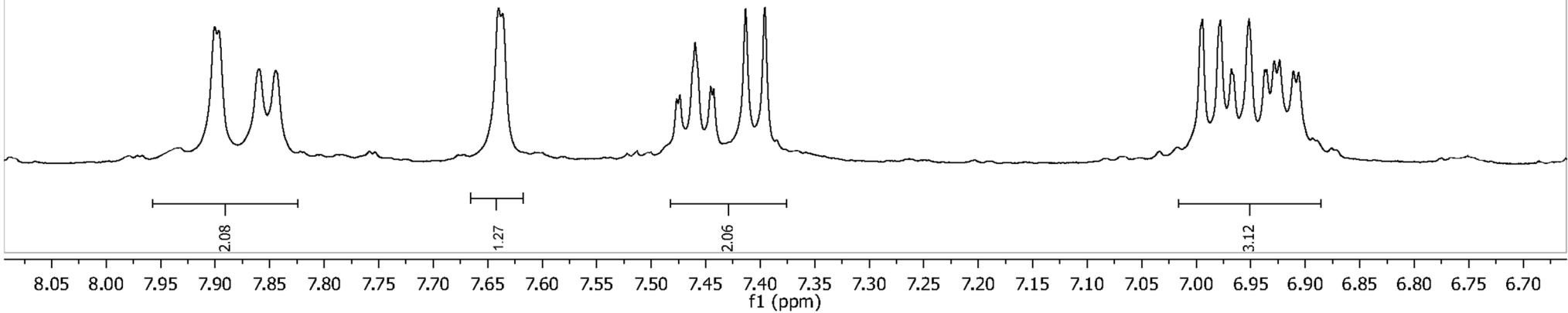
NSAH-E-3N

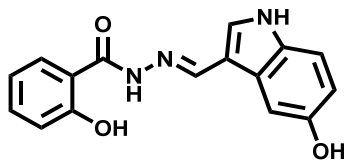




500 MHz, CD₃CN

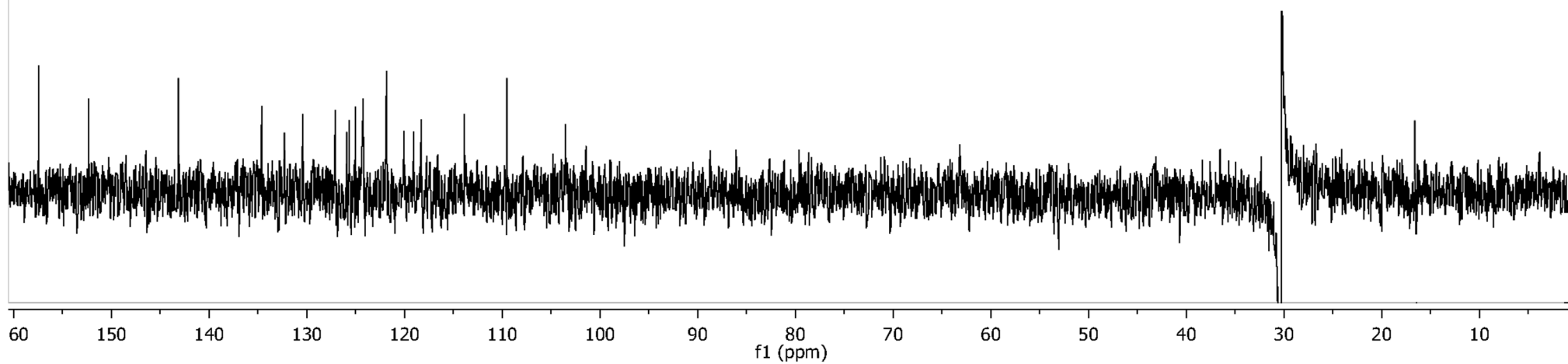
NSAH-E-3N

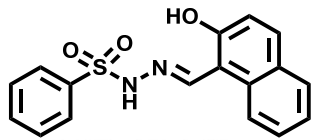




125 MHz, CD₃CN

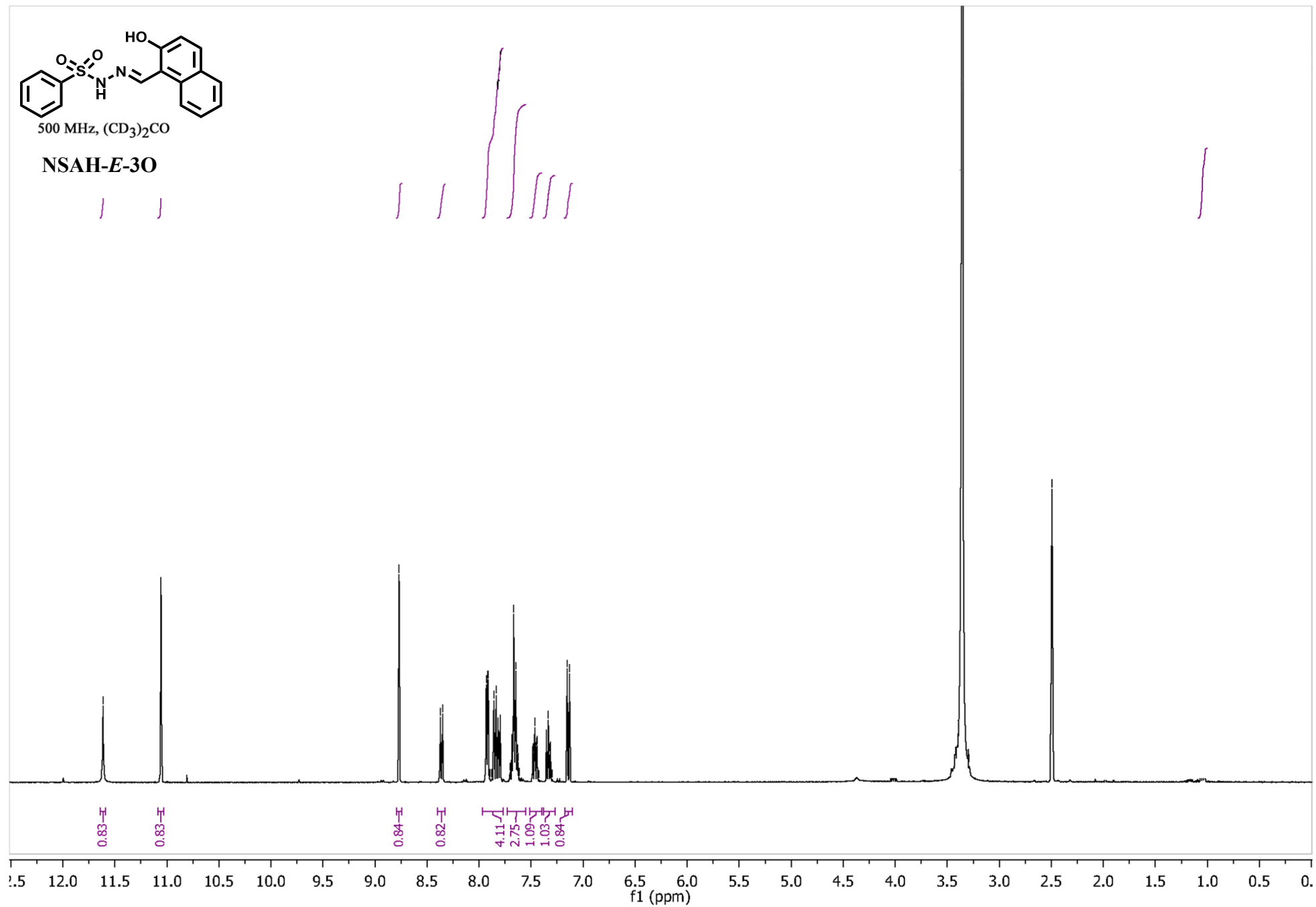
NSAH-E-3N

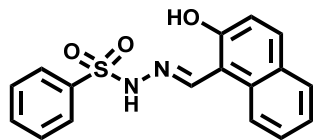




500 MHz, (CD₃)₂CO

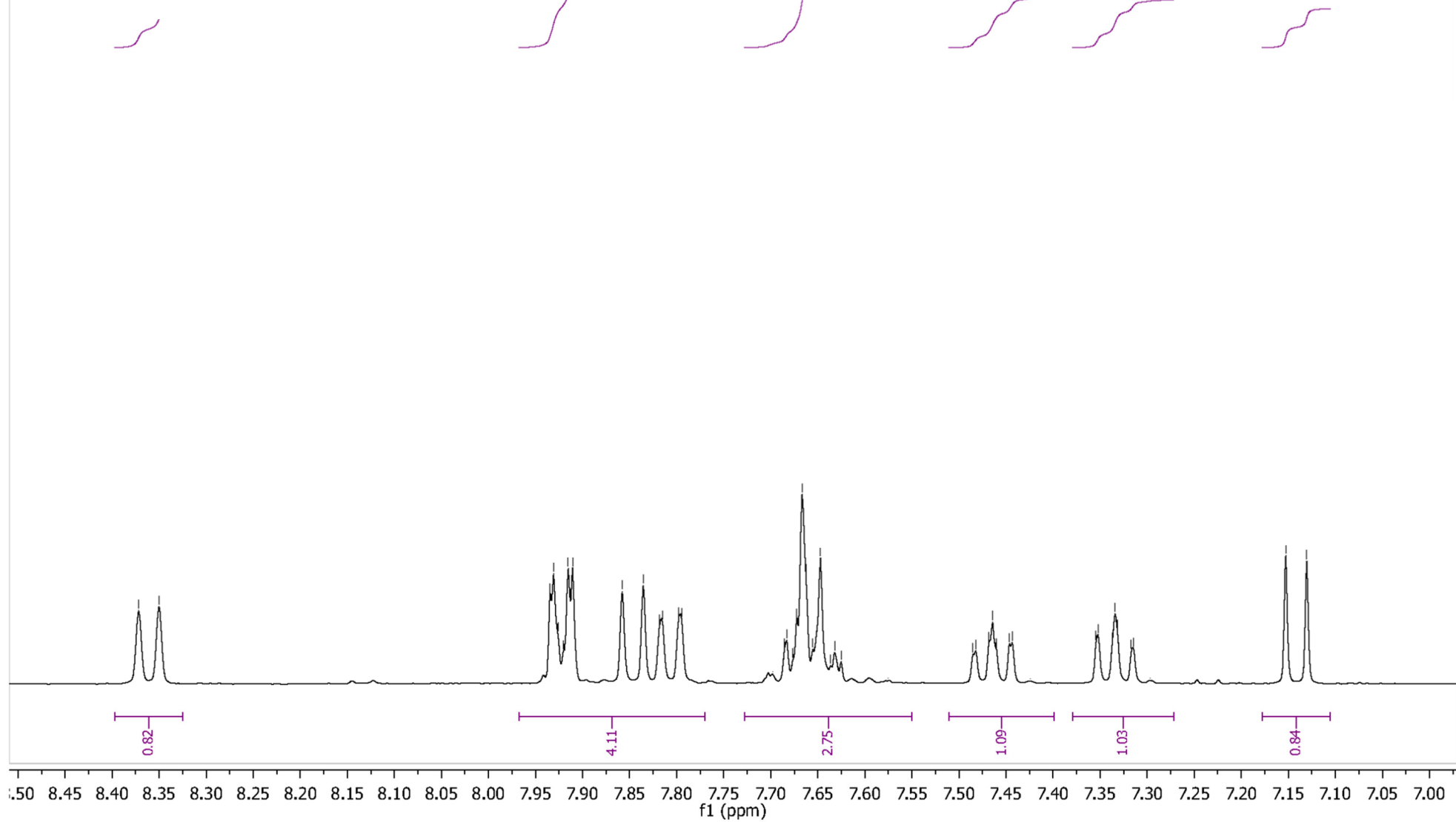
NSAH-E-30

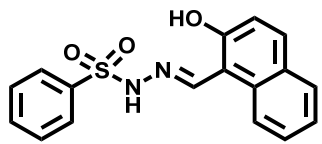




500 MHz, (CD₃)₂CO

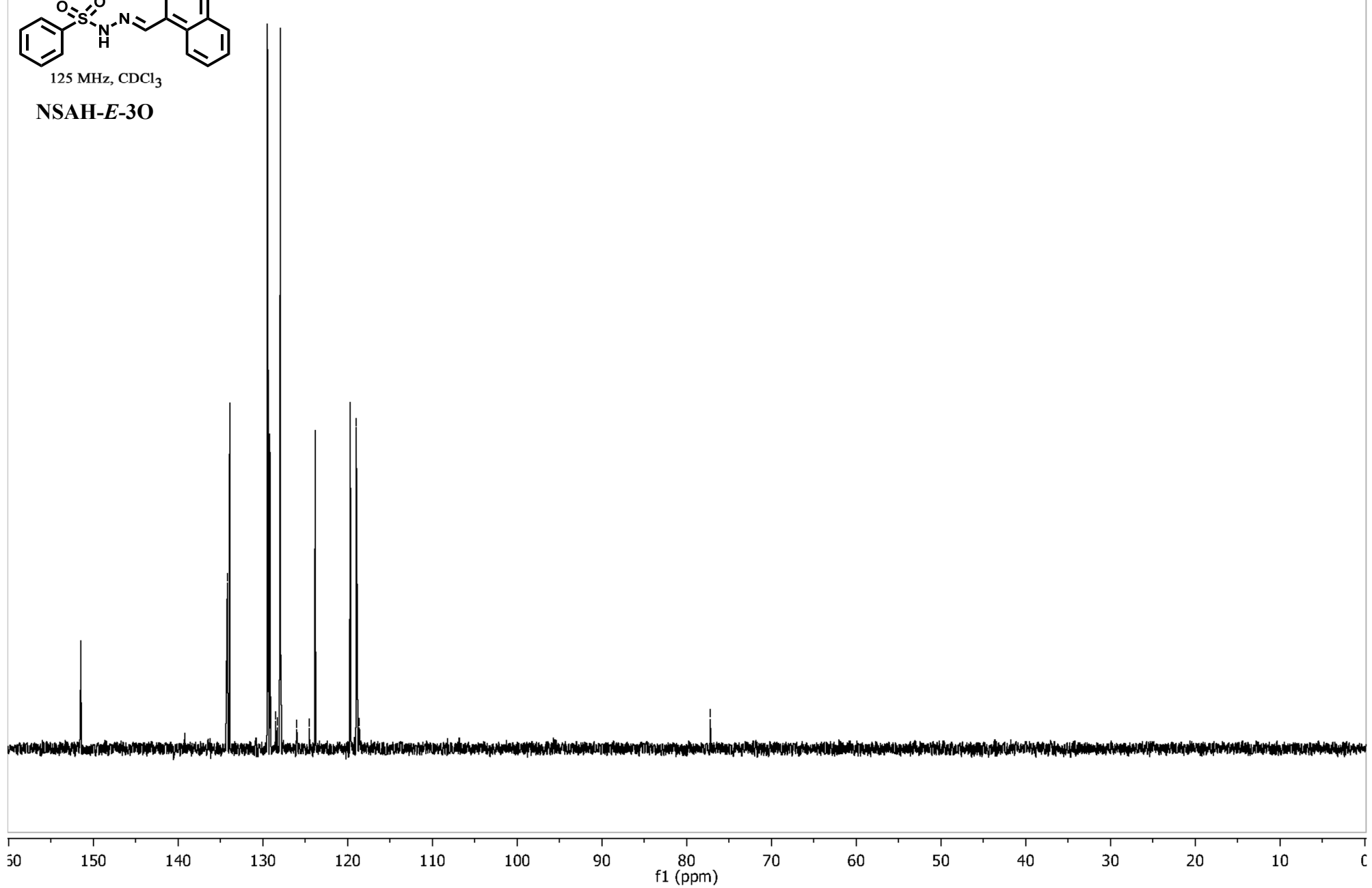
NSAH-E-30

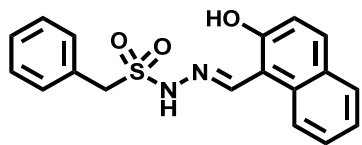




125 MHz, CDCl₃

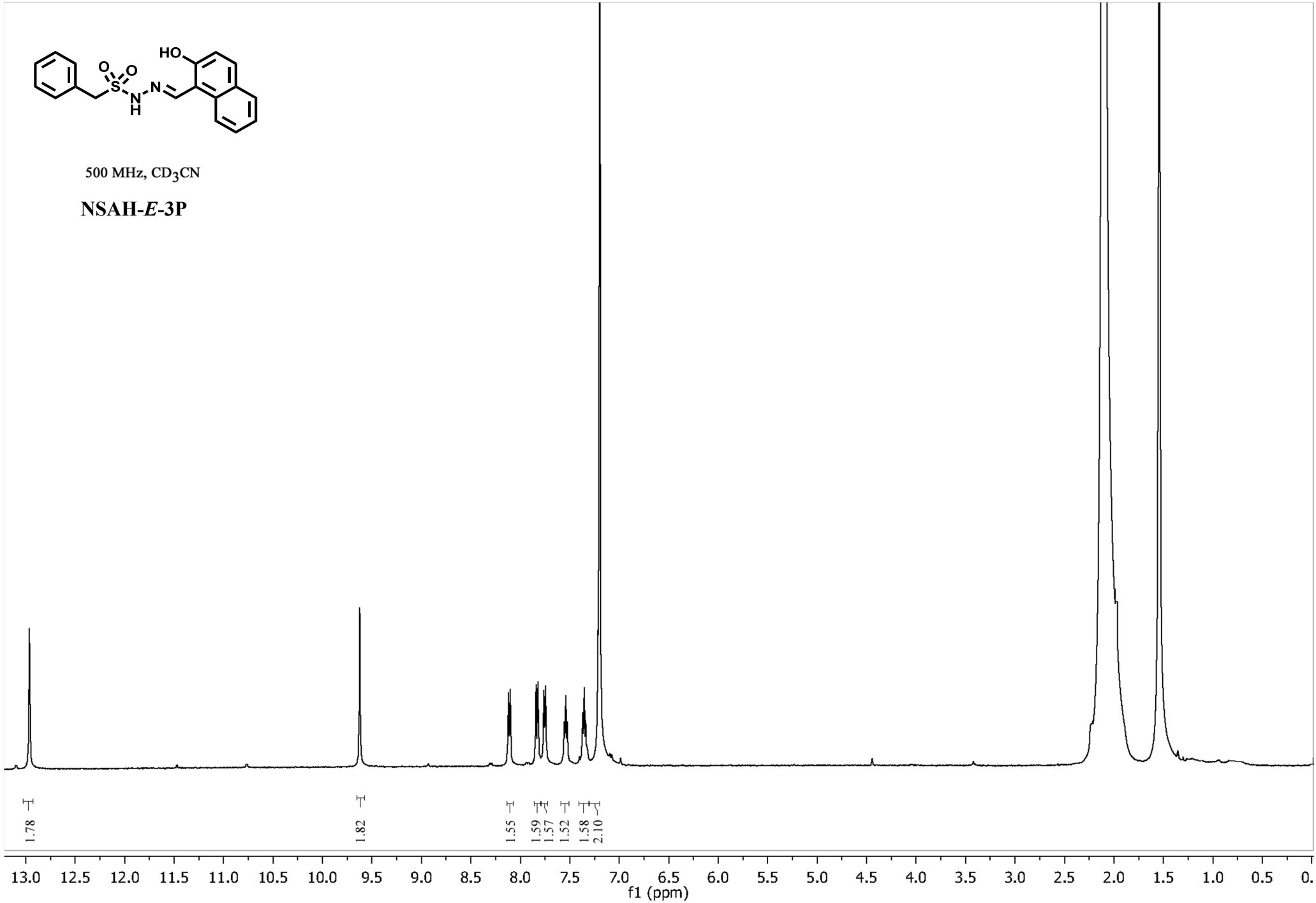
NSAH-*E*-3O

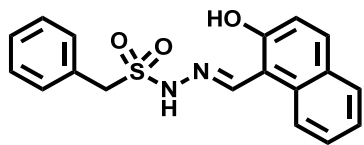




500 MHz, CD₃CN

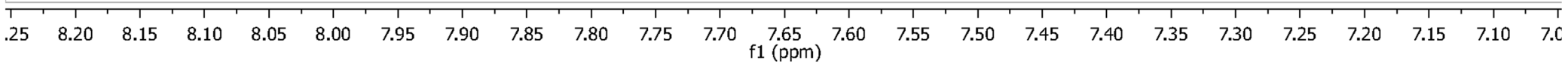
NSAH-E-3P

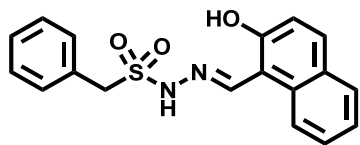




500 MHz, CD₃CN

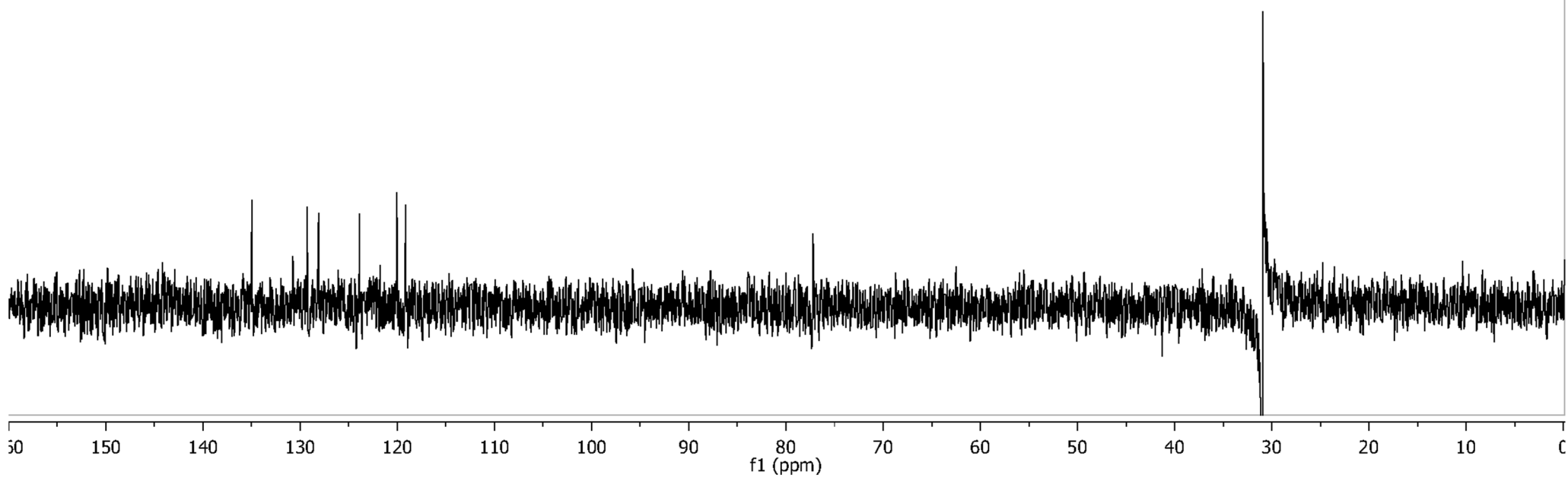
NSAH-E-3P

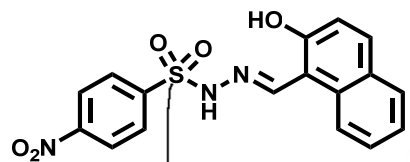




125 MHz, CD₃CN

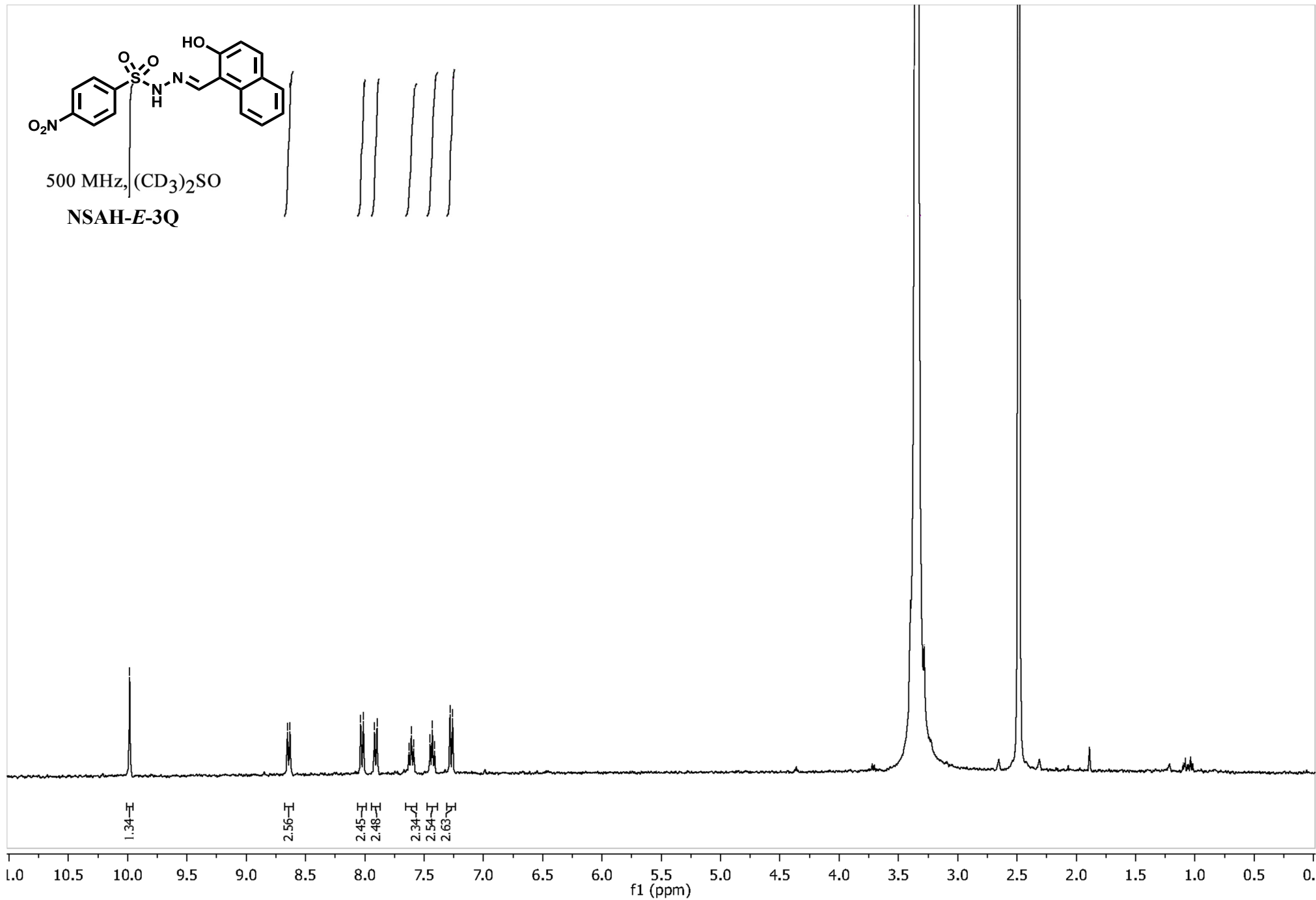
NSAH-E-3P

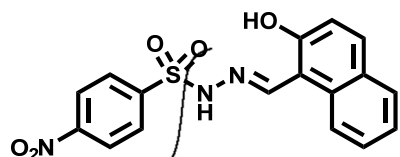




500 MHz, (CD₃)₂SO

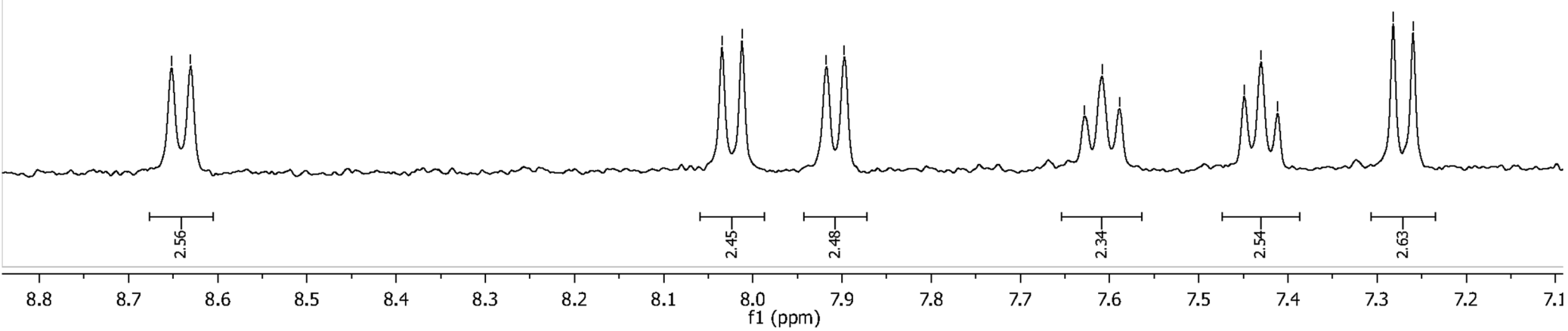
NSAH-E-3Q

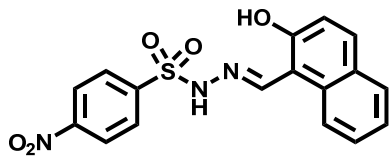




500 MHz, (CD₃)₂SO

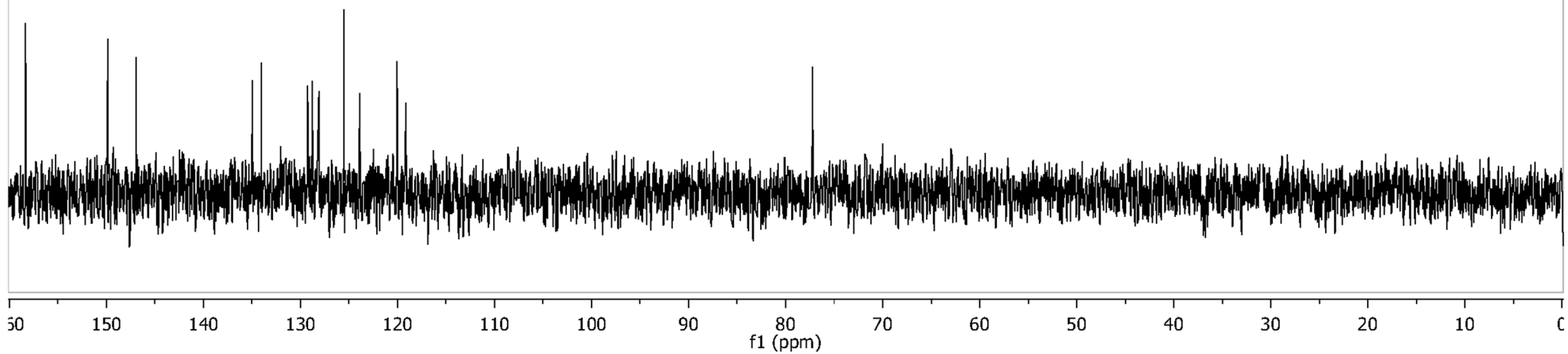
NSAH-E-3Q

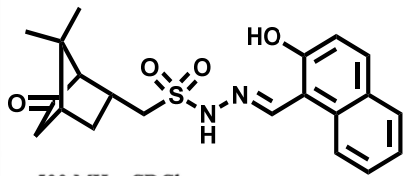




125 MHz, CCID₃

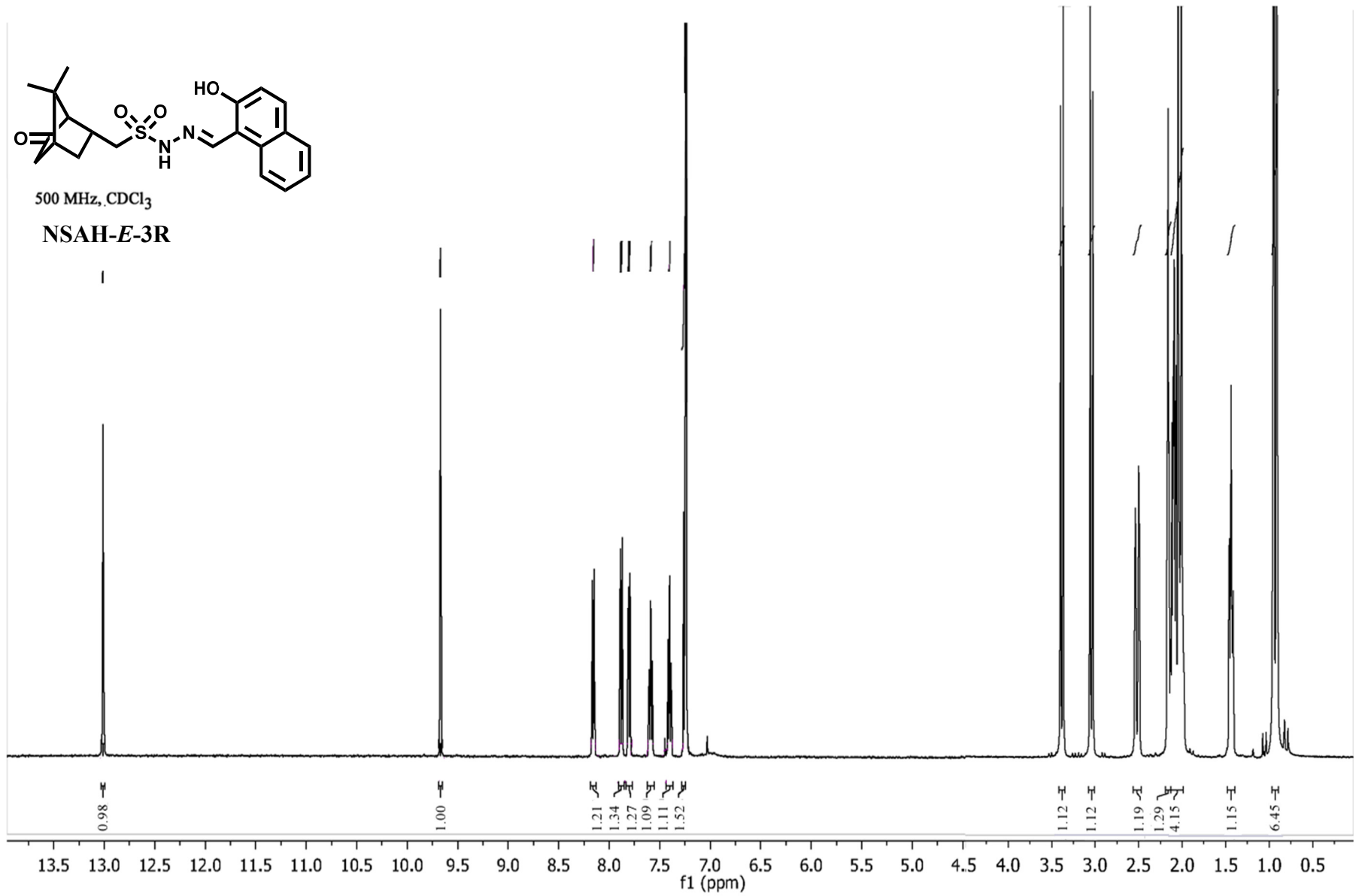
NSAH-E-3Q

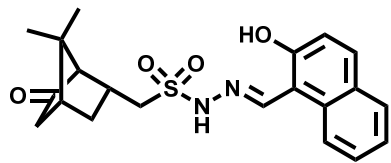




500 MHz, CDCl₃

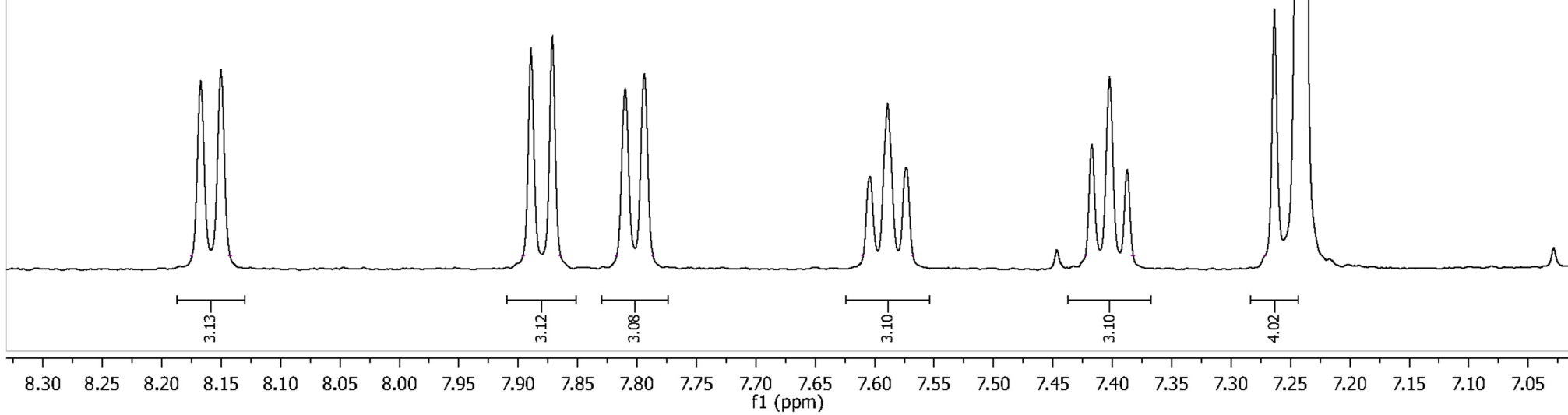
NSAH-E-3R

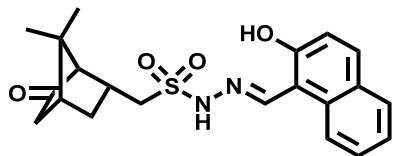




500 MHz, CDCl₃

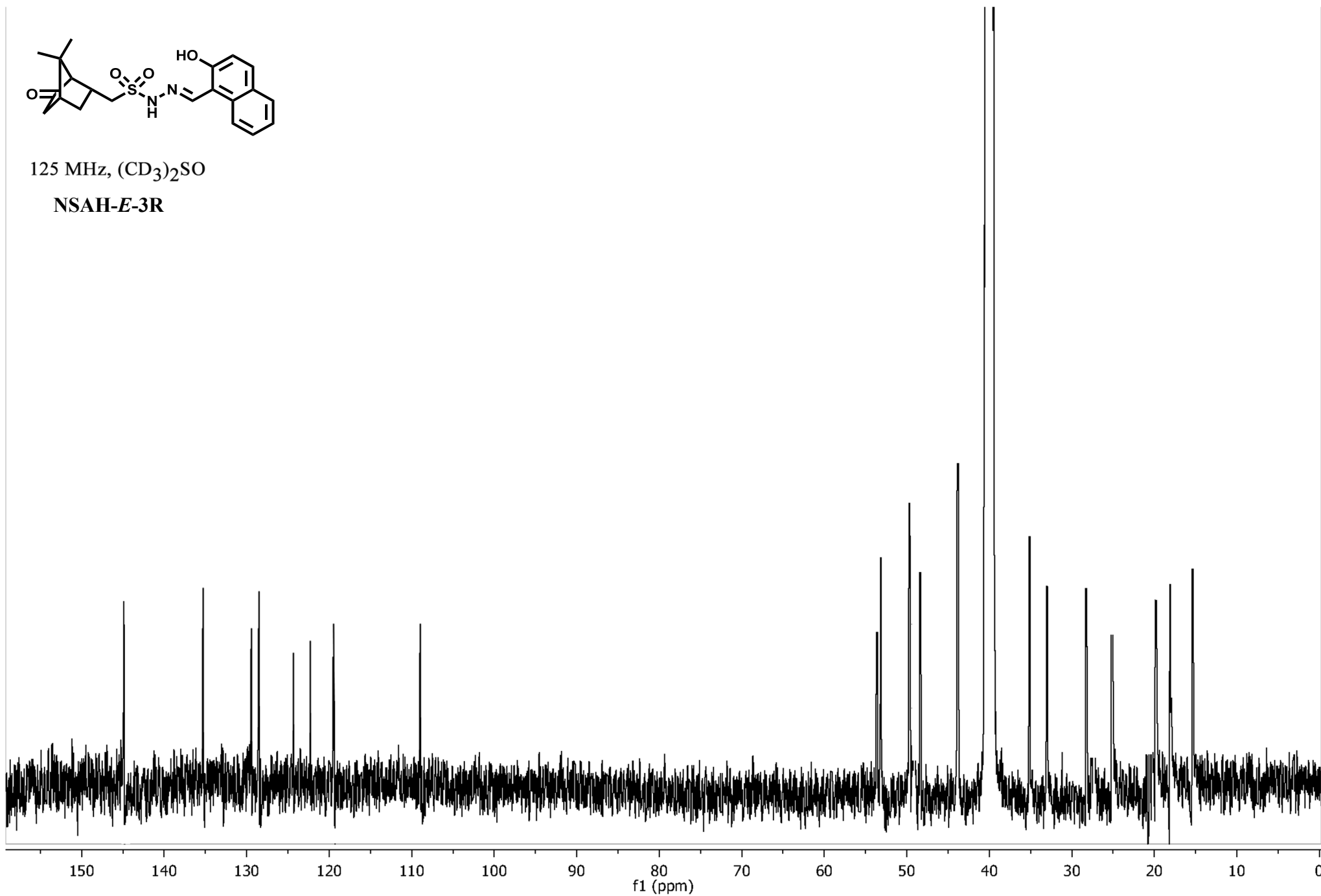
NSAH-E-3R

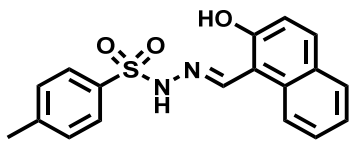




125 MHz, (CD₃)₂SO

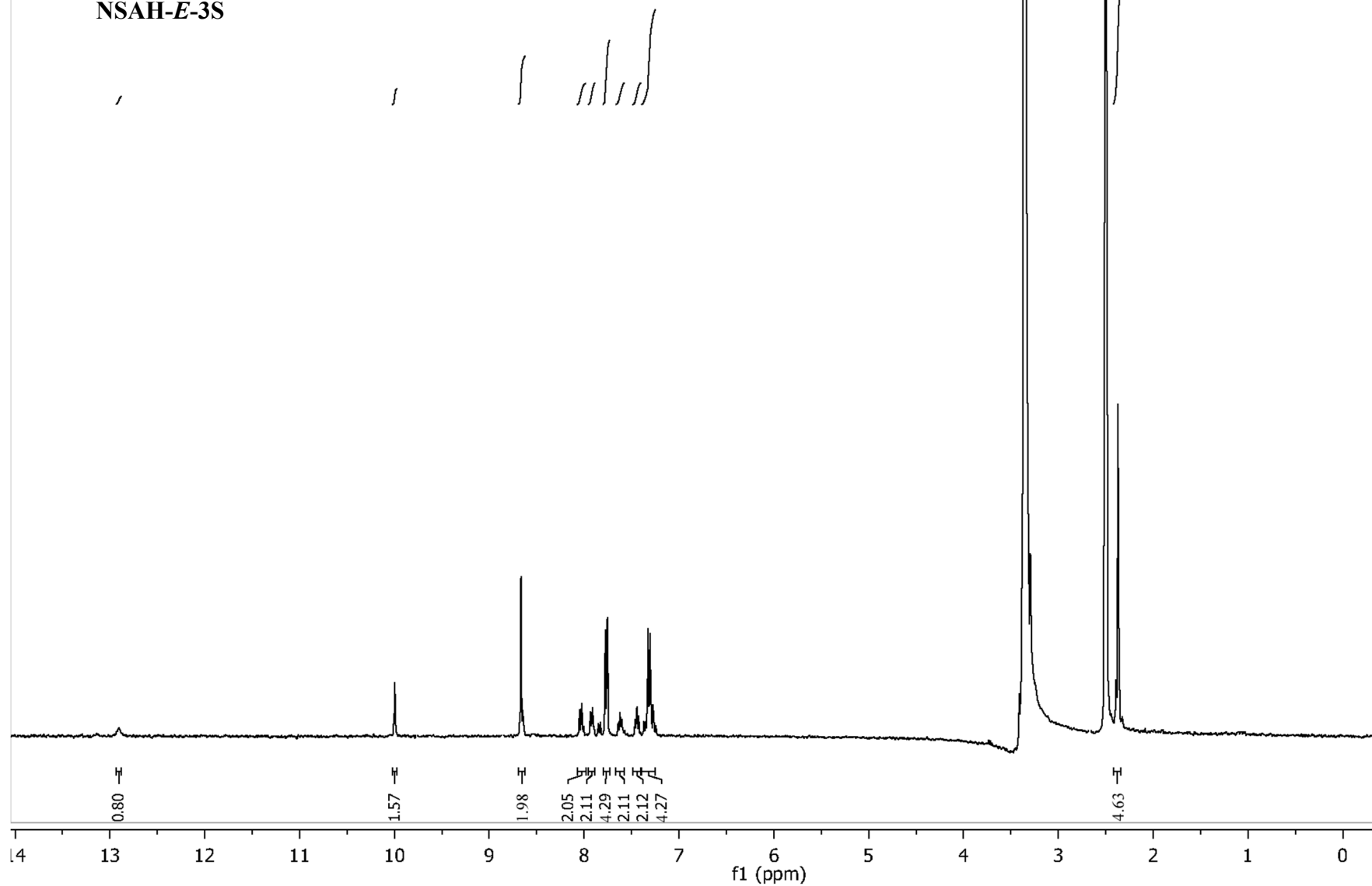
NSAH-E-3R

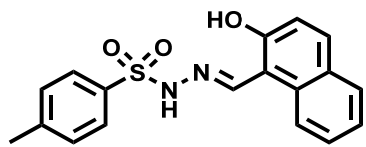




(CD₃)₂SO 500 MHz

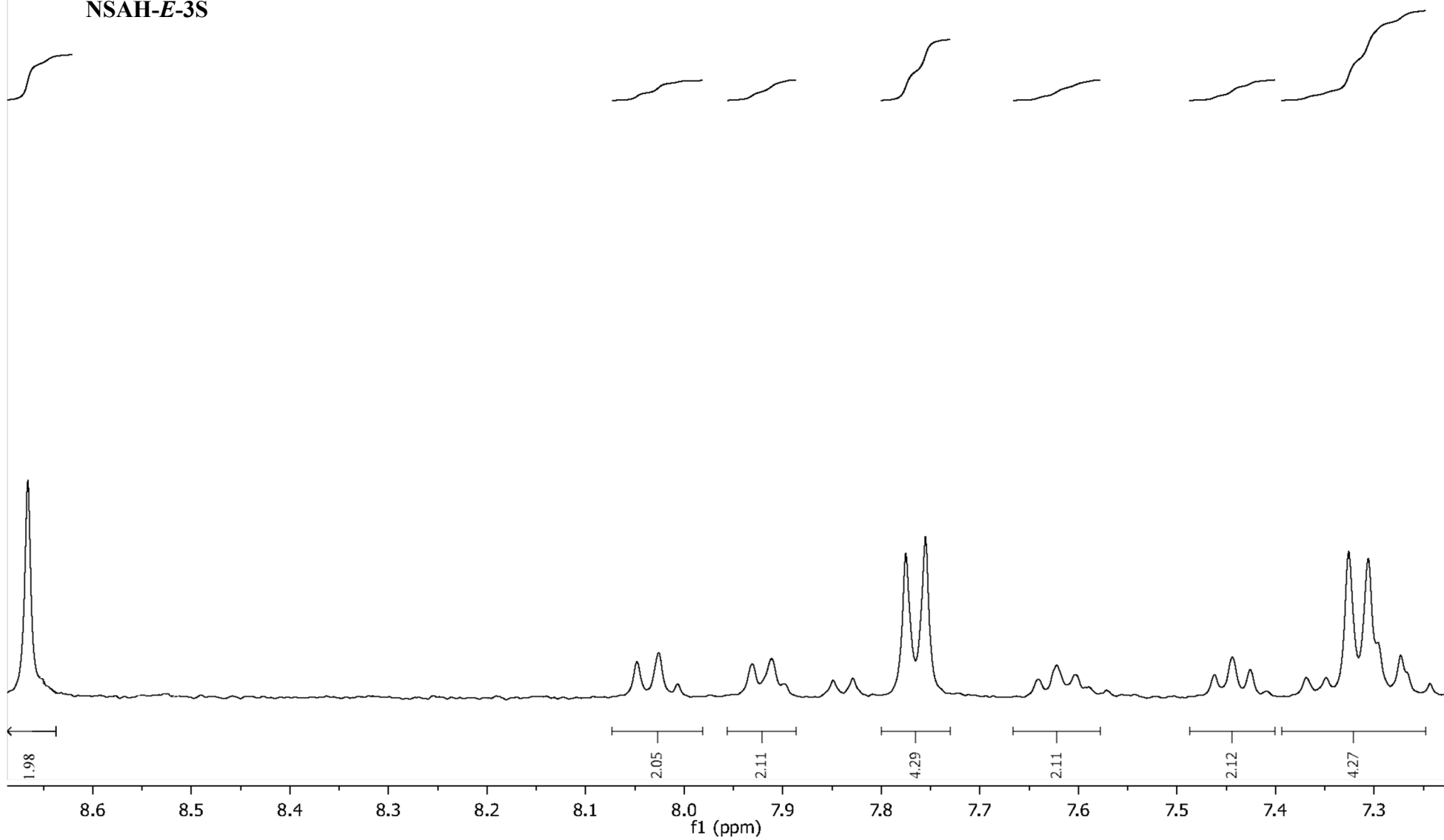
NSAH-E-3S

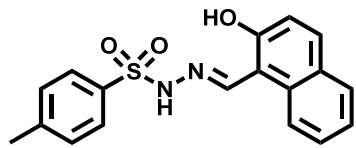




(CD₃)₂SO 500 MHz

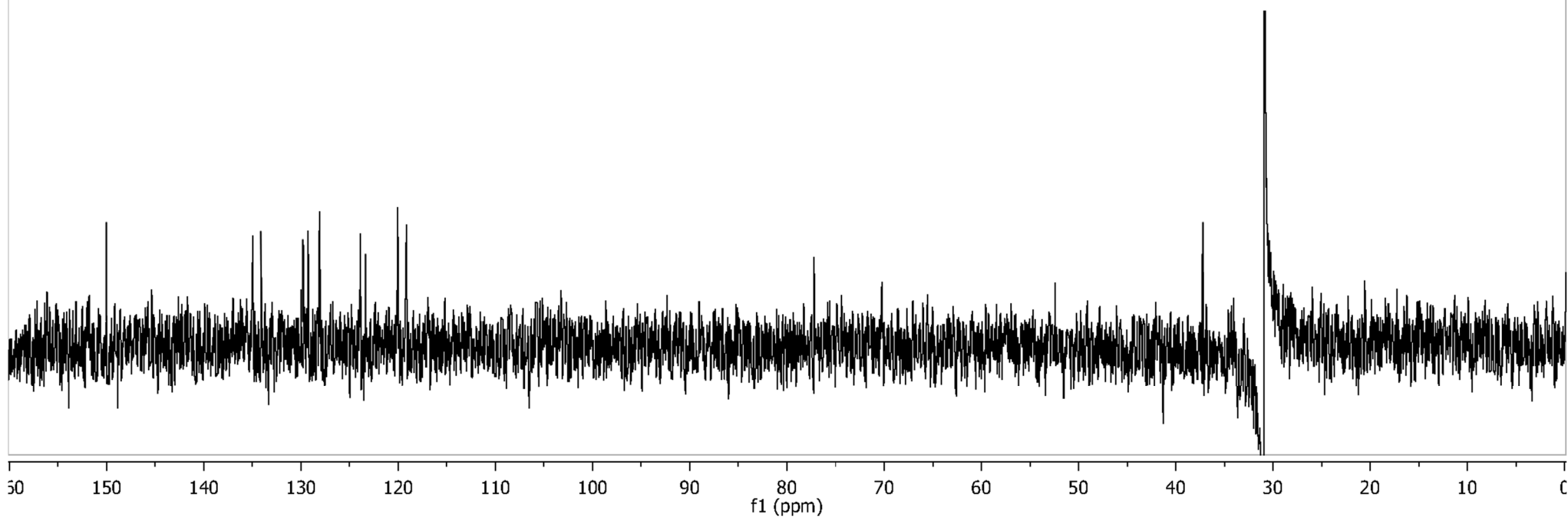
NSAH-E-3S

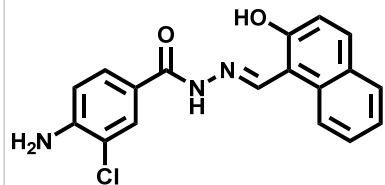




125 MHz, CDCl₃

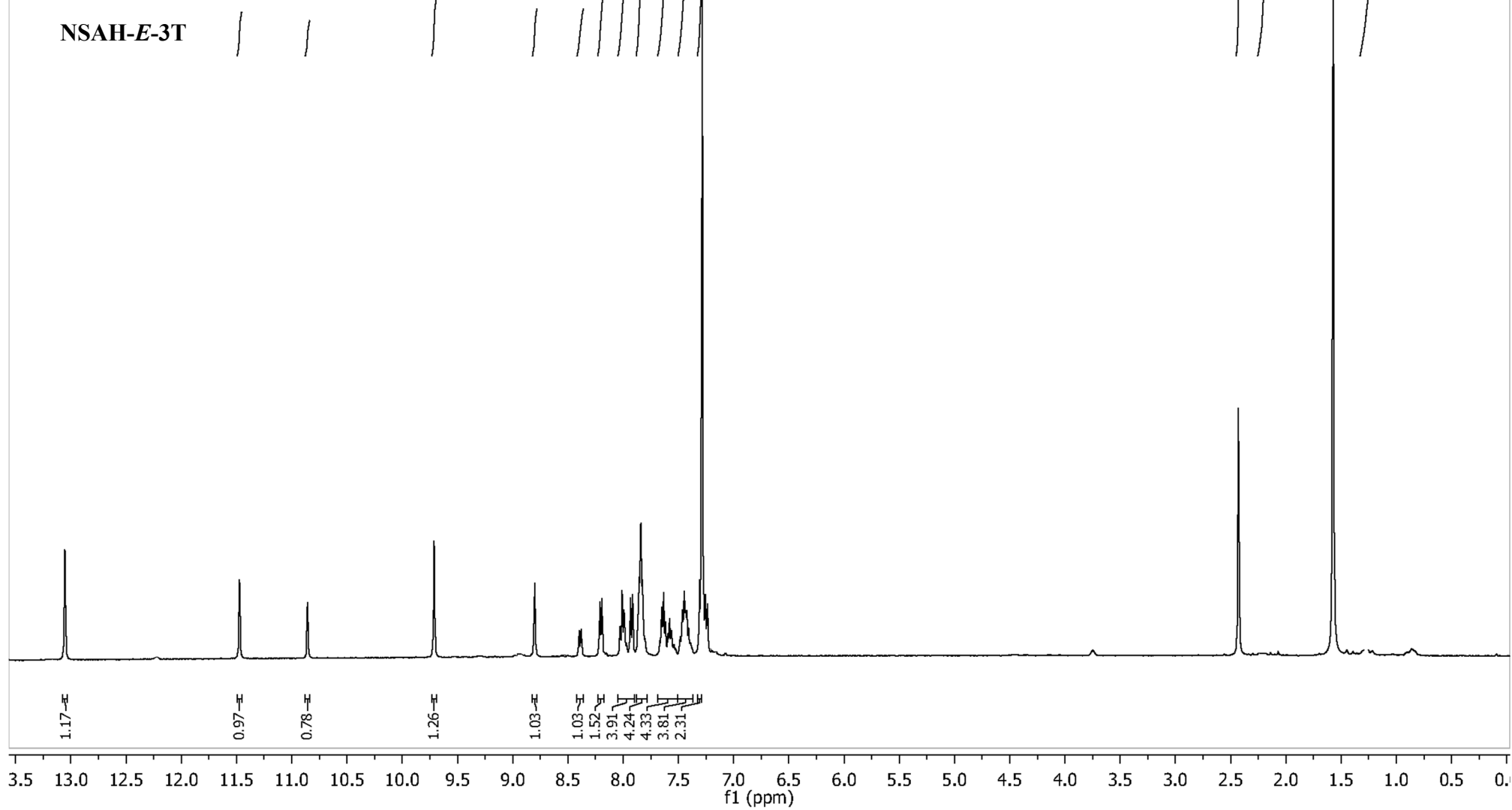
NSAH-E-3S

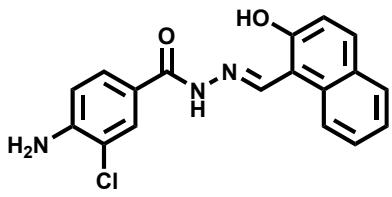




500 MHz,
CDCl₃

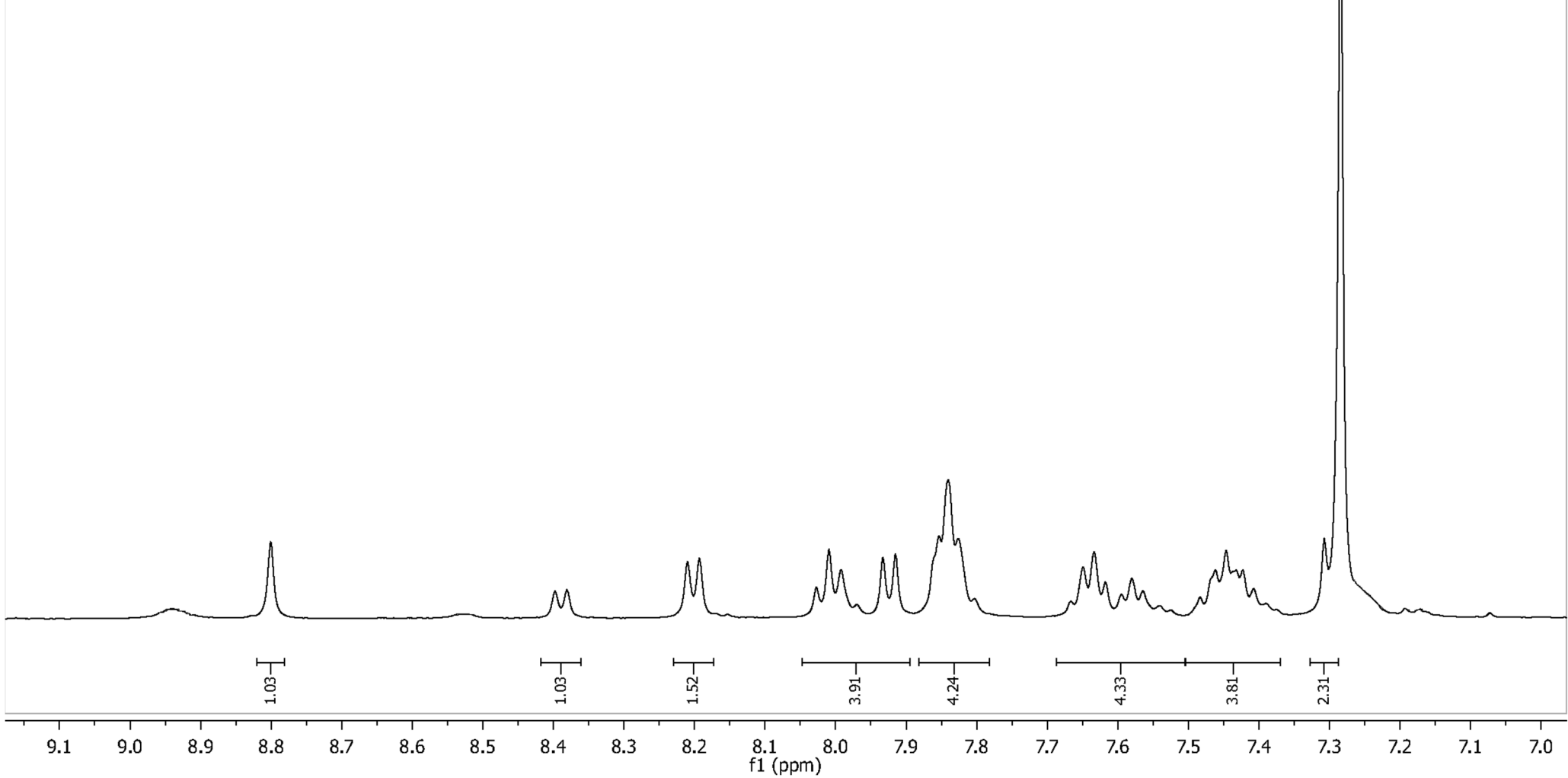
NSAH-E-3T

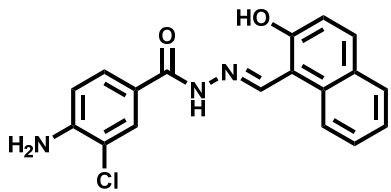




500 MHz,
CDCl₃

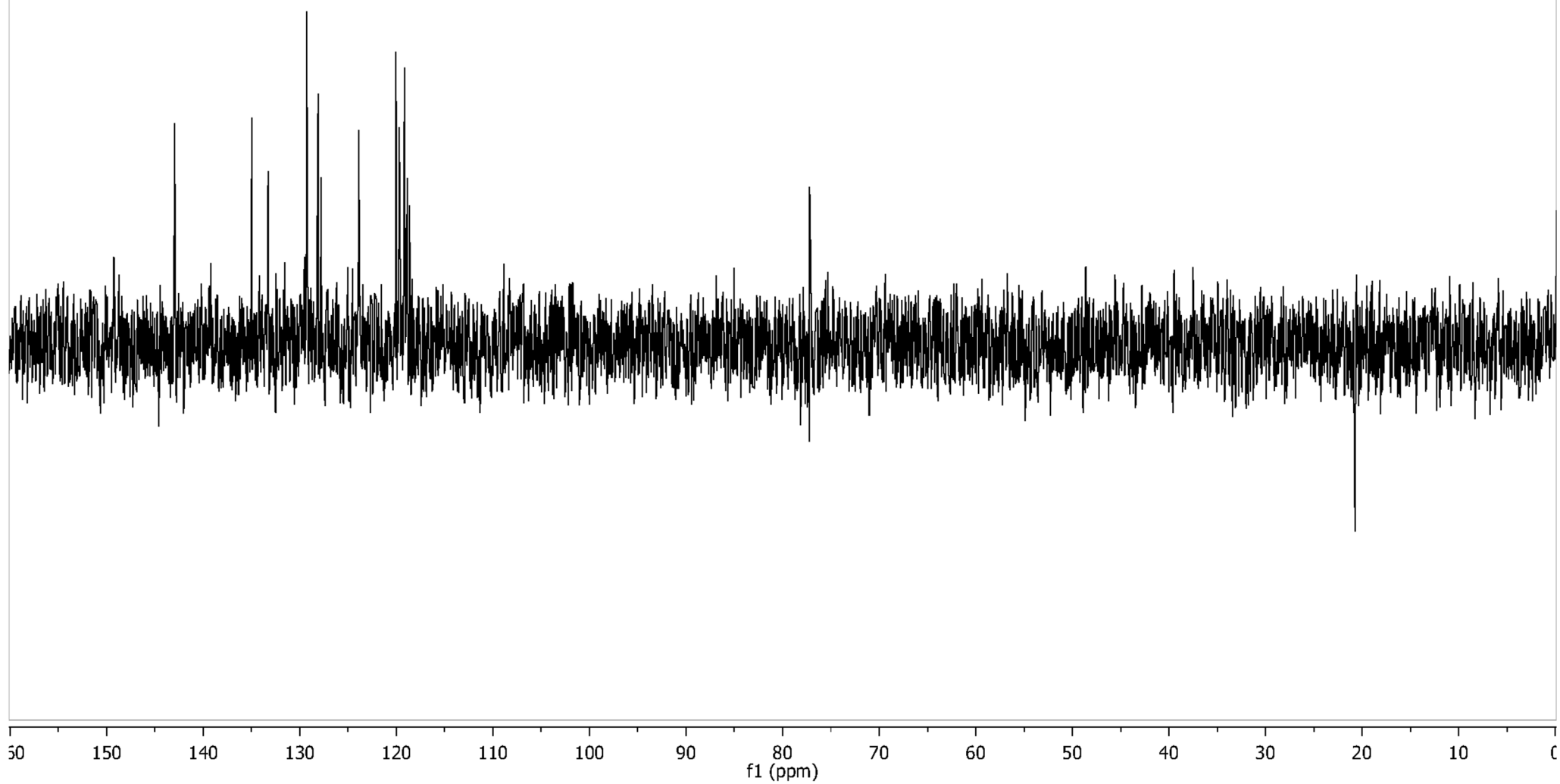
NSAH-E-3T

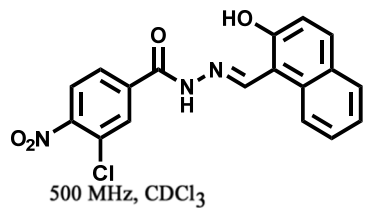




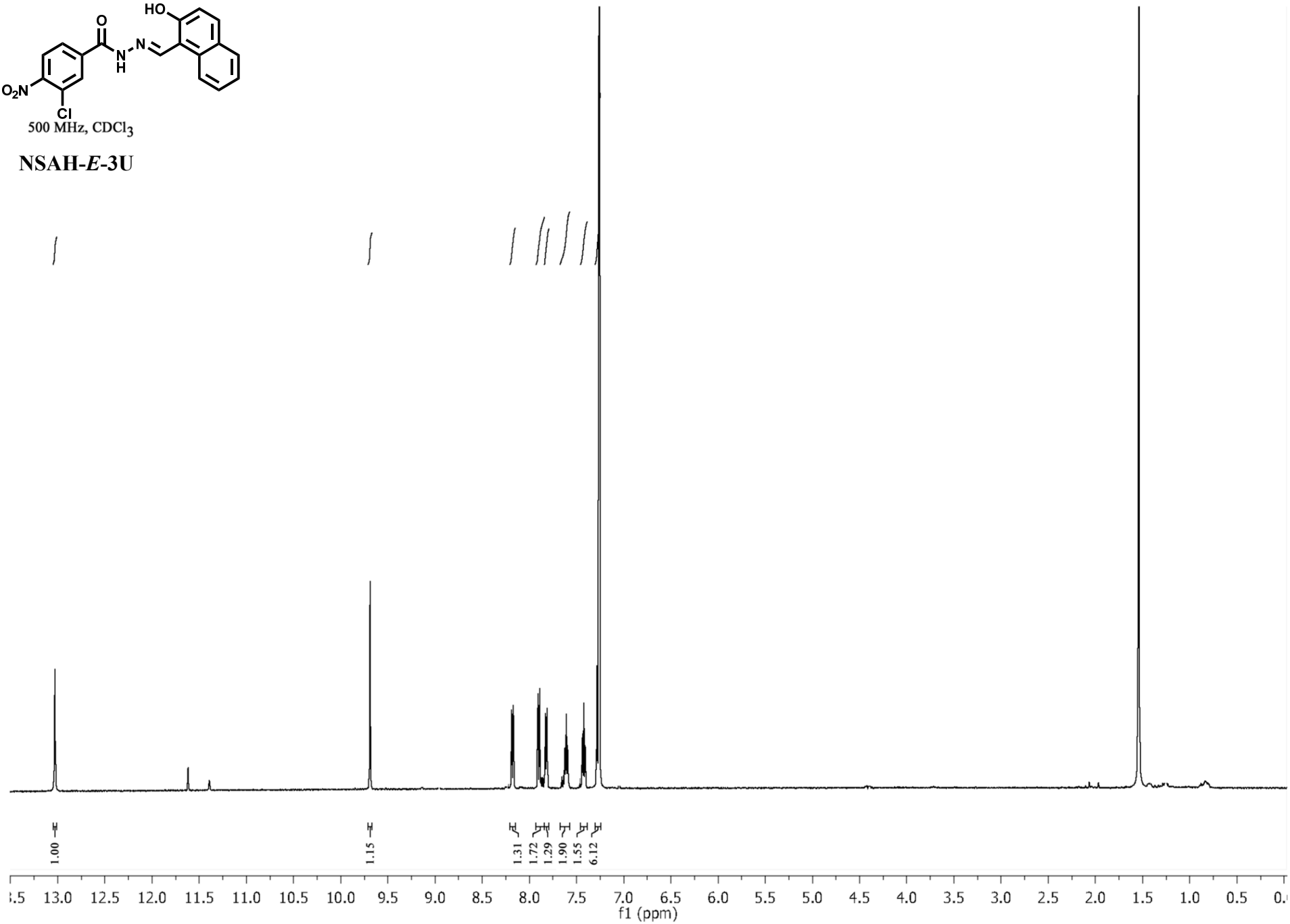
125 MHz,
CDCl₃

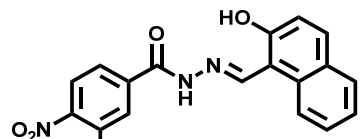
NSAH-E-3T





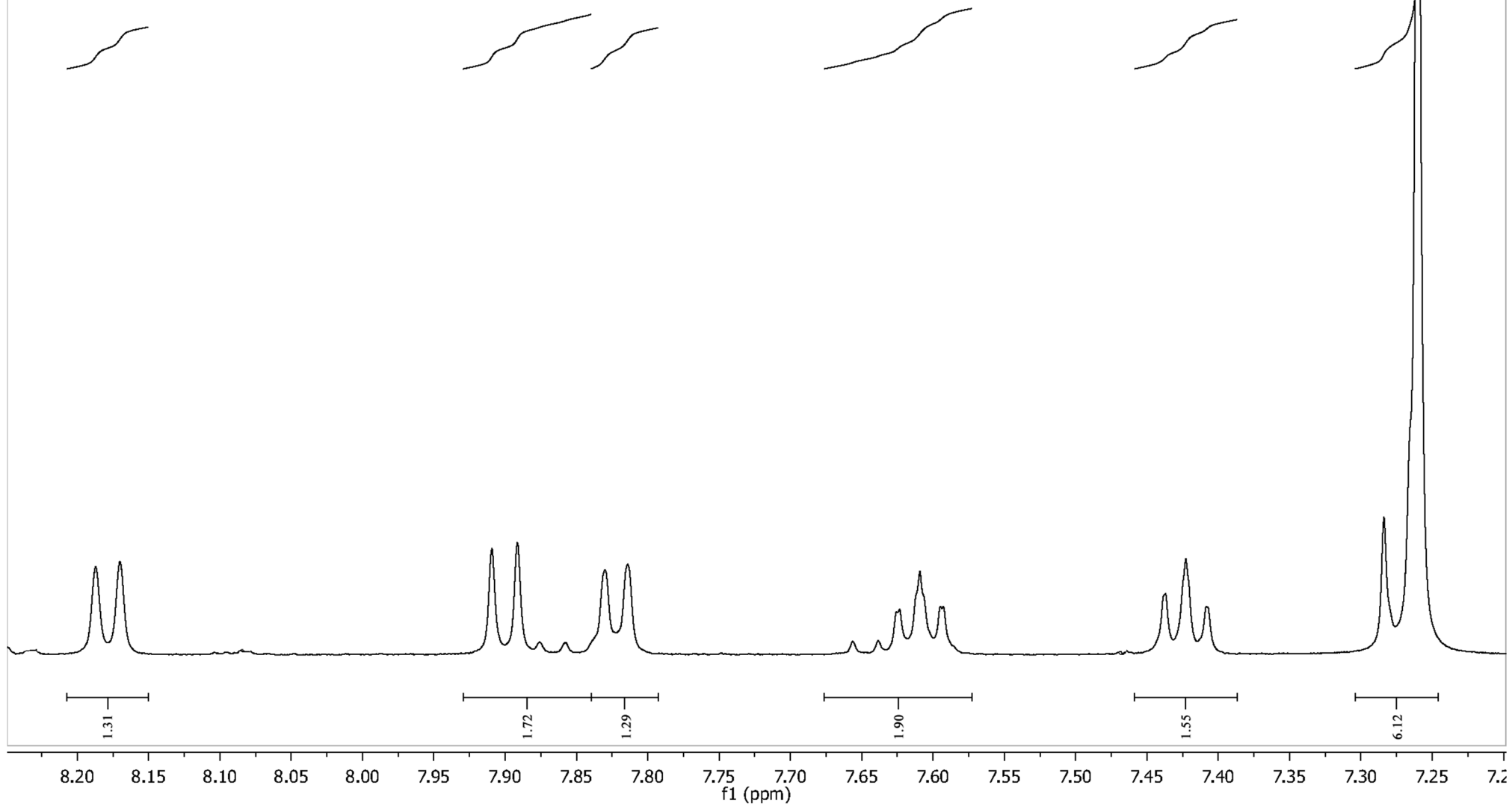
NSAH-E-3U

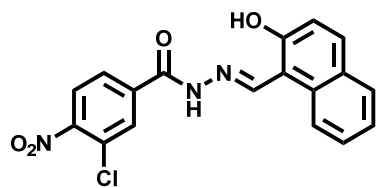




500 MHz, CDCl₃

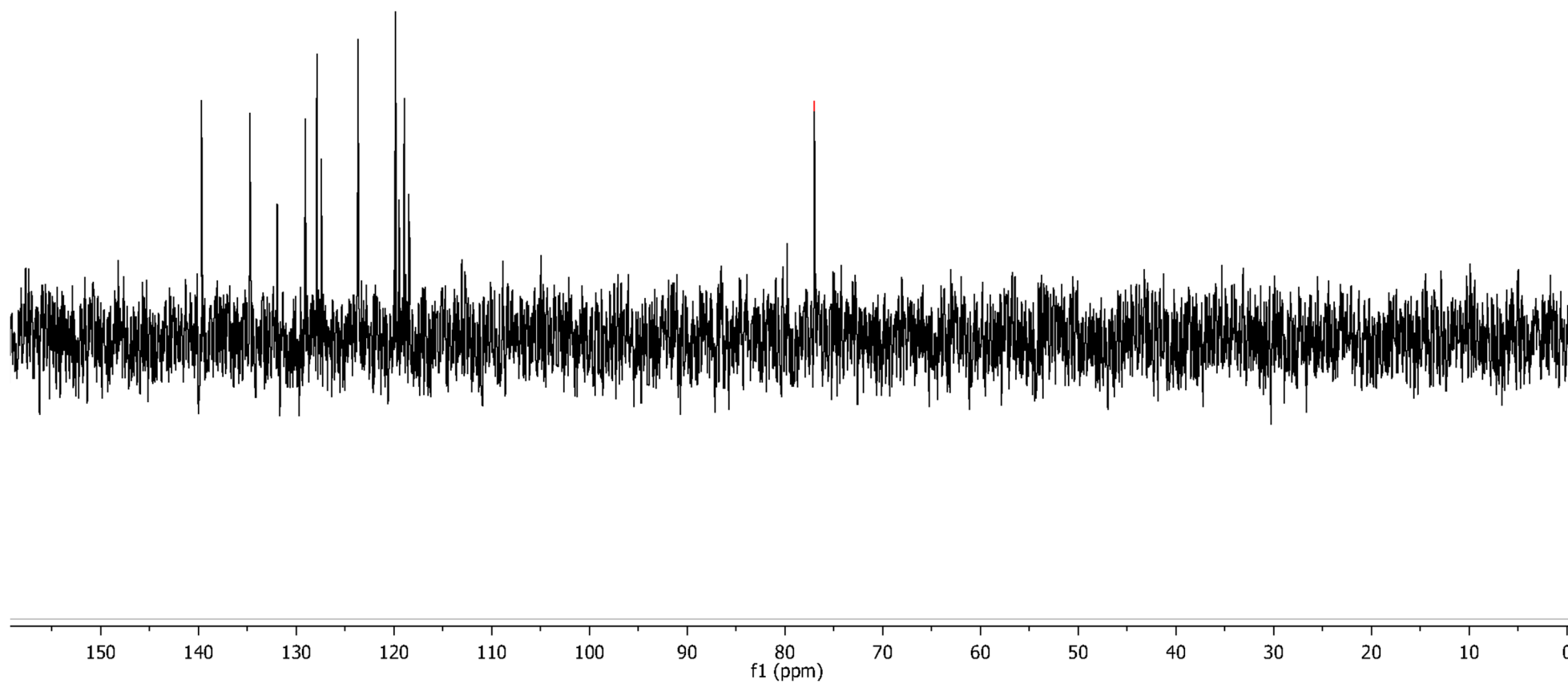
NSAH-E-3U

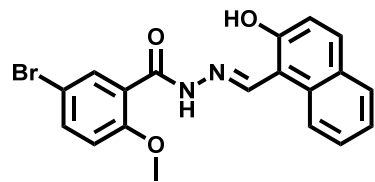




125 MHz, CDCl₃

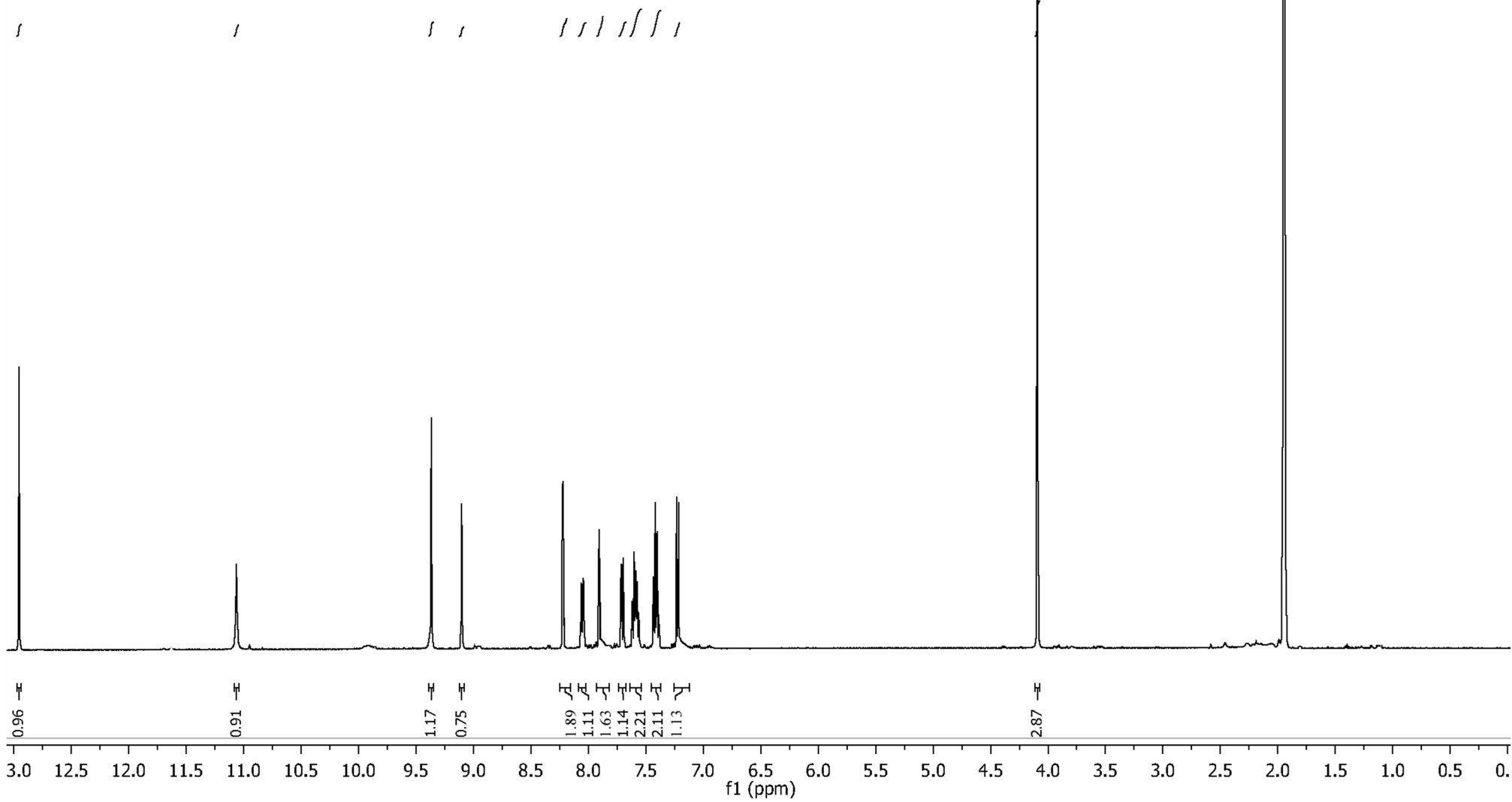
NSAH-*E*-3U

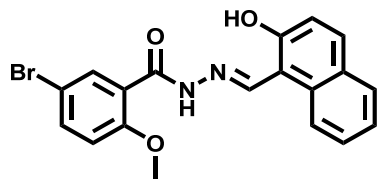




500 MHz, CD₃CN

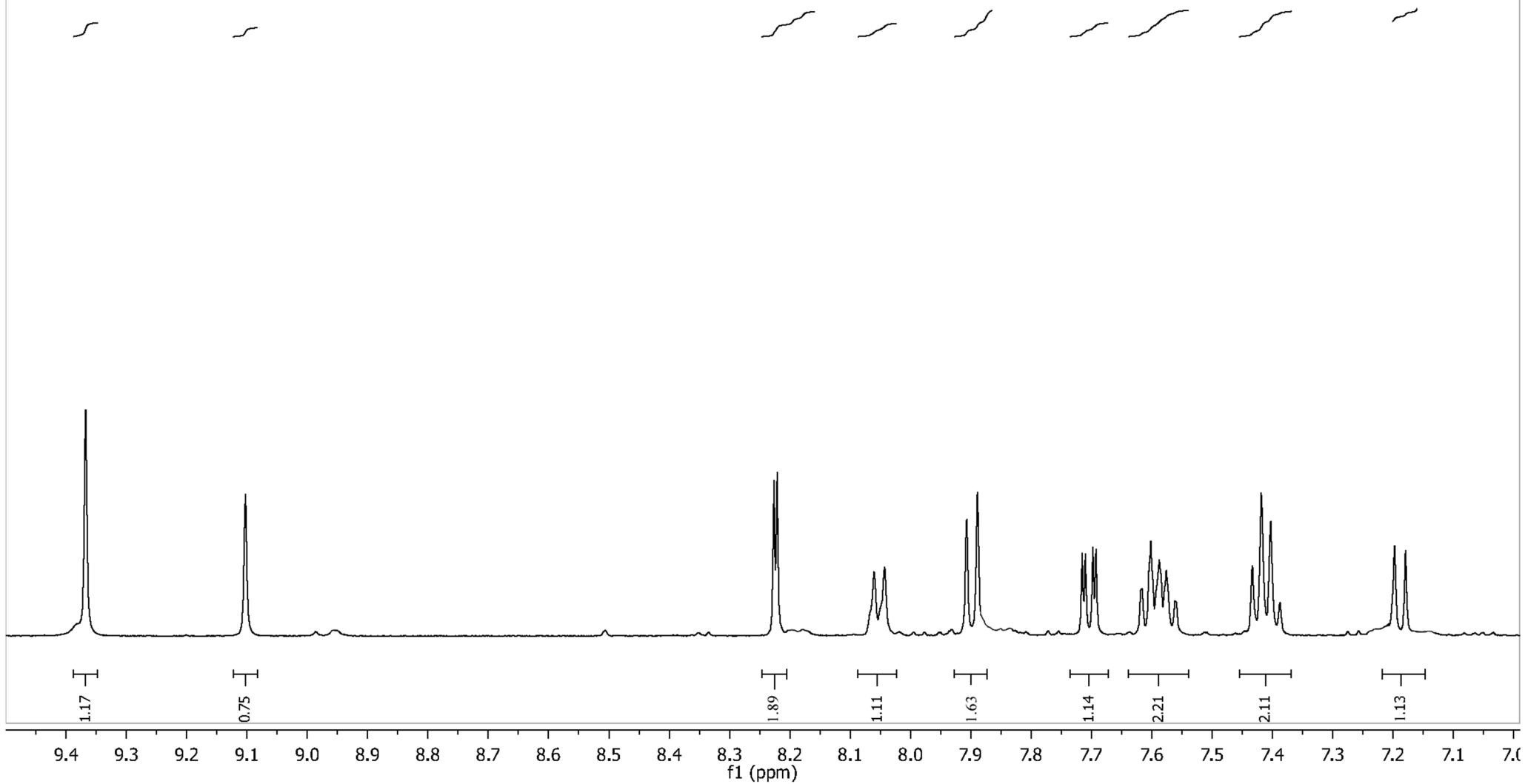
NSAH-E-3V

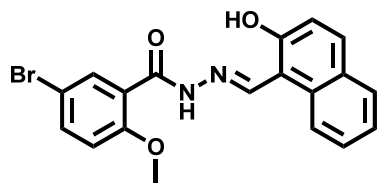




500 MHz, CD₃CN

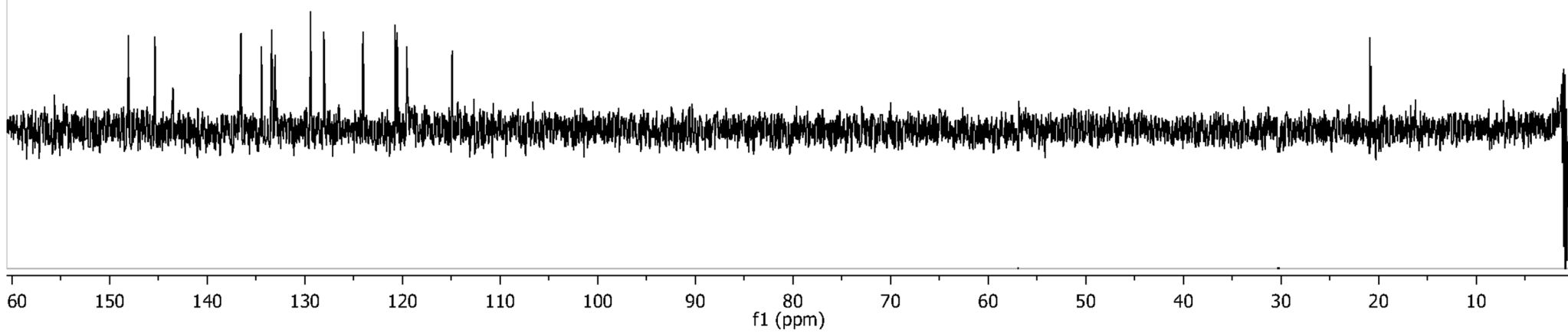
NSAH-E-3V

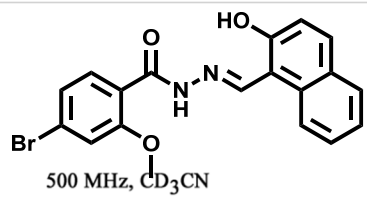




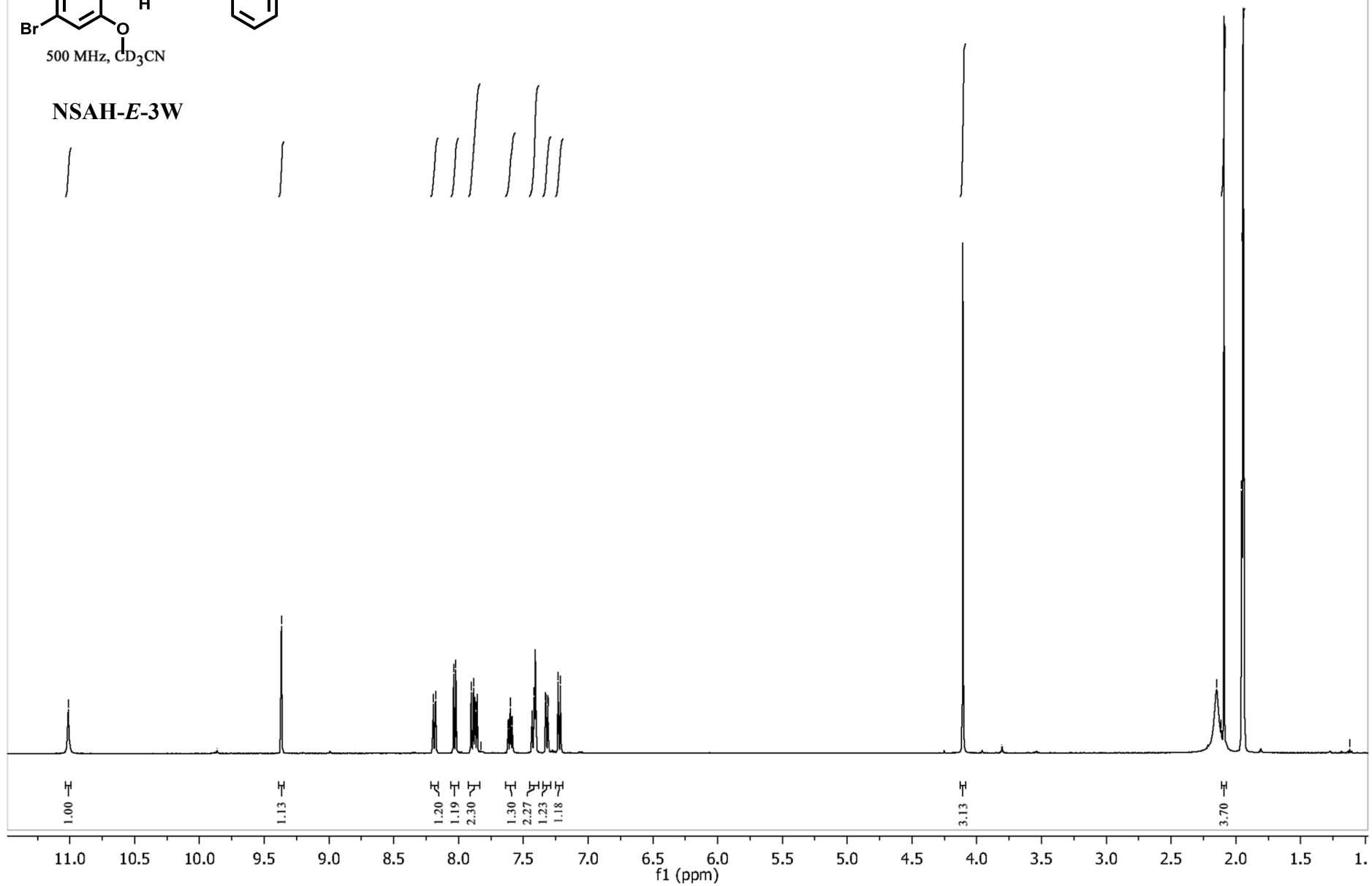
125 MHz, CD₃CN

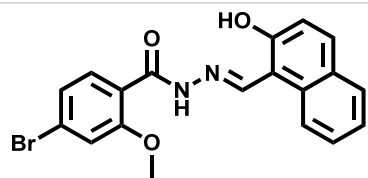
NSAH-E-3V





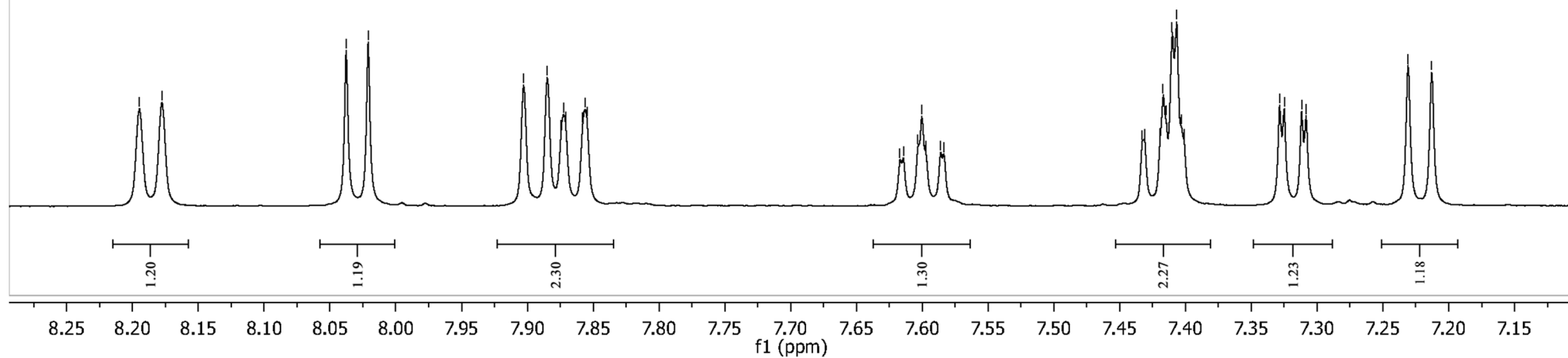
NSAH-E-3W

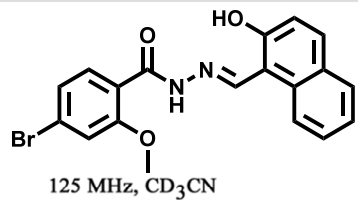




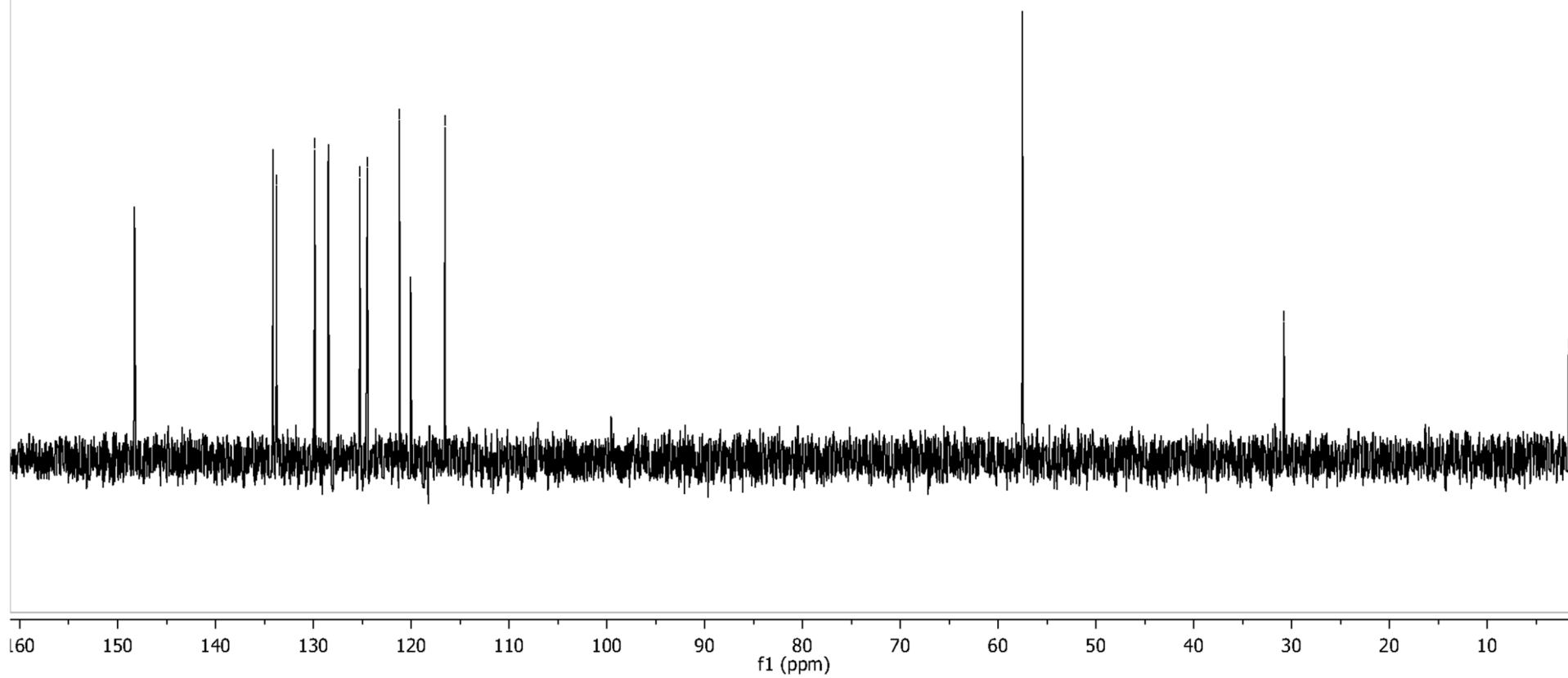
500 MHz, CD₃CN

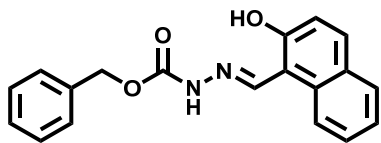
NSAH-E-3W





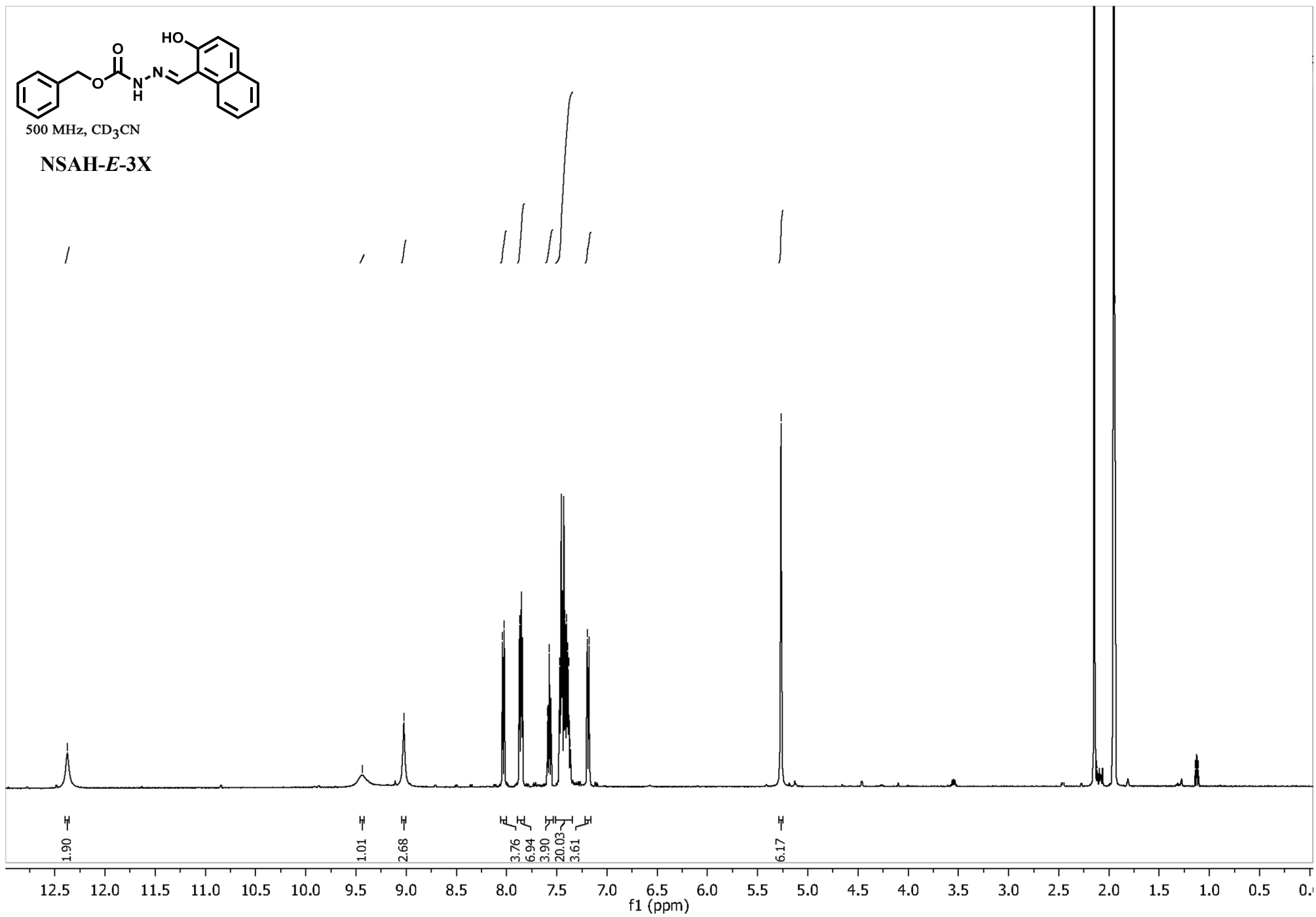
NSAH-*E*-3W

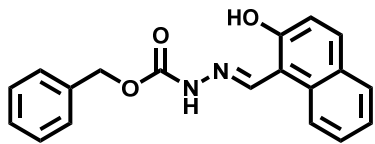




500 MHz, CD₃CN

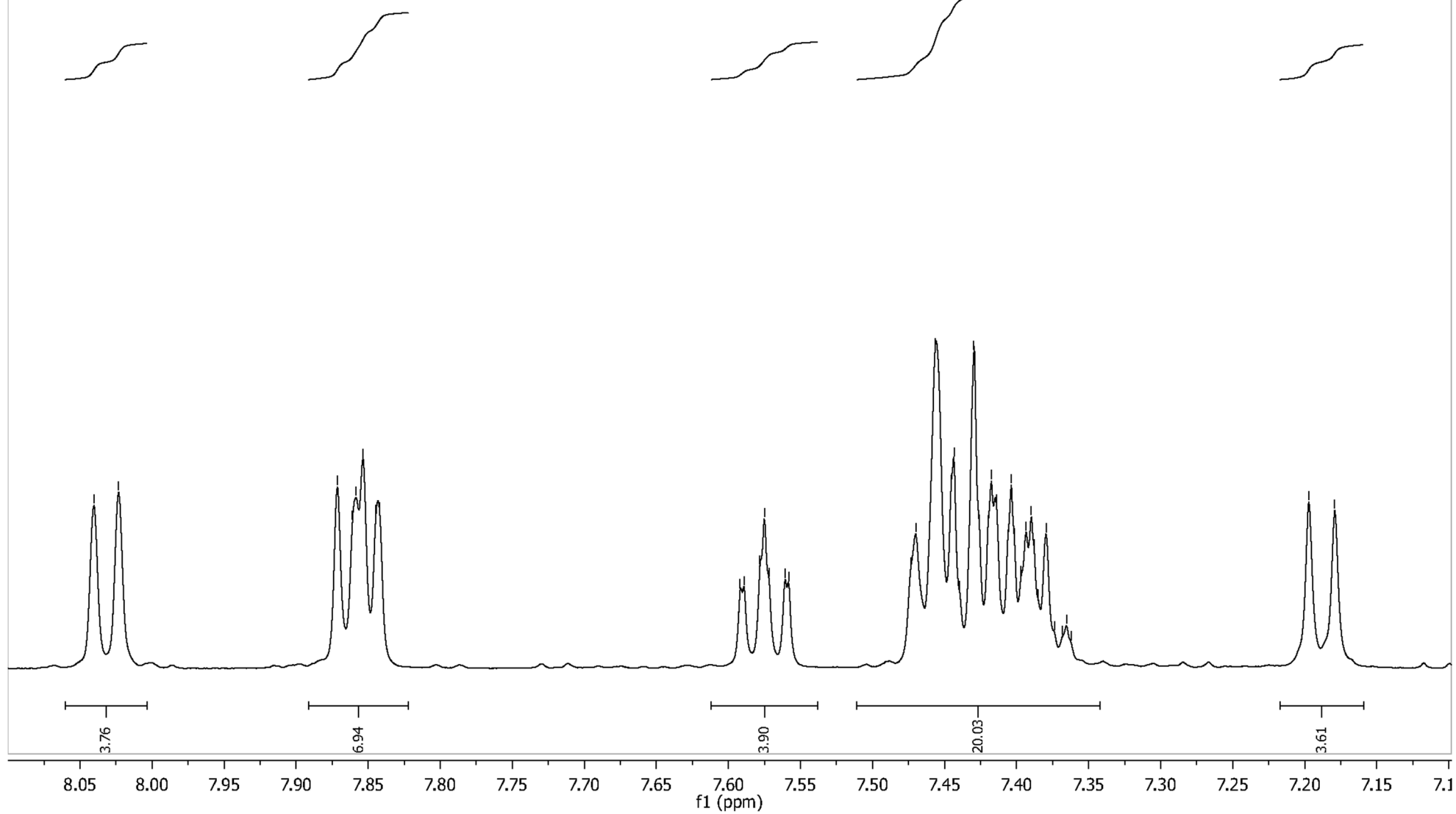
NSAH-E-3X

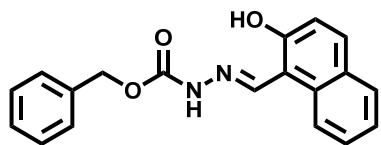




500 MHz, CD₃CN

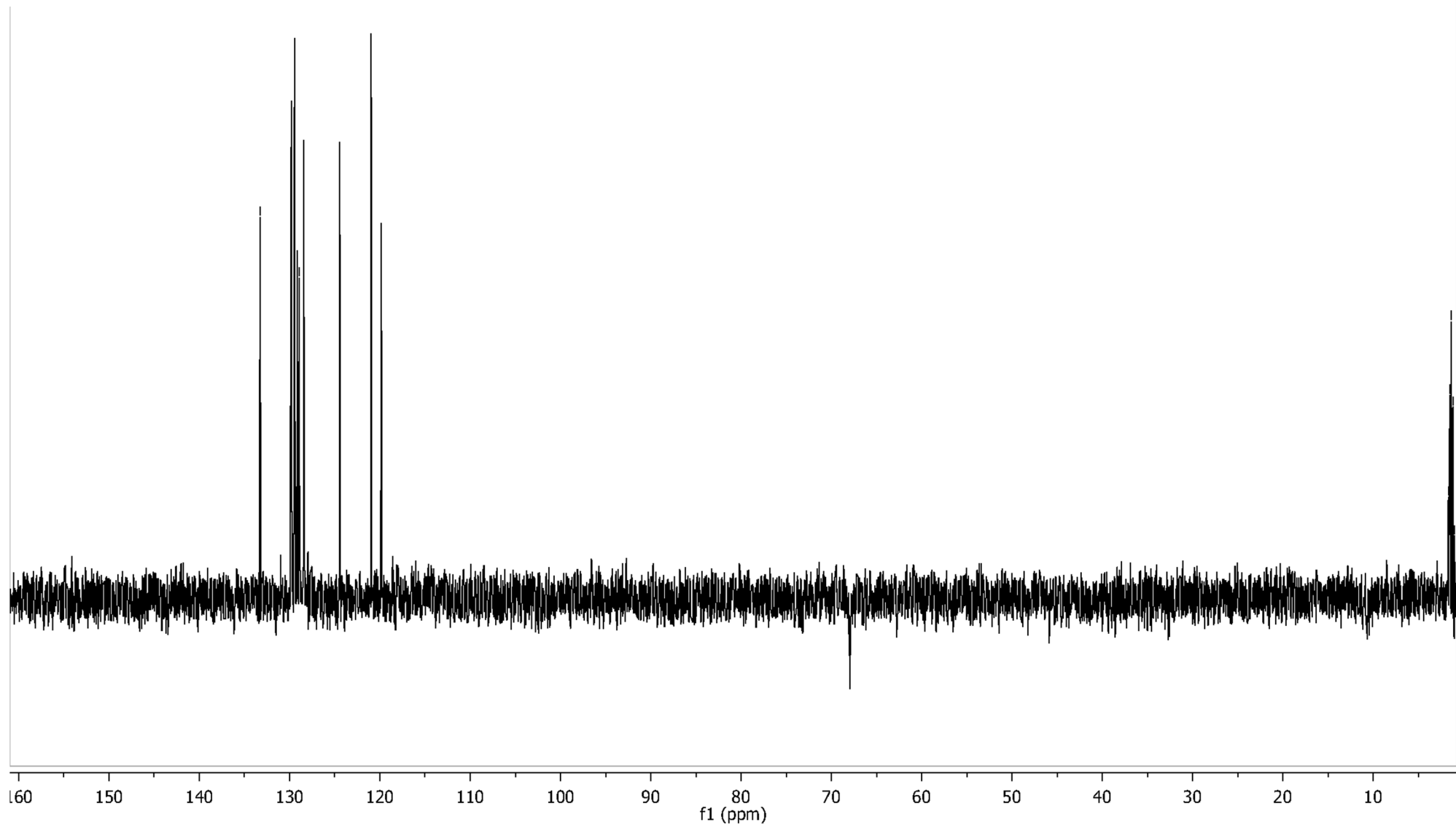
NSAH-E-3X

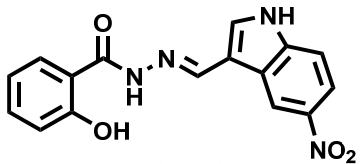




125 MHz, CD₃CN

NSAH-*E*-3X

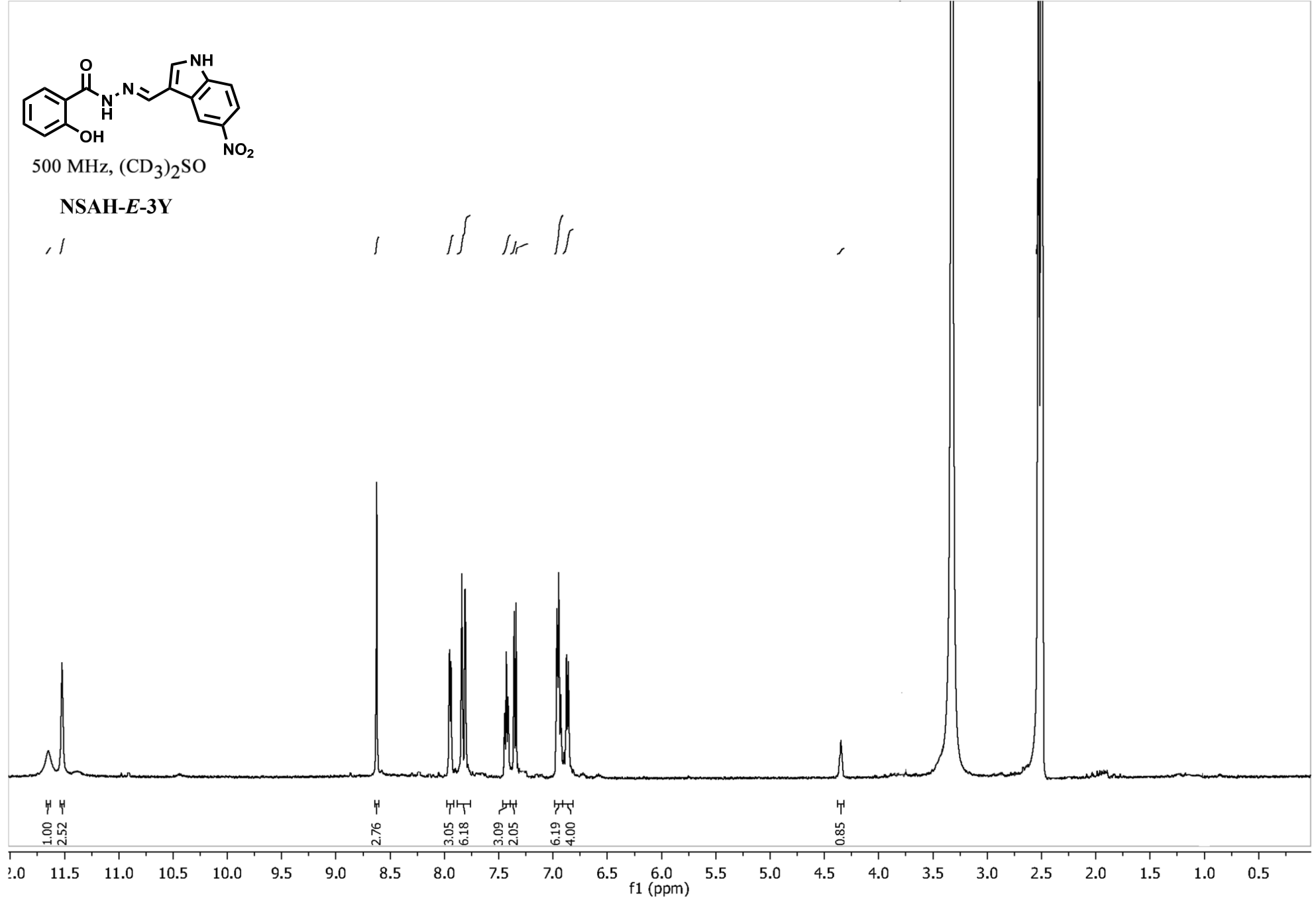


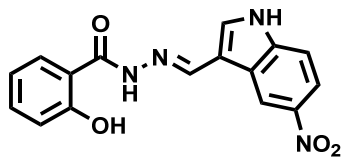


500 MHz, (CD₃)₂SO

NSAH-E-3Y

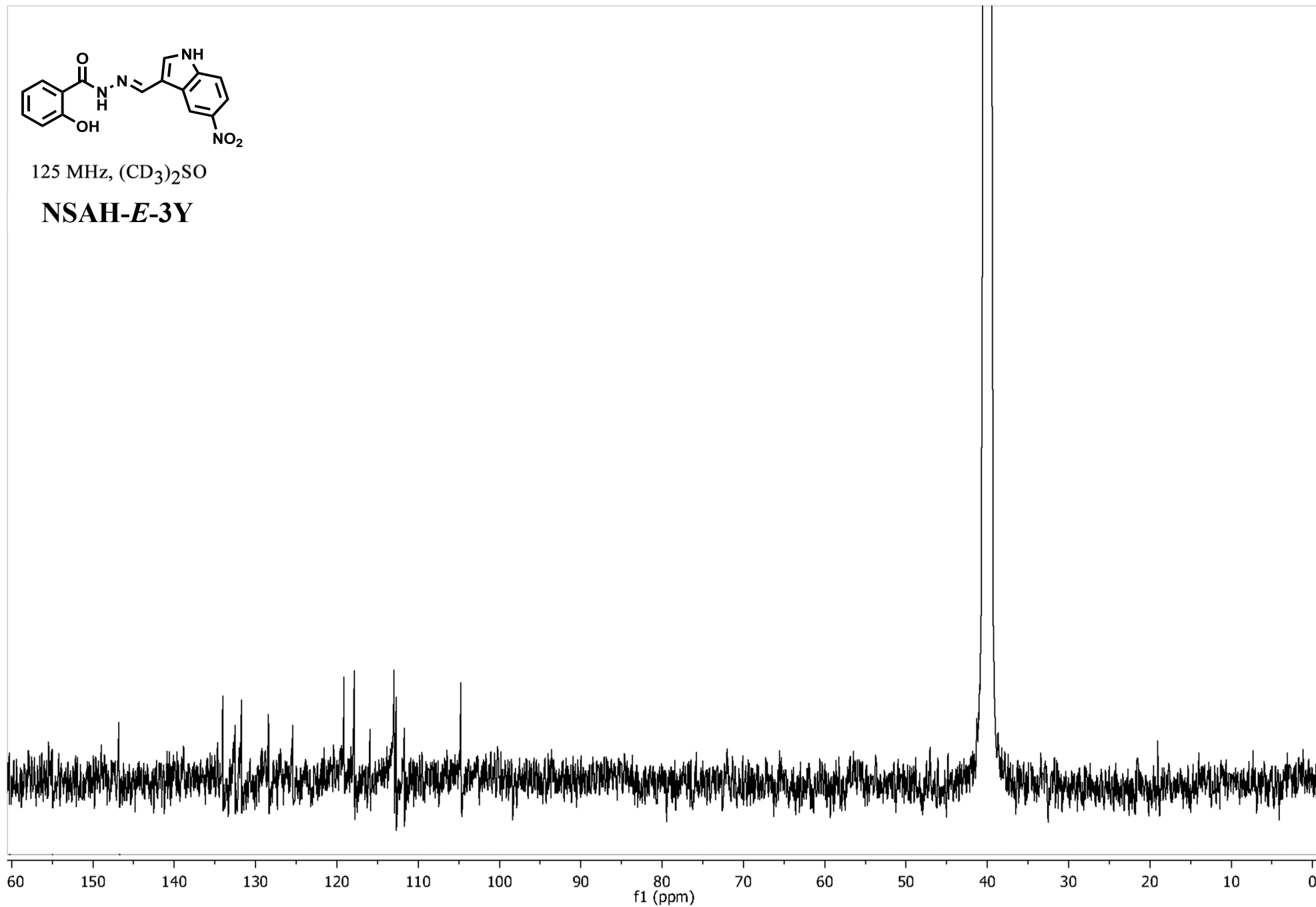
Handwritten annotations above the spectrum: *1 1 1 1 1*

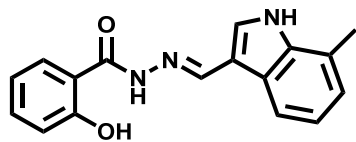




125 MHz, (CD₃)₂SO

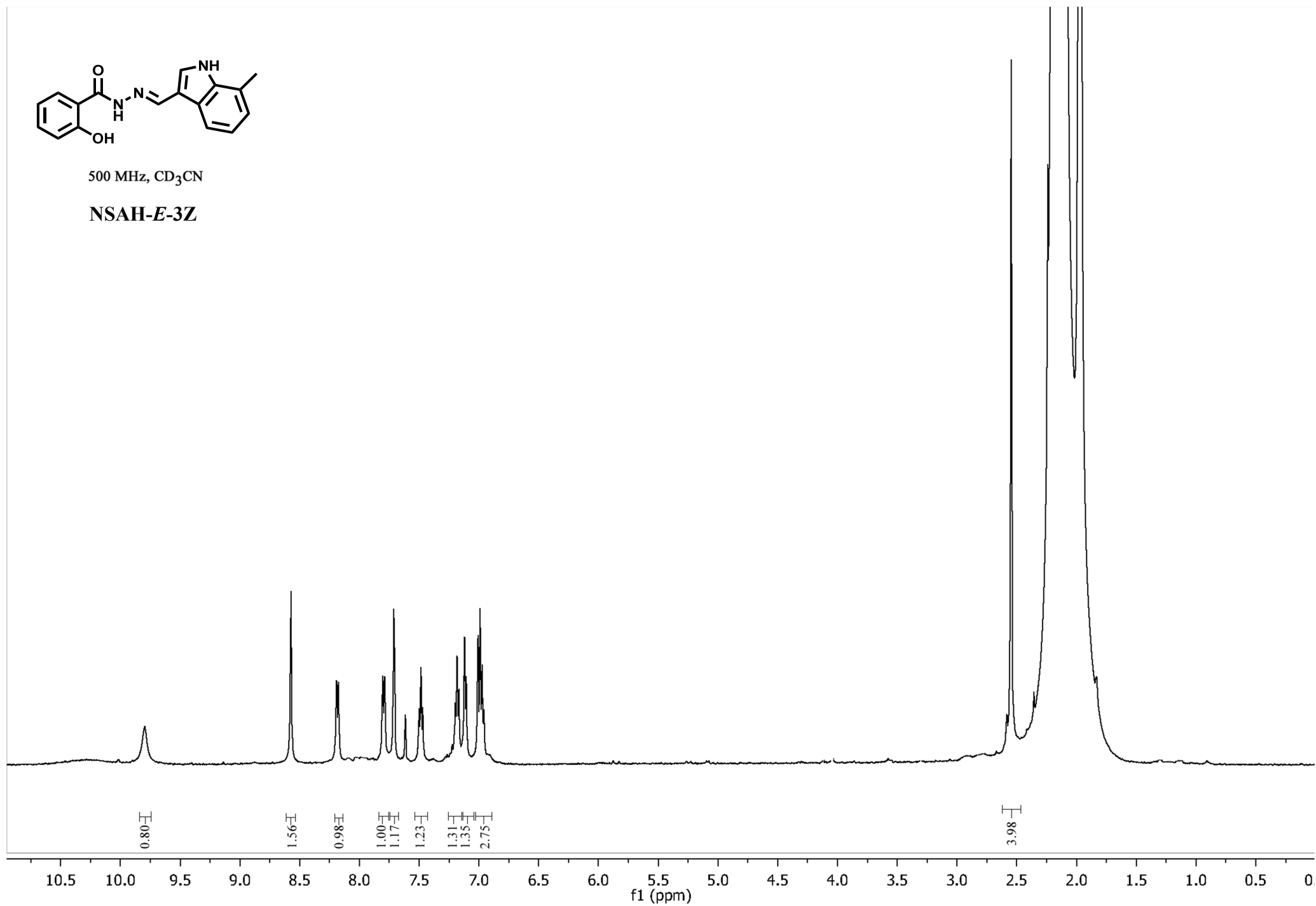
NSAH-E-3Y

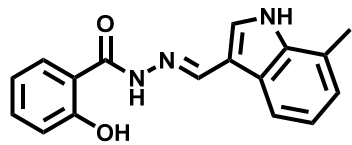




500 MHz, CD₃CN

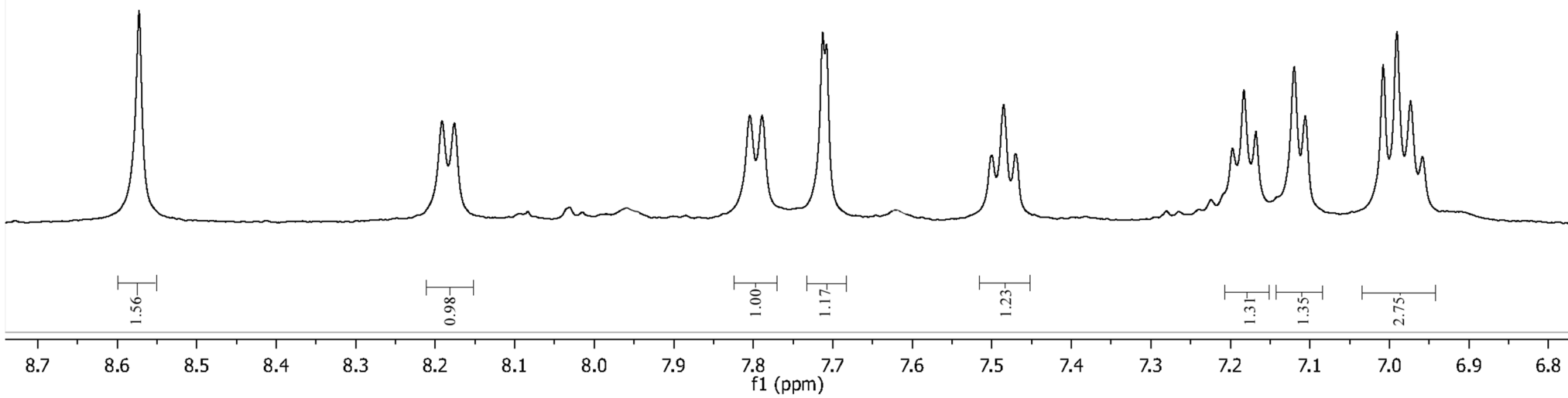
NSAH-*E*-3Z

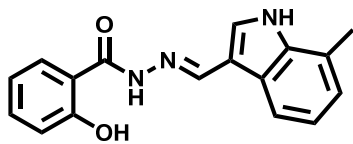




500 MHz, CD₃CN

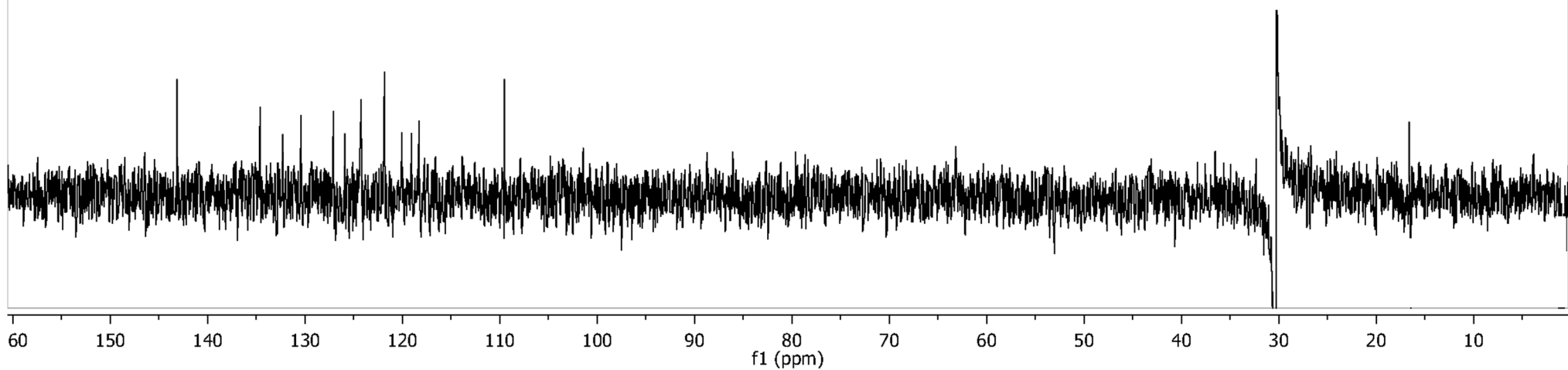
NSAH-E-3Z

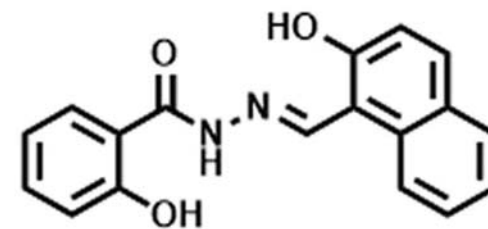
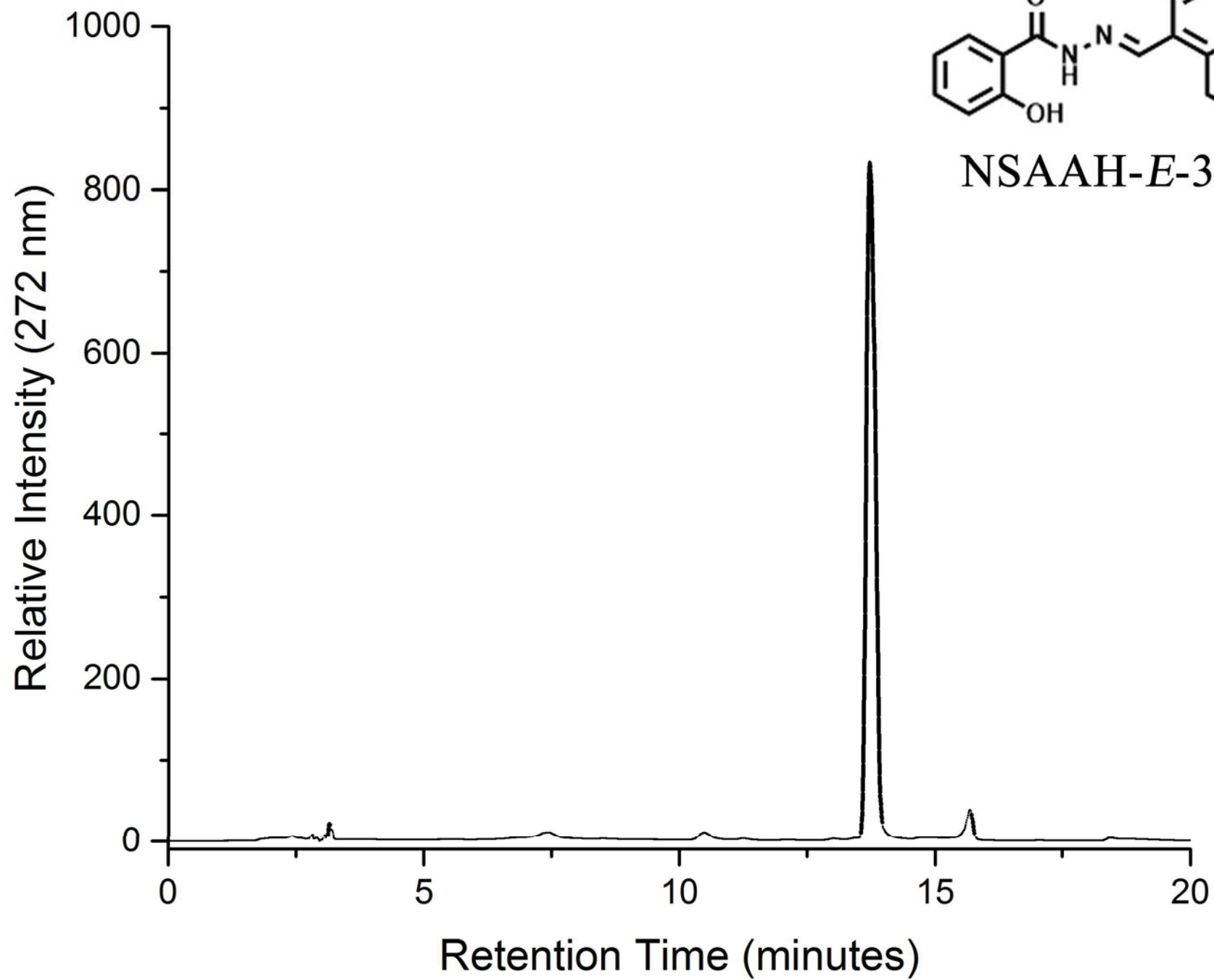




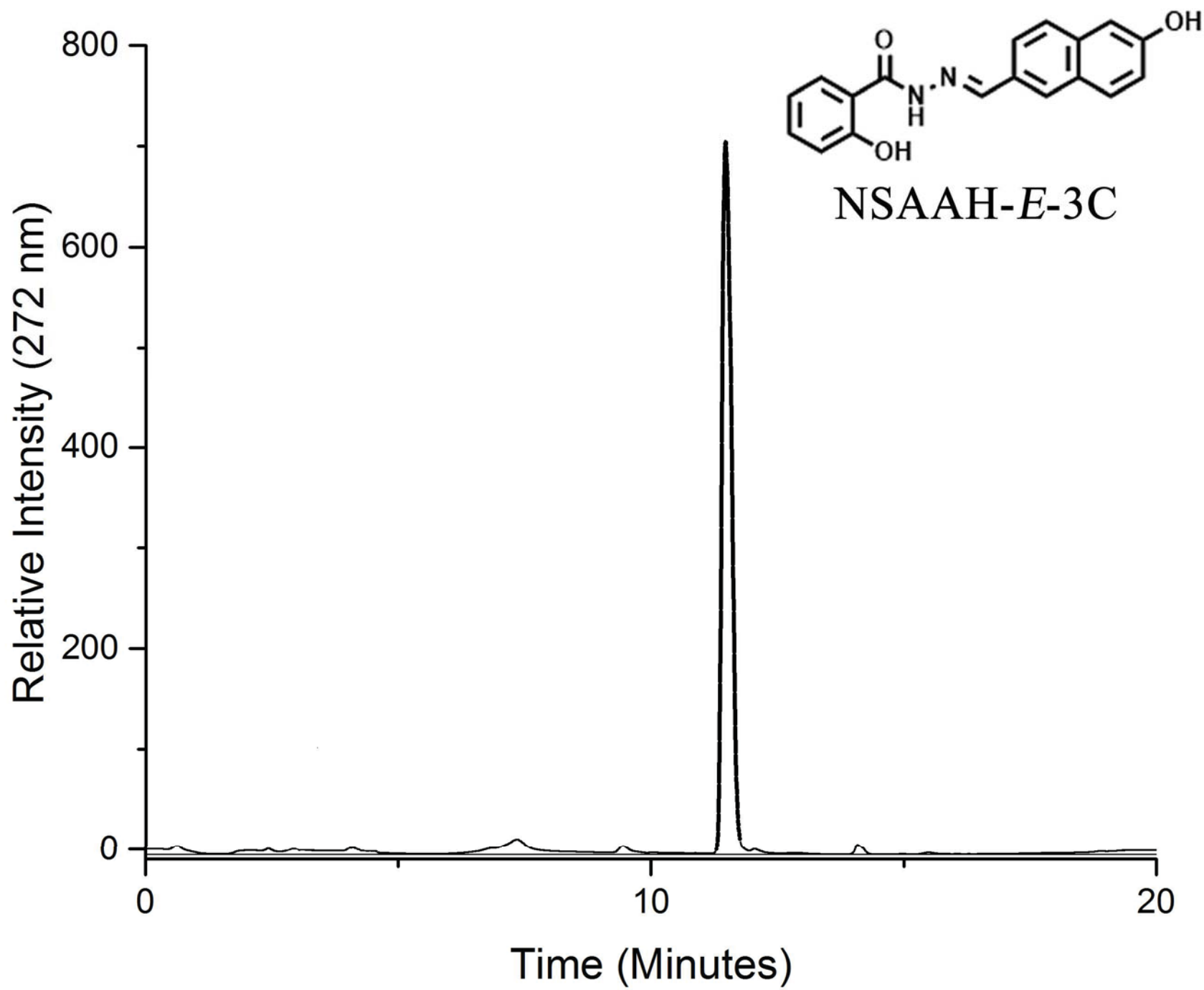
125 MHz, CD₃CN

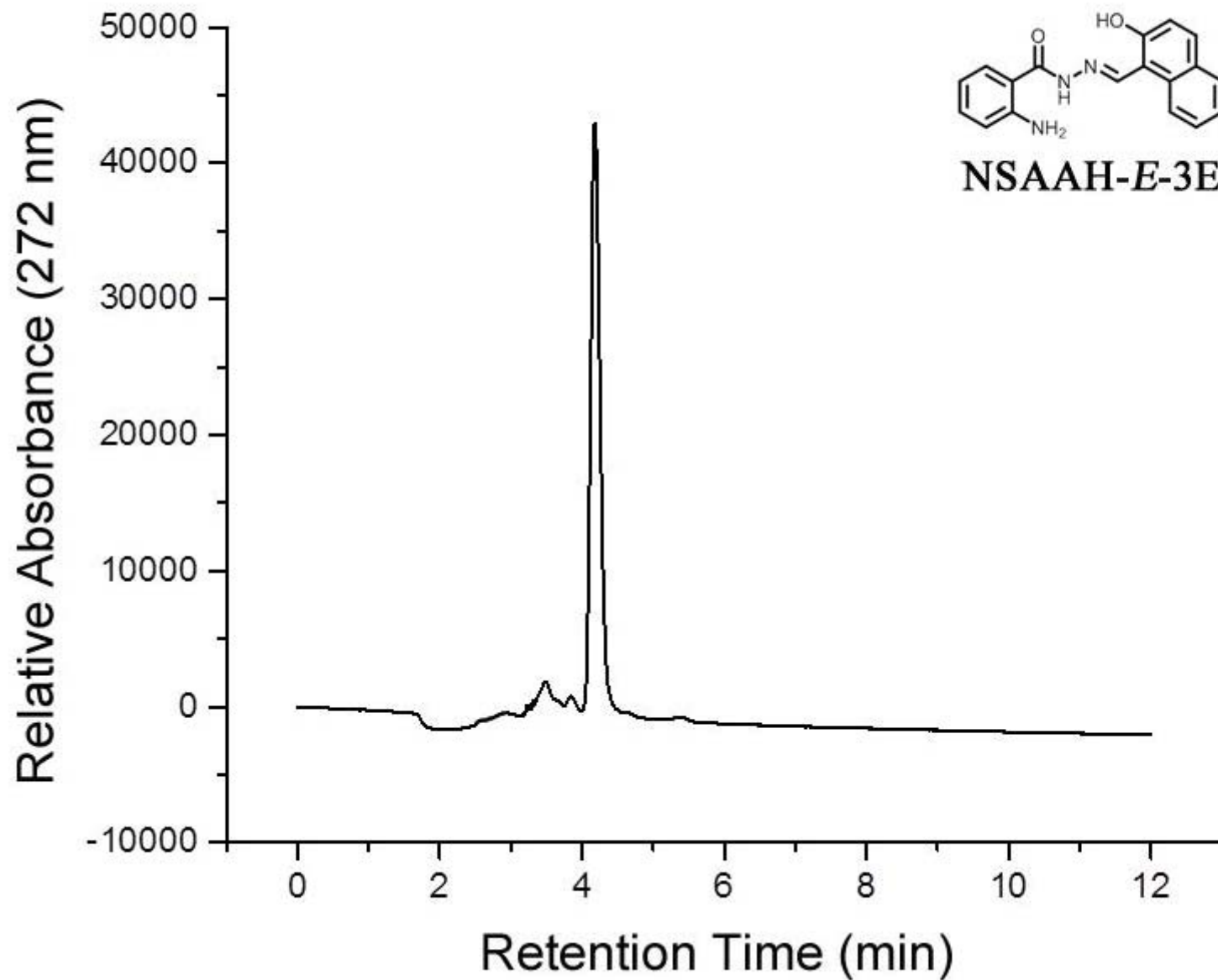
NSAH-*E-3Z*

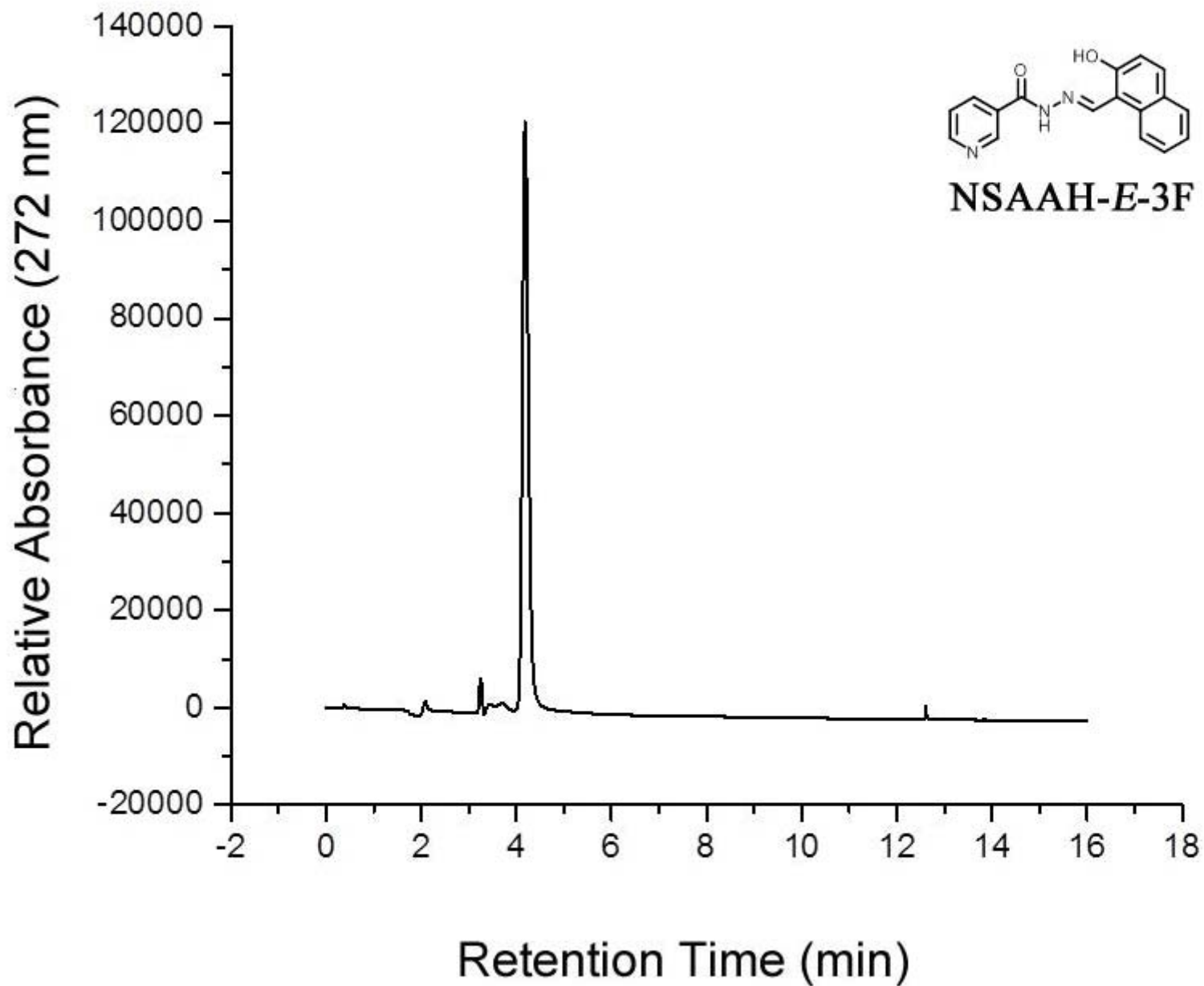


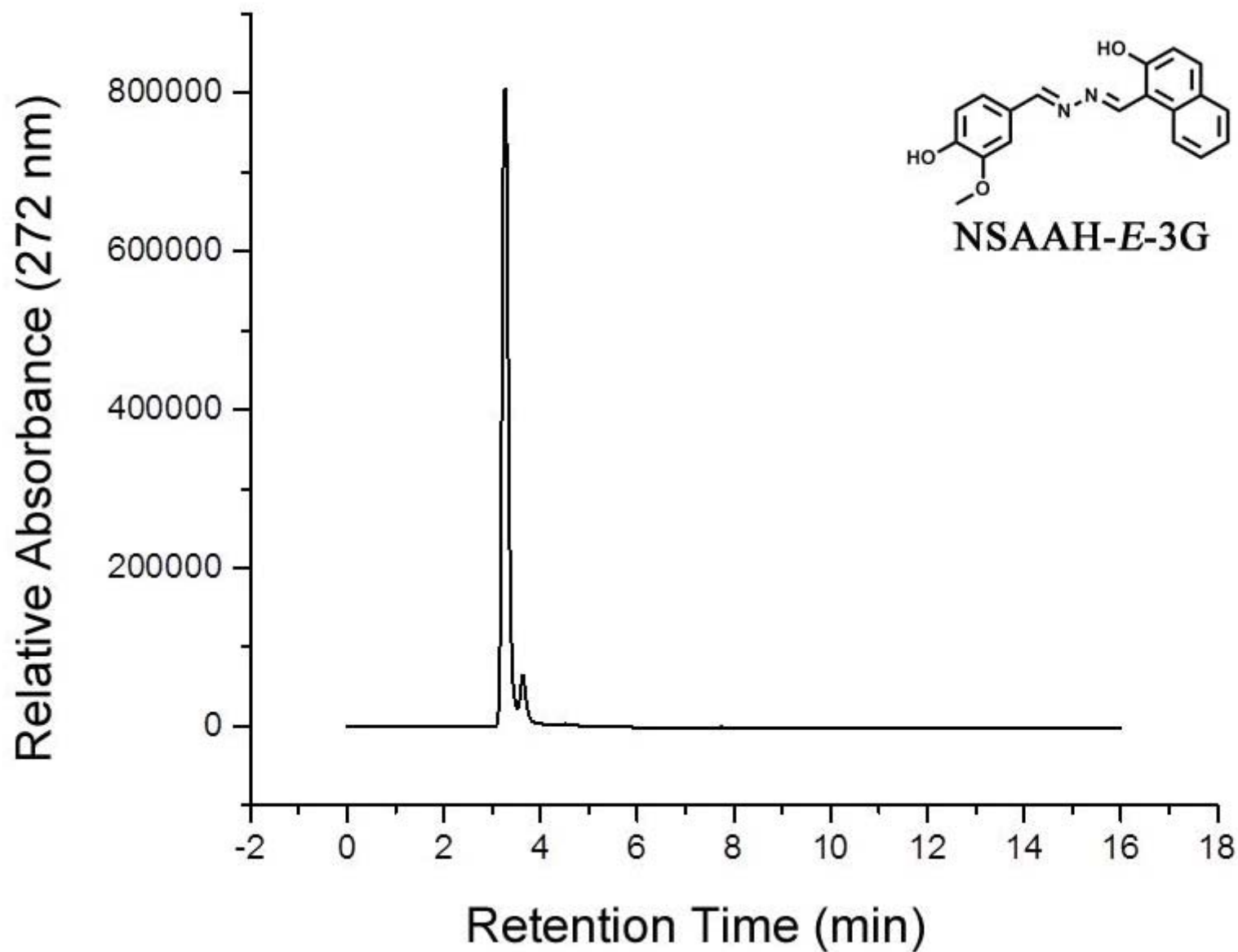
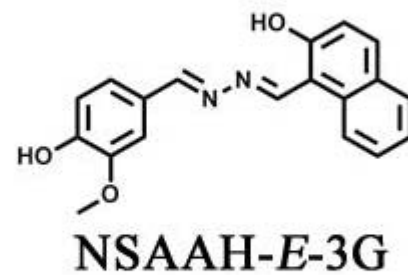


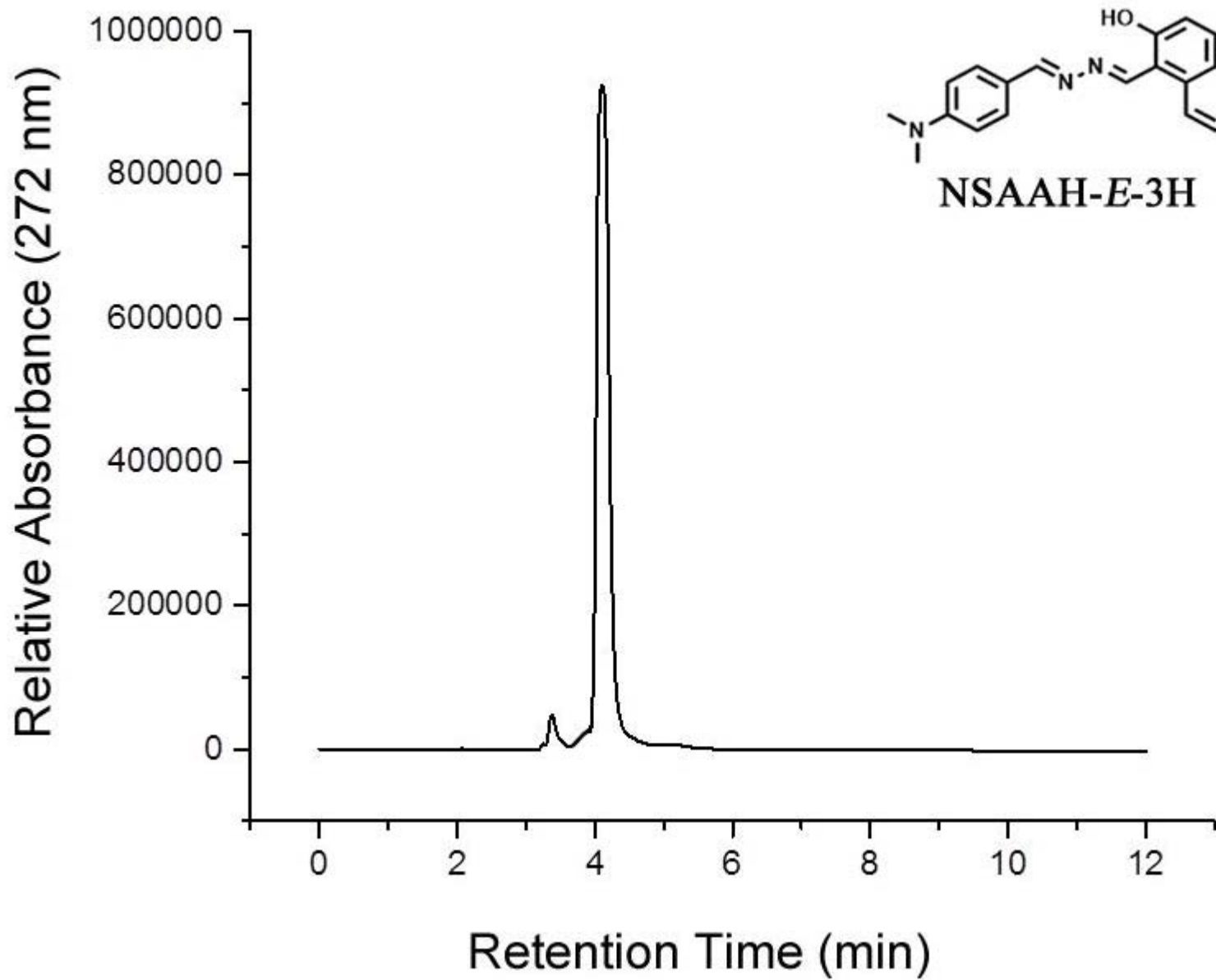
NSAAH-*E*-3A

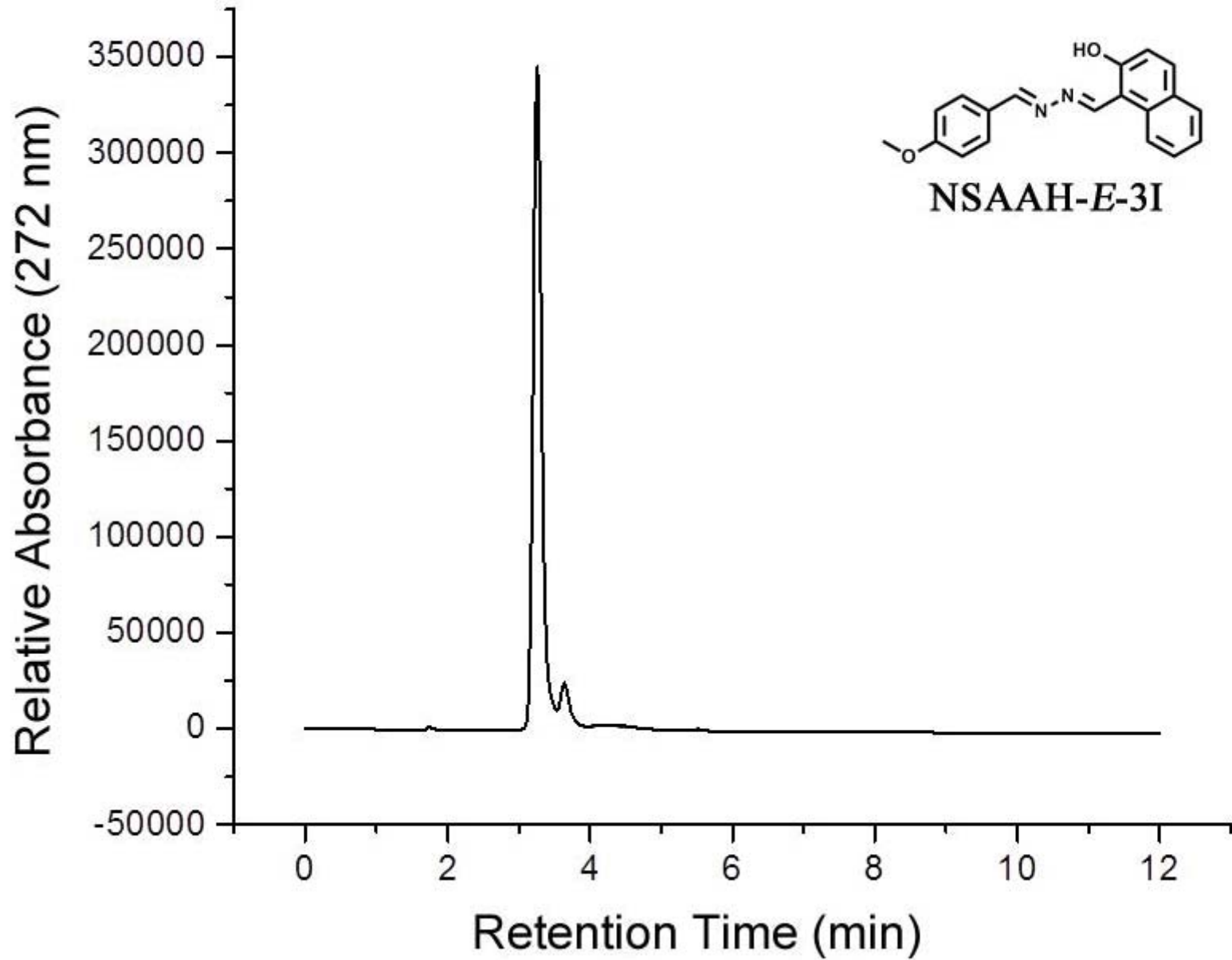


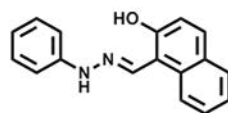




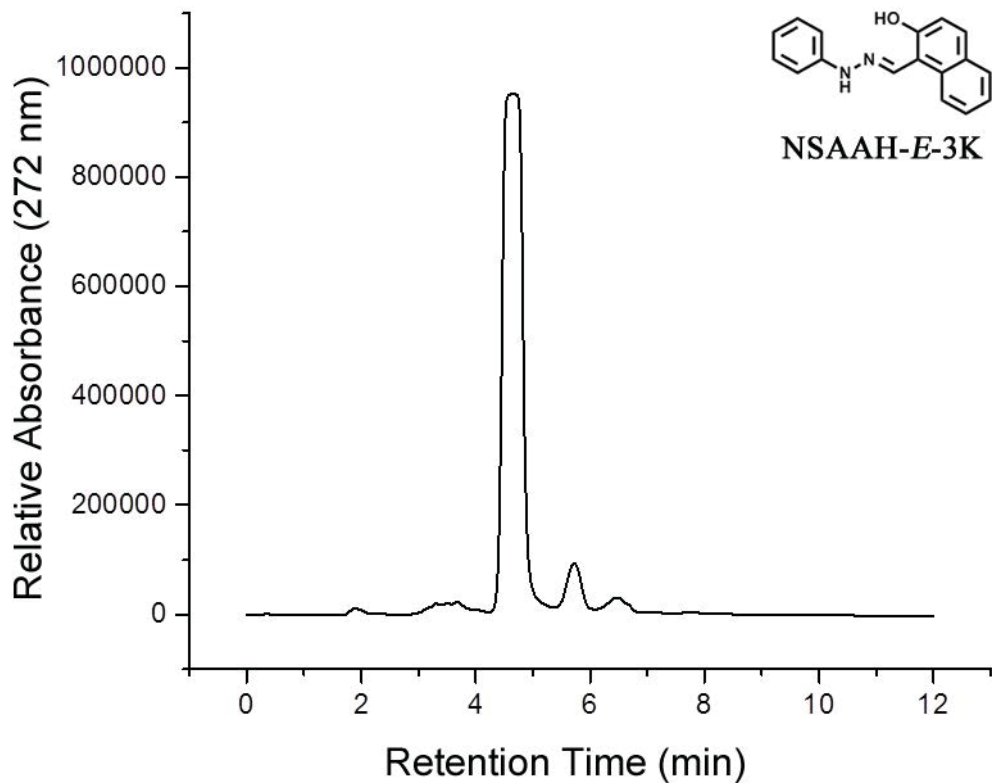


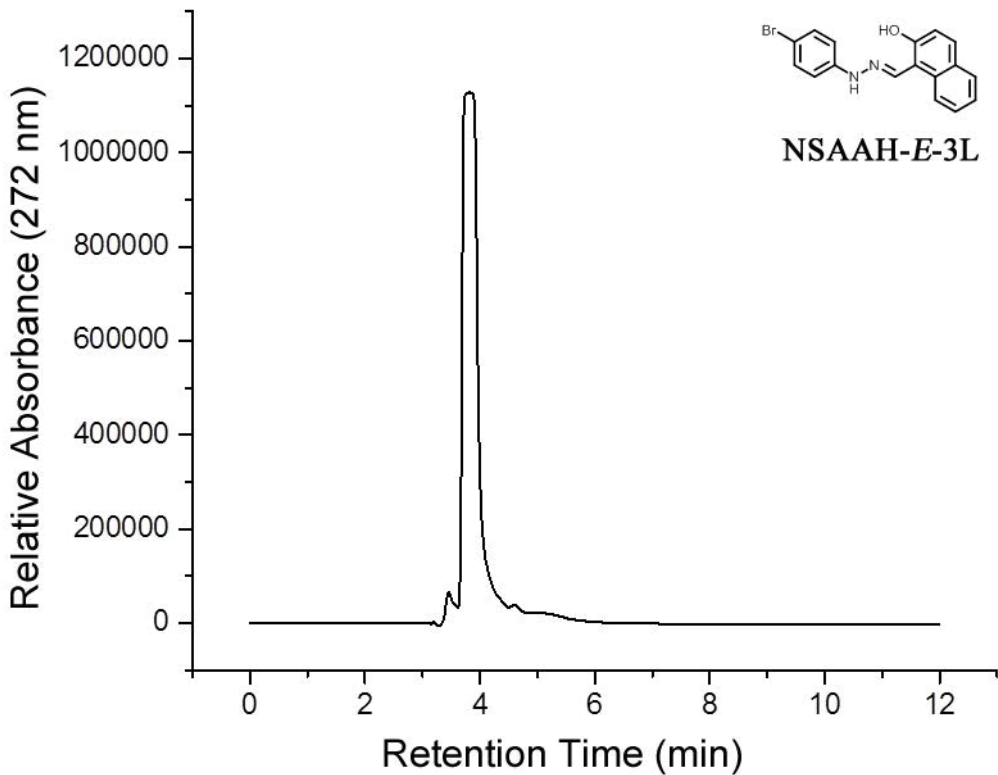


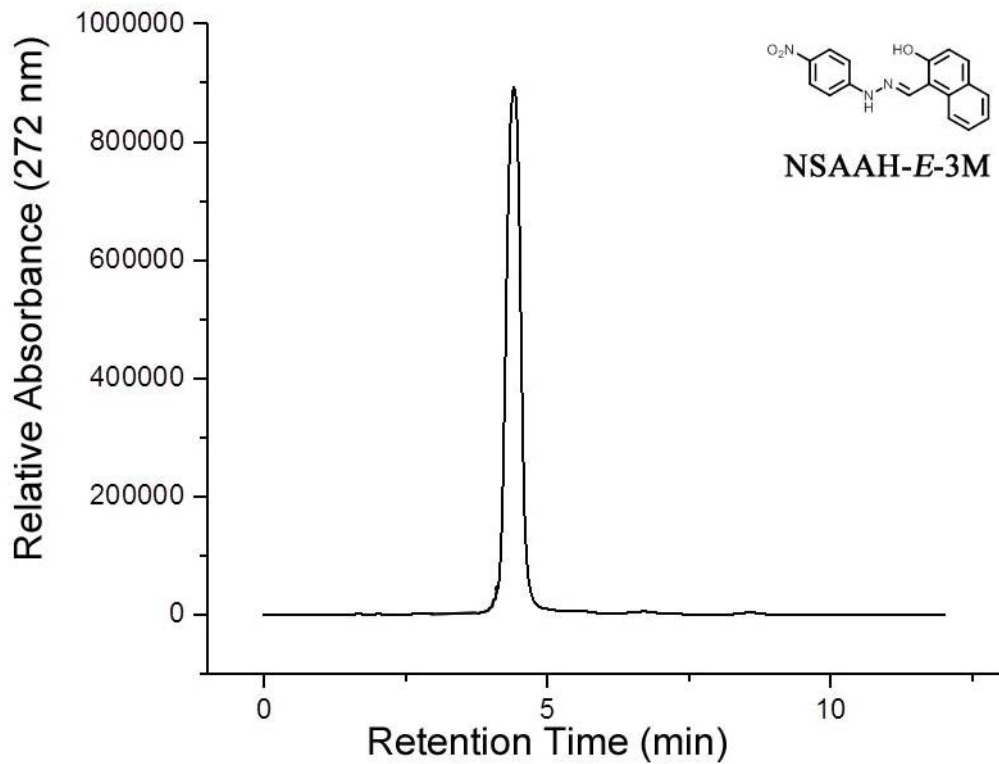


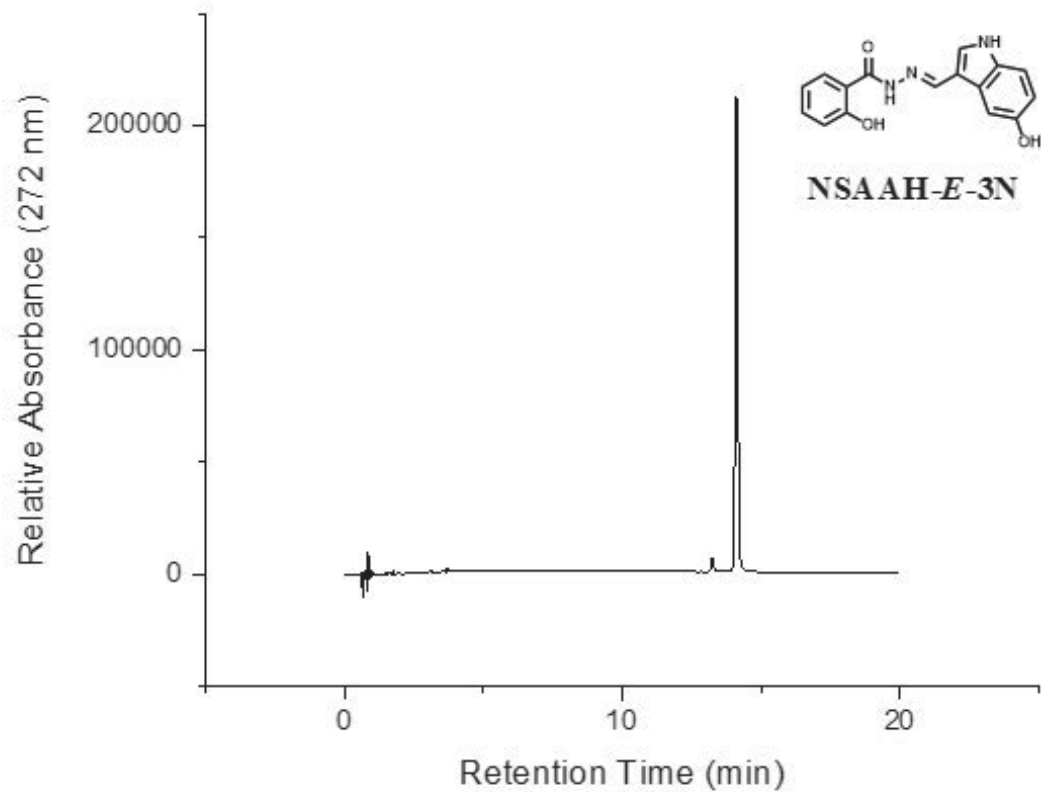


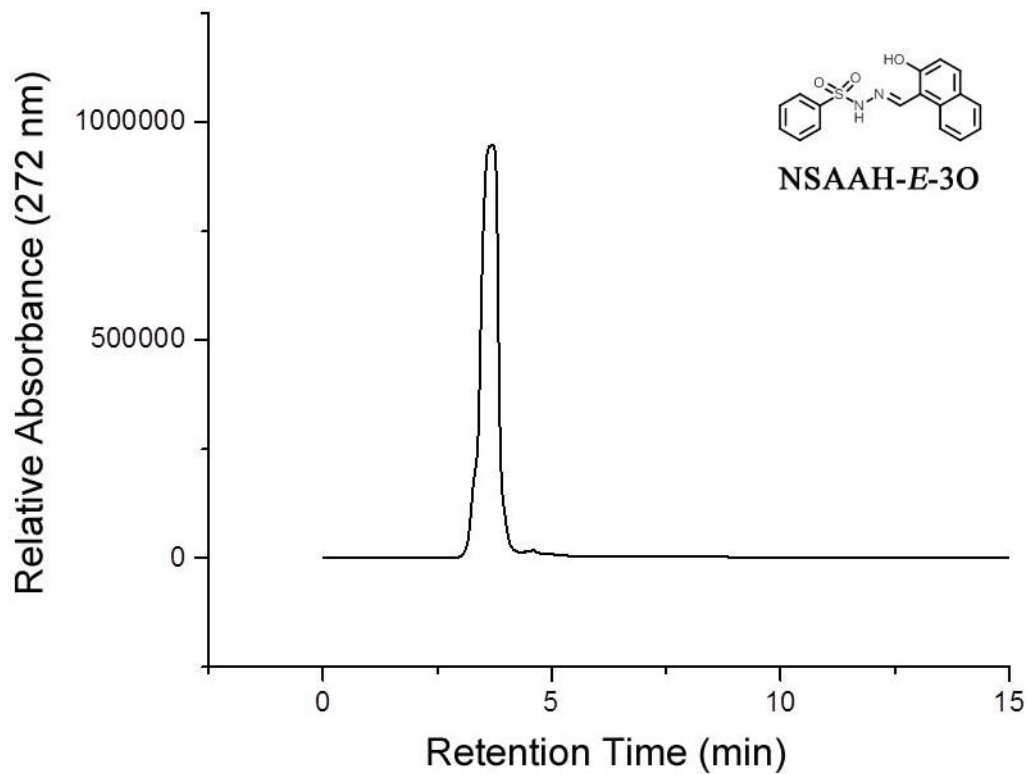
NSAAH-E-3K

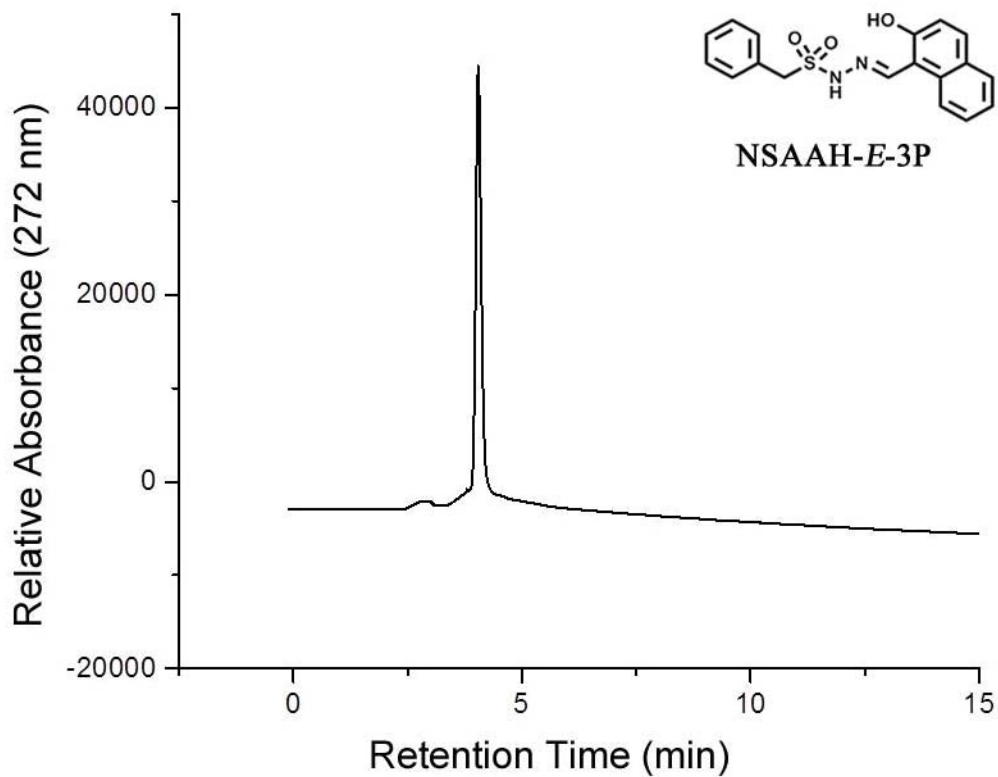


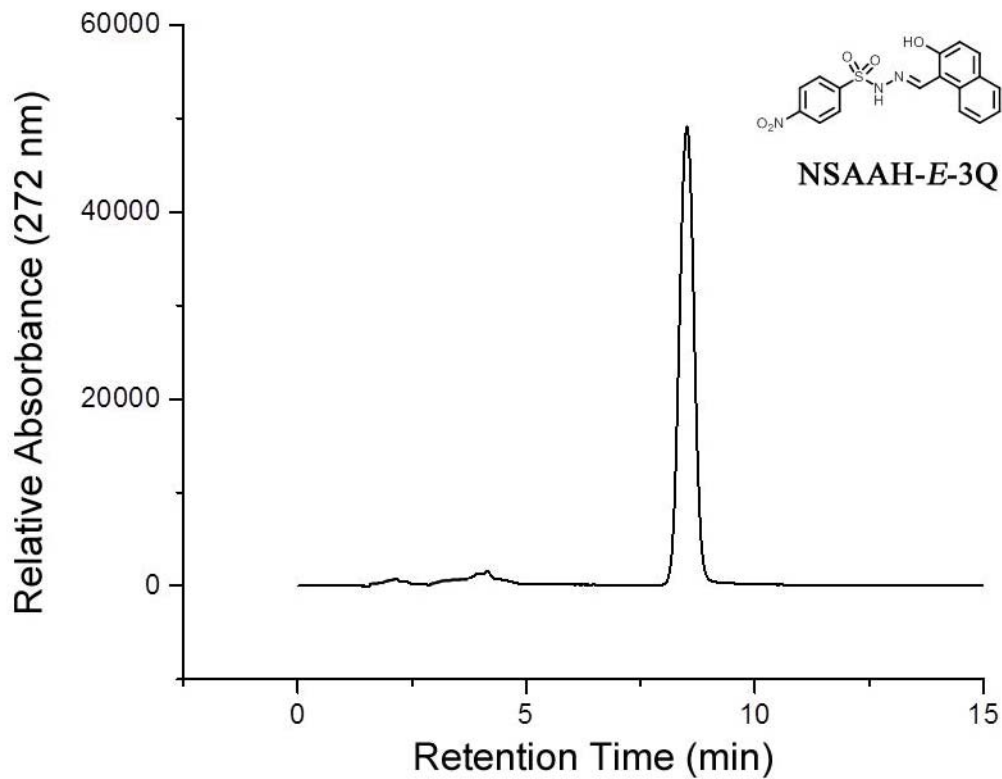


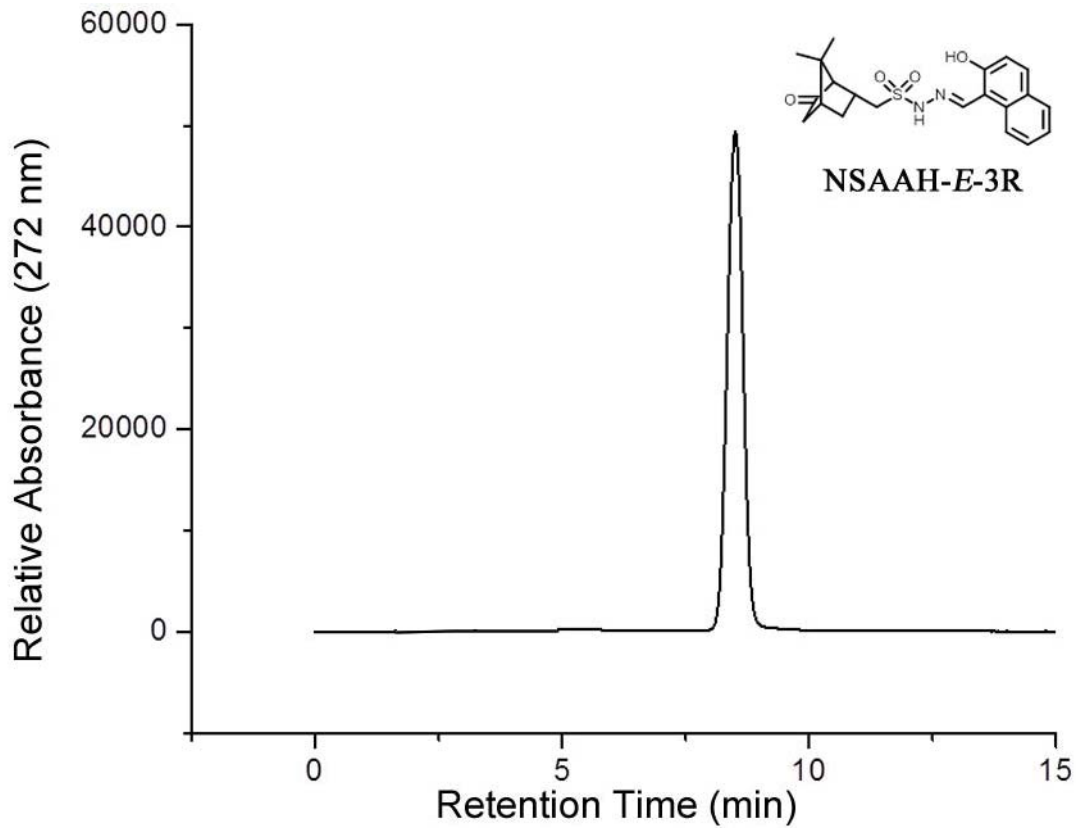




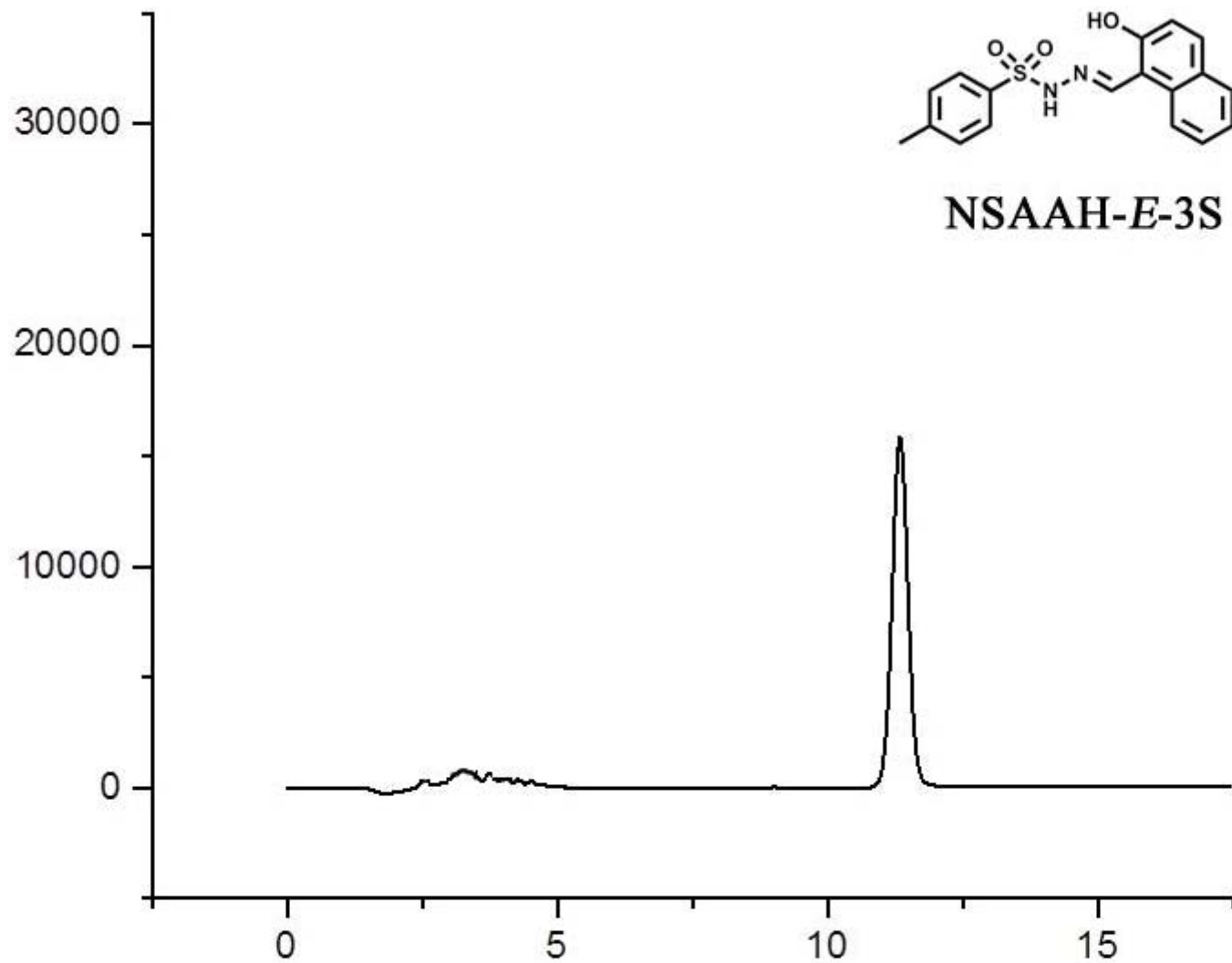






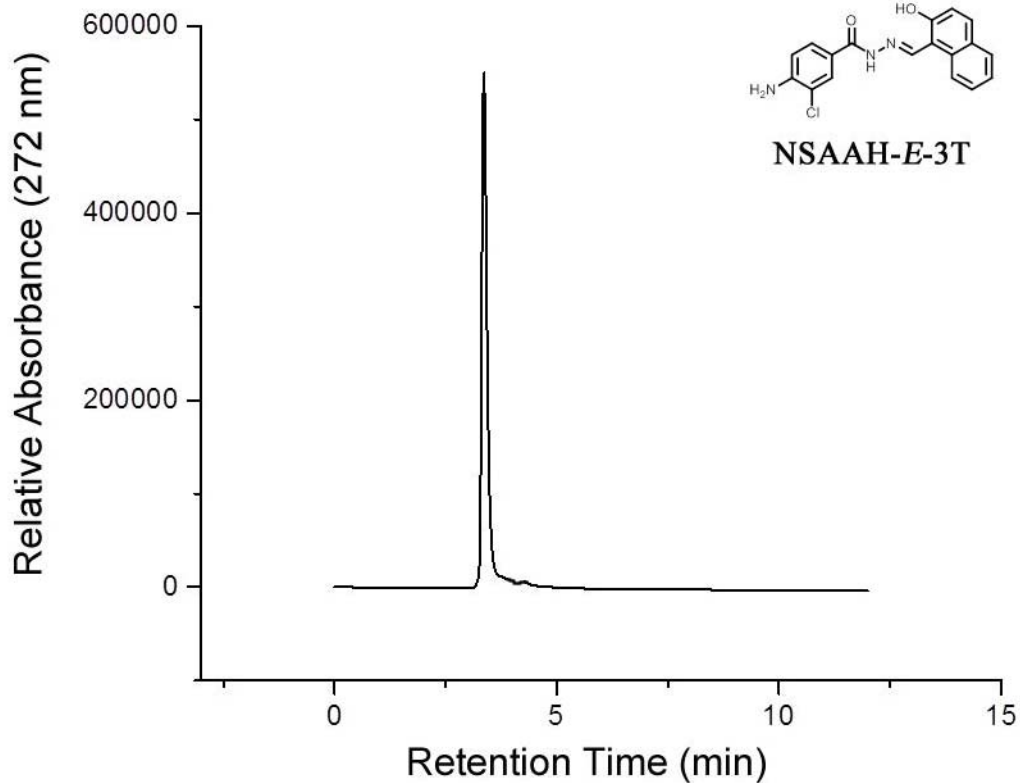


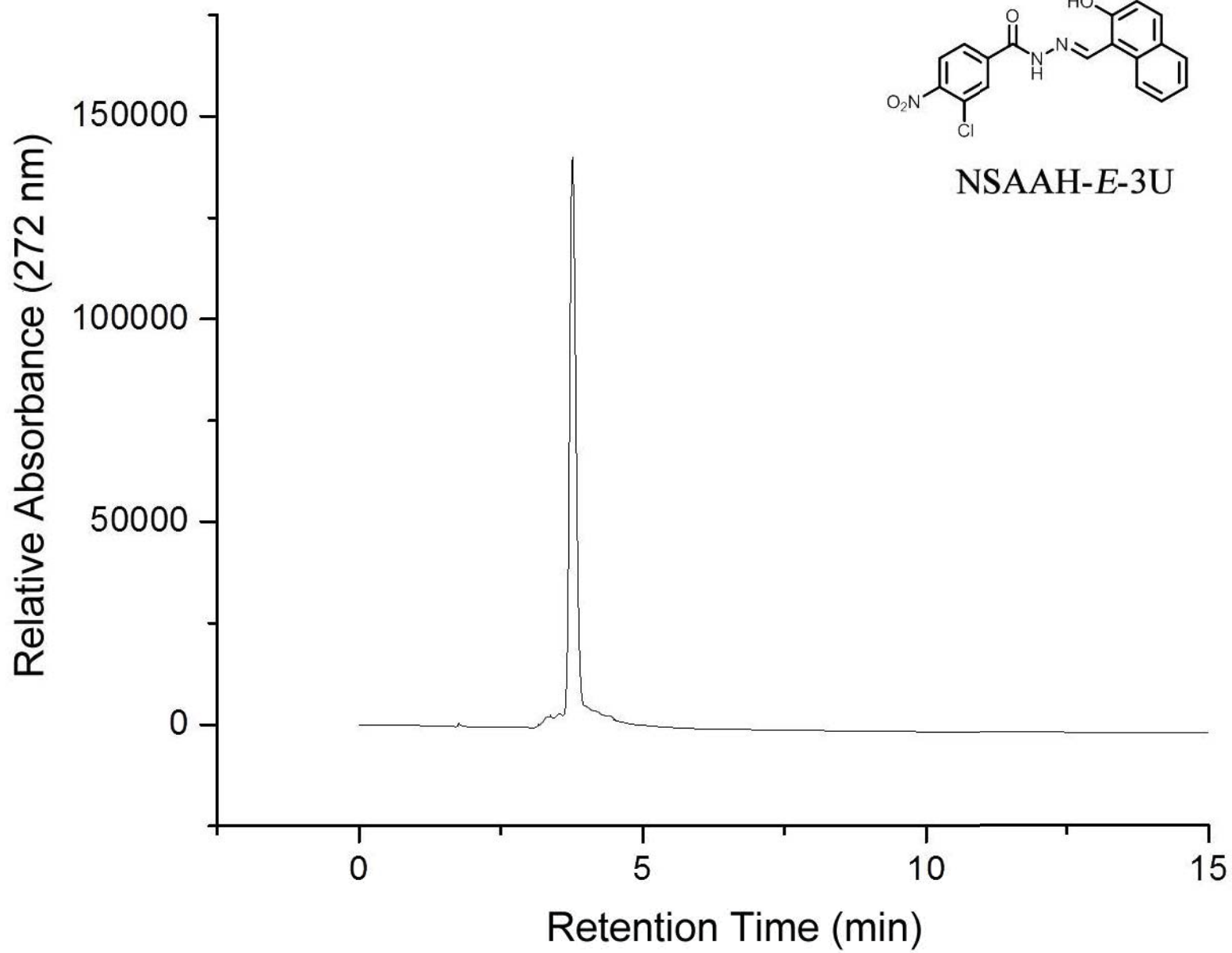
Relative Absorbance (272 nm)

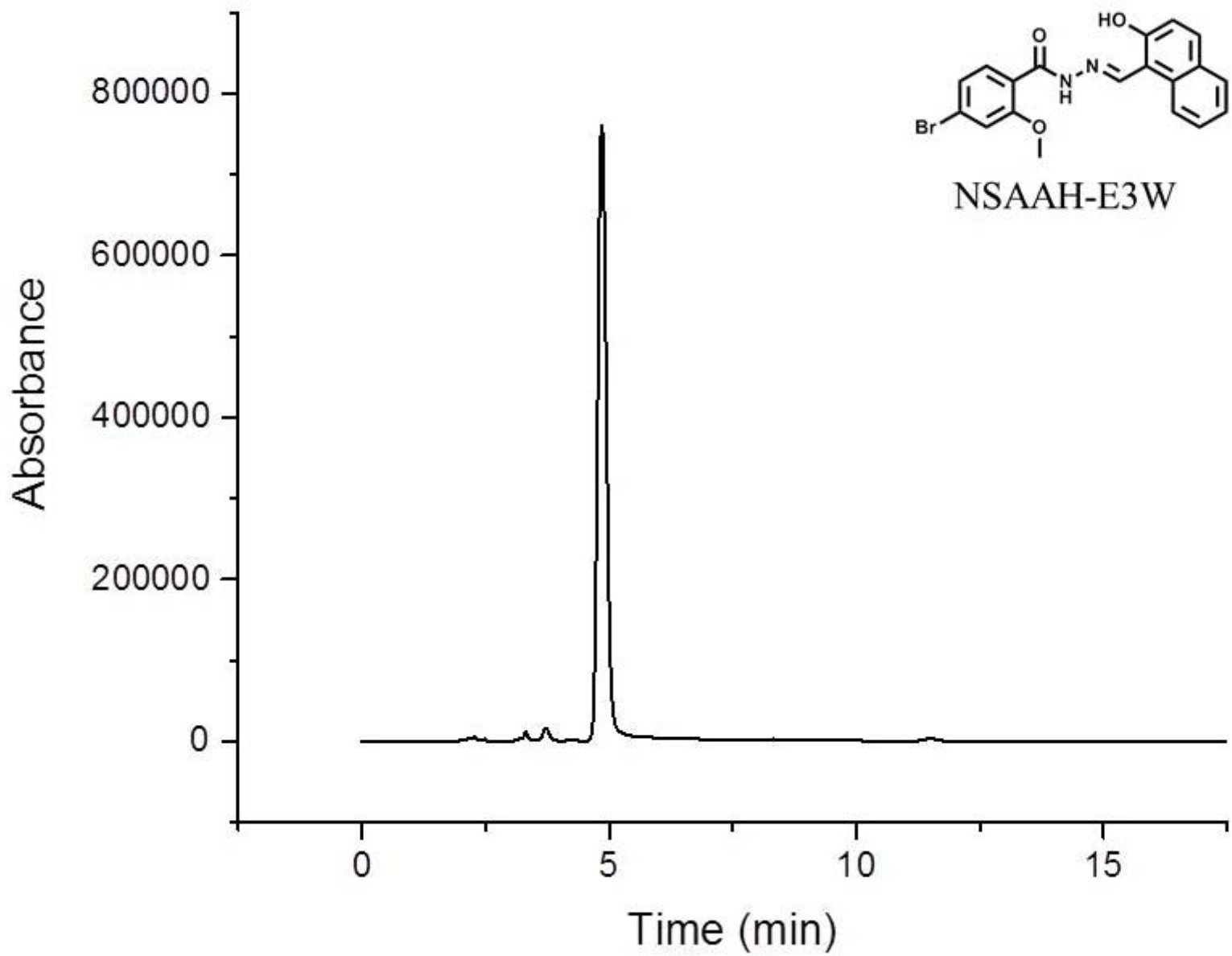


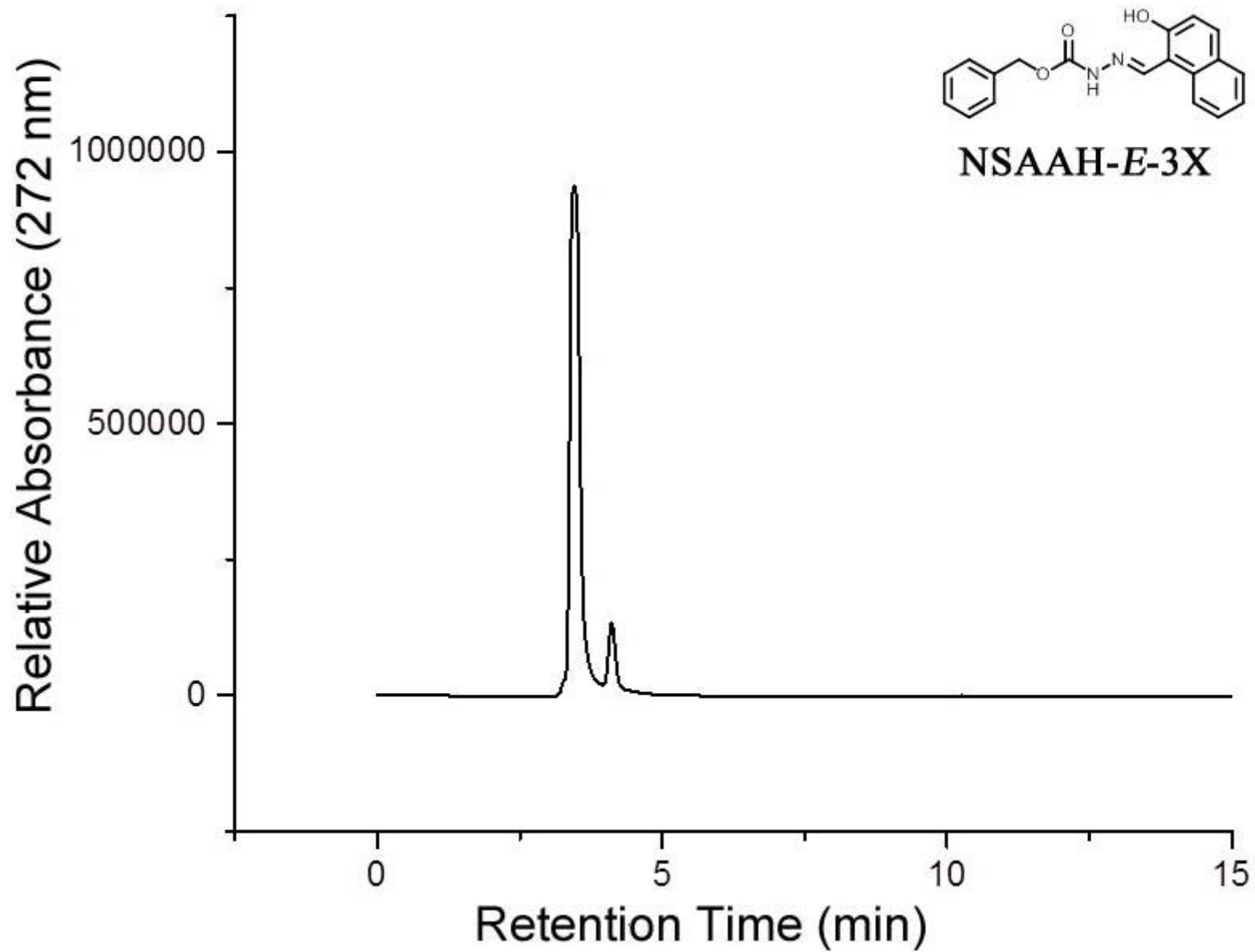
NSAAH-E-3S

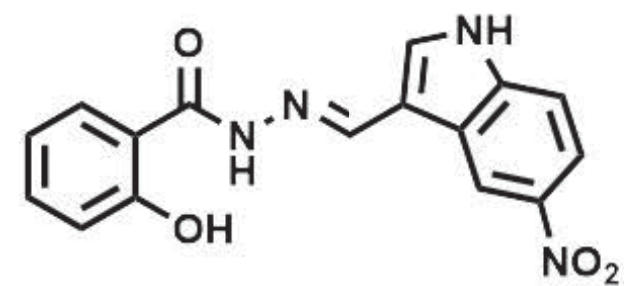
Retention Time (min)



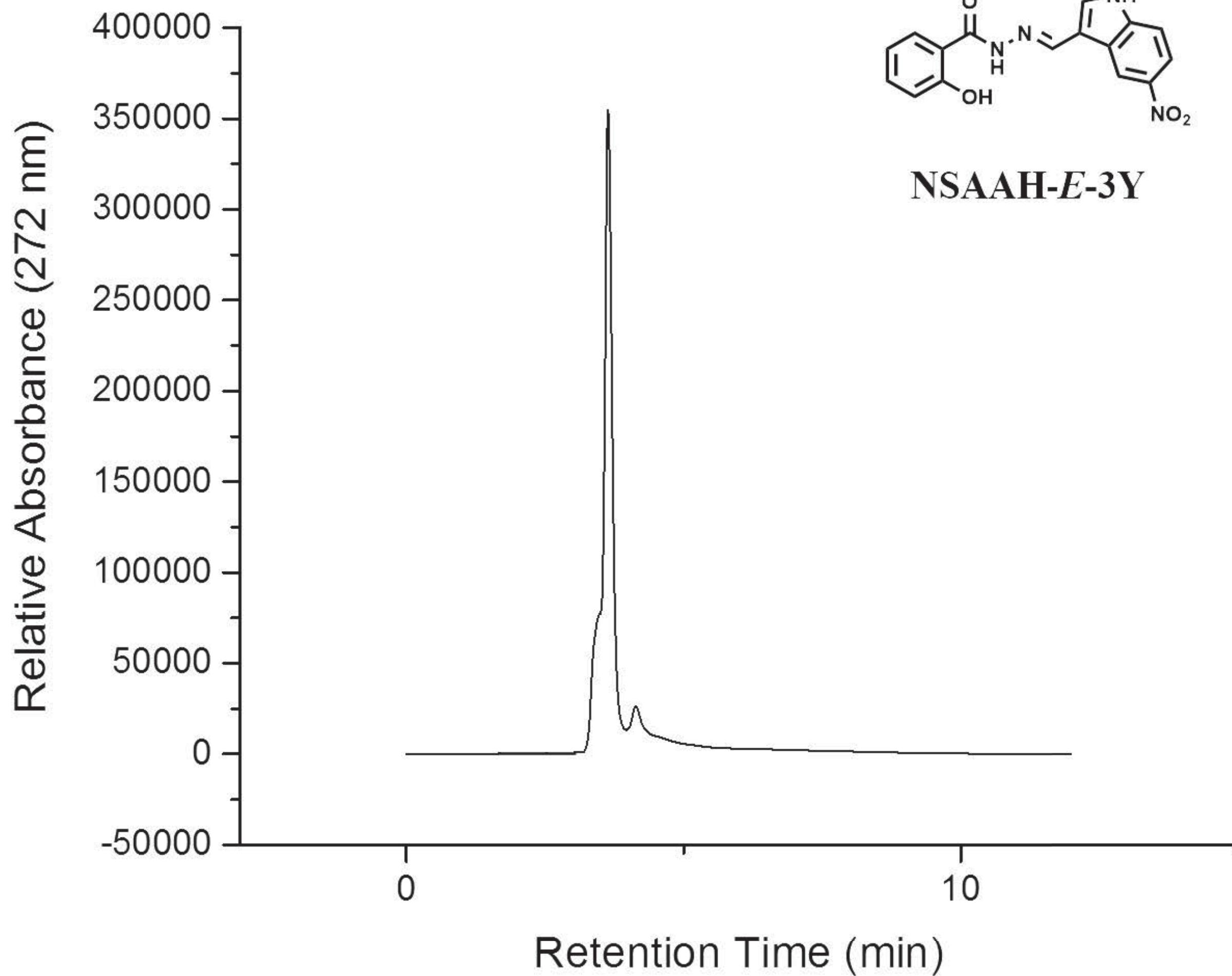


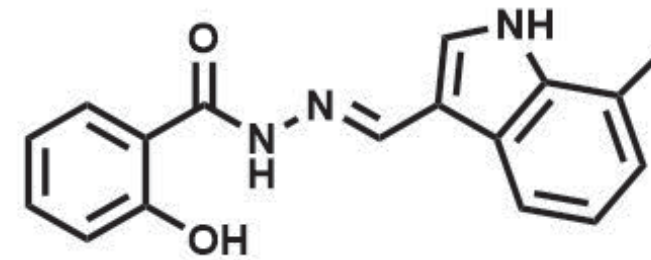






NSAAH-E-3Y





NSAAH-*E*-3Z

